MATHEMATICAL AND EXPERIMENTAL MODELS FOR STUDYING SOMATOSENSORY FEEDBACK VIA PRIMARY AFFERENT MICROSTIMULATION

by

James Arthur Hokanson

B.S. Biomedical Engineering, Washington University in St. Louis, 2006

B.S. Electrical Engineering, Washington University in St. Louis, 2006

Submitted to the Graduate Faculty of

the Swanson School of Engineering in partial fulfillment

of the requirements for the degree of

Doctor of Philosophy

University of Pittsburgh

2013

UNIVERSITY OF PITTSBURGH

SWANSON SCHOOL OF ENGINEERING

This dissertation was presented

by

James Arthur Hokanson

It was defended on

November 18, 2013

and approved by

A.P. Batista, Ph.D., Assistant Professor, Bioengineering Department

R.A. Gaunt, Ph.D. Assistant Professor, Physical Medicine and Rehabilitation Department

C.C. McIntyre, Ph.D. Associate Professor, Biomedical Engineering,

Case Western Reserve University

D.J. Simons, Ph.D., Professor, Neurobiology Department

Dissertation Director: D.J. Weber, Ph.D., Associate Professor, Departments of Bioengineering and Physical Medicine and Rehabilitation

MATHEMATICAL AND EXPERIMENTAL MODELS FOR STUDYING SOMATOSENSORY FEEDBACK VIA PRIMARY AFFERENT MICROSTIMULATION

James Arthur Hokanson, PhD

University of Pittsburgh, 2013

A significant problem with current prostheses is the challenge of controlling the device without being able to 'feel' it. Without somatosensory feedback, cognitively demanding visual and attentional processes must be relied upon. However, restoring somatosensory feedback offers the possibility of changing a prosthetic from an extracorporeal tool into a part of the user's body, while enabling a far more natural control scheme. Although artificial somatosensory feedback of prostheses has been attempted since the 1960s, clinical implementations are lacking.

This thesis will focus on the use of electrical stimulation to artificially activate the nervous system to restore feedback. With recent advances in electrode design, the possibility of implanting hundreds of electrodes into the nervous system is becoming a reality. However, current stimulation protocols are oriented towards using only a few electrodes. It is likely that new stimulation paradigms will be needed in order to fully take advantage of multichannel microelectrode arrays.

This dissertation examines new methods for studying somatosensory feedback. Dorsal root ganglia microstimulation with concurrent nerve-cuff recordings is used to evaluate stimulation thresholds and the types of neurons first recruited. Computational models are developed to explore recruitment beyond threshold as well as the impact of simultaneous stimulation on changing neural recruitment. Finally, an experimental model is developed that uses the cortical response to primary afferent stimulation to assess information transfer to the

brain. Together, these models offer new approaches for improving somatosensory feedback stimulation paradigms.

TABLE OF CONTENTS

LIST OF TABLES

LIST OF FIGURES

PREFACE

When writing my dissertation, I thought that this section would be the easiest to write. Now, as it is the last thing I write, I realize I was quite wrong. I owe so much thanks to so many people and I surely cannot thank you all adequately here. If you're reading this and thinking that you deserve a bit of thanks for your help and support you are only partially correct. More than likely you deserve much more appreciation and thanks from me than you realize. THANK YOU for your support!

I would be remiss if I didn't mention my biggest supporter through all of this, my wife Laura. Thank you Laura Ann for everything, especially your patience.

1.0 INTRODUCTION

1.1 THE NEED FOR SOMATOSENSORY FEEDBACK

Somatosensory feedback is critical for normal motor function. For some this knowledge may be self-evident. Anyone that has tried knows how difficult it is to type on a keyboard while wearing gloves. We rely on our ability to feel the keys to type, although our awareness of our using this knowledge is often subconscious. When holding objects we naturally maintain a precise amount of force that prevents slippage yet is not overly strong (Westling and Johansson 1984), meaning we can carry a heavy cup when necessary, but at the same time not crush it.

For some, disease or injury has led to a loss of somatosensory feedback which negatively impacts their ability to perform daily tasks. In some cases of diabetic neuropathy, the loss of foot sensation is so great that they are more likely to fall (Maurer et al. 2005). People that experience a large loss of sensory fibers due to disease have difficulty in maintaining steady-state levels of active muscular contraction that are necessary for postural stability (Sanes et al. 1984). In some extreme cases constant visual attention is needed in order to make any movements (Cole and Sedgwick 1992, see also Bastian 1887). Feedback also provides us with safety cues. As described by Tims, tissue damage and loss commonly associated with leprosy is actually a side result of loss of sensation and the inability to properly protect an insensate limb (Tims et al. 1967, Pfeiffer 1969). From personal communication with a missionary who had worked with

lepers, he mentioned that even though it is often possible to prevent limb loss, lack of sensation often leads to a lack of ownership, such that an insentient limb becomes not worth saving since it no longer belongs to the person it is physically attached to. Similarly, appropriate feedback attributed to an artificial hand has been shown to lead to perceptions of embodiment (Marasco et al. 2011).

In some cases it may be possible to artificially restore this loss of sensation using engineering approaches. It is this goal that motivates the work done in this thesis. The thesis will focus on artificial electrical stimulation in the peripheral nervous system where the pathway from the point of stimulation to the brain is intact, but because of limb loss or peripheral neuropathy, the body is unable to naturally sense things such as touch or limb position. The discussion will primarily focus on artificial sensory feedback in prosthetic users since historically that population has been the focus of development for these technologies. That being said, the principles discussed should be generalizable to other populations with damaged peripheral receptors (distal neuropathies). The problem and the general approach are illustrated in Figure 1.1.

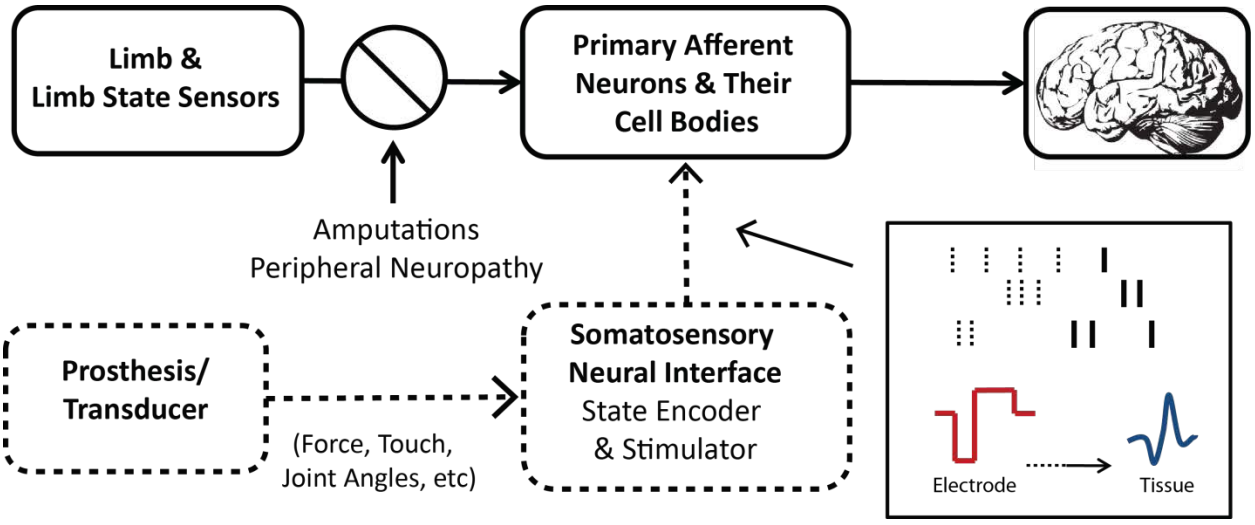

Figure 1.1: Problem and general approach. Normally our limb senses things such as pressure, temperature, or joint angles. Sometimes these signals are not properly sensed and transmitted to our brain, such as due to amputation or peripheral neuropathy. To restore these feedback signals requires a transducer to first sense them, and a neural interface to transfer these signals back into the nervous system.

It is estimated that there are nearly two million people living with limb loss in the United States (Ziegler-Graham et al. 2008). Based on CDC data, there are approximately 185,000 amputations that occur in the United States each year (Owings and Kozak, 1996). Roughly half of the amputations are due to trauma, and another half due to diabetes (Ziegler-Graham et al. 2008).

In studies regarding the priorities of prosthetic users, comfort and durability appear to be the highest priorities (Atkins et al. 1996, Biddiss et al. 2007). However, in terms of "future work", individuals with upper-limb loss rated needing less visual attention as one of their top priorities (Atkins et al. 1996). Similarly, sensory feedback was rated highly in a study by Biddiss et al. (2007) after issues like weight and glove durability. It is expected that sensory feedback will become especially important as prostheses become more advanced and offer more degrees-

of-freedom for control, especially with the ability to control individual finger movements (Belter et al. 2013).

1.2 ARTIFICIAL SOMATOSENSORY FEEDBACK

1.2.1 Brief History

To make a more naturally controlled prosthetic, designers in the 1940's and 1950s started working on extracting neural signals from the residual limb of amputees to control a device (Battye et al. 1955, Alter 1966, Childress 1985). By the 1960s many groups had completed prototypes and started testing of these devices (Cowell 196, McKenzie 1965a, McKenzie 1965b). Immediately it became apparent that a user's ability to control these new devices was poor and that sensory feedback was needed to improve performance (Wiener 1951, Mckenzie 1965a, Alter 1966, Mann 1968).

Although some groups report mild success, nothing is currently being used clinically to provide artificial sensory feedback. Instead prosthetic users must rely on visual feedback, causing a significant increase in cognitive load and concentration required to perform tasks, and making limb movements while performing other tasks much more difficult if not impossible (Mann 1968). The realization of the importance of sensory feedback for improving brain-machine interfaces has led to a resurgence in interest in providing artificial sensory feedback (Abbott 2006, Lebedev 2006, Suminski et al. 2010, Weber et al. 2011). Given that this problem was first described over a half century ago, it is relevant to understand where the field has been and perhaps why we have not made more progress.

Beginning in the late 1960's to early 1970's a series of papers were published on artificial sensory feedback. Two generic approaches to providing this feedback were suggested. The first, commonly referred to as sensory substitution, aims to replace one type of sensory input with another. As an example, Mann describes a system which uses vibration on the skin of a limb stump to convey elbow position to a prosthetic user (Mann, 1968). In this case, the primary afferents that would normally convey elbow position information are being replaced with cutaneous input to a different part of the body which must then be interpreted as representing elbow angle. Other labs also examined this approach, typically using either vibration (Mann 1968, Alles 1970, Mann 1970), electro-cutaneous stimulation (Beeker 1967, Pfeiffer 1968, Shannon 1979), or sound (Pfeiffer et al. 1969, Tims et al. 1967). The authors of these articles claimed some success. Mann (1970), for example, indicated that matching task errors were reduced by 50% with tactile feedback.

An alternative approach involves trying to directly activate the primary afferent neurons which are no longer receiving appropriate input. This lack of input may be due to limb loss or receptor damage (as may be the case with diabetic neuropathy). Importantly, in most of these cases, some portion of the peripheral nerve remains intact and artificial activation of any given neuron will ultimately be interpreted by the body as if that activation had occurred from receptor activation (Dhillon et al. 2004). This does not mean that artificial stimulation will feel completely natural. A nerve may have thousands of neurons and currently available electrode arrays have approximately 100 electrodes (for motor neuron stimulation, Norman et al. 2012). Additionally, peripheral damage can lead to changes in the physiology of the peripheral nerves (spontaneous action potential generation) and to changes in higher order connectivity (cortical remapping) (Dhillon et al. 2004), which may make it impossible to drive completely natural

sensations after a long post-injury period. Despite these challenges it is thought that interpretation of activation of the normal neural pathways, even if imperfect, would be less of a cognitive burden than sensory substitution approaches, and certainly has the potential to lead to much more natural feedback.

In 1973, Clippinger reported use of an implanted electrical stimulator for direct nerve activation through electrical stimulation (Clippinger, 1973). Results from three subjects were reported, although more significant testing had been done on only two. The prosthesis included a strain-gauge for monitoring the degree of hand opening. This signal was tied into an electrode on the surface of the median nerve. To provide a feedback signal the stimulation frequency delivered on the electrode varied in proportion to the degree of hand closure (i.e. with strain). For the two patients in whom more significant testing had been conducted, the paper says "Both state the prosthesis is more like their normal hand and that they have fewer problems with fine prehension of small and breakable objects." In a much more detailed 1974 (Clippinger et al. 1974) follow-up, they mention that comparative functional testing between the conventional prosthesis and the sensory feedback system was not performed.

In 1975, Reswick reported results from a study that relied on an implanted interneural electrode to provide sensory stimulation (Reswick et al. 1975). Unlike in Clippinger's work, the single patient being tested continued to use their cable-powered prosthesis during testing (instead of EMG). Using a block size discrimination task, there was found to be no difference when electrical stimulation feedback was present. Their primary conclusion was that the sensory stimuli being delivered were being ignored in favor of the residual feedback available from the cable system. Future studies were suggested but, as far as I can tell, none were published.

There is a dearth of publications on artificial sensory feedback after the 1970's. Childress (1985) mentions that powered prosthetics finally gained significant clinical traction in the late 1970's. It is possible that there was an attention and funding shift from theoretical feedback to practical issues impacting current clinical practices. Körner (1979) suggests that sensory feedback, although useful, might not be as important as previously thought given the current state of prostheses, and should only be attempted in a limited set of patients where it is very clear that a device with feedback is needed. Similar sentiment is given by Northmore-Ball and colleagues (Northmore-Ball et al. 1980). It is possible that the type of feedback possible with these systems, given the technology available at the time, was ultimately deemed not useful enough to warrant further study. Scott (1990) expresses a similar sentiment that the 1980's allowed for sufficient development in prosthetic technology that a return to sensory feedback is now needed/warranted. Finally, in 1976 the United Stated Food and Drug Administration introduced the Medical Devices Act, arguably making it much more difficult to try new approaches in human subjects. It is interesting to consider what impact this might have had on researchers considering direct nerve stimulation procedures for sensory feedback or the much simpler option (in terms of regulations) of using surface electrodes to extract motor control signals.

Although research into sensory substitution approaches is still ongoing (e.g. Antfolk et al. 2013, Christiansen et al. 2013), it is felt that ultimately direct nerve stimulation approaches will be preferable. A good example of the current state of the art is the work by Dr. Ken Horch. Dr. Horch has inserted longitudinal intrafascicular electrodes (LIFEs) into the nerves of amputee patients. Although multiple electrodes are sometimes inserted, usually only one or two electrodes are used (Dhillon and Horch 2005, Horch et al. 2011). Horch and colleagues have demonstrated

the ability to evoke graded sensations referred to phantom limbs, as well as to use these signals during motor control tasks (Dhillon et al. 2004, Dhillon and Horch 2005, Horch et al. 2011). It is unclear the extent to which this level of sensory feedback is actually useful, although there is a growing awareness that this type of stimulation might mitigate phantom limb pain (Horch et al. 2011), regardless of the sensory feedback outcomes.

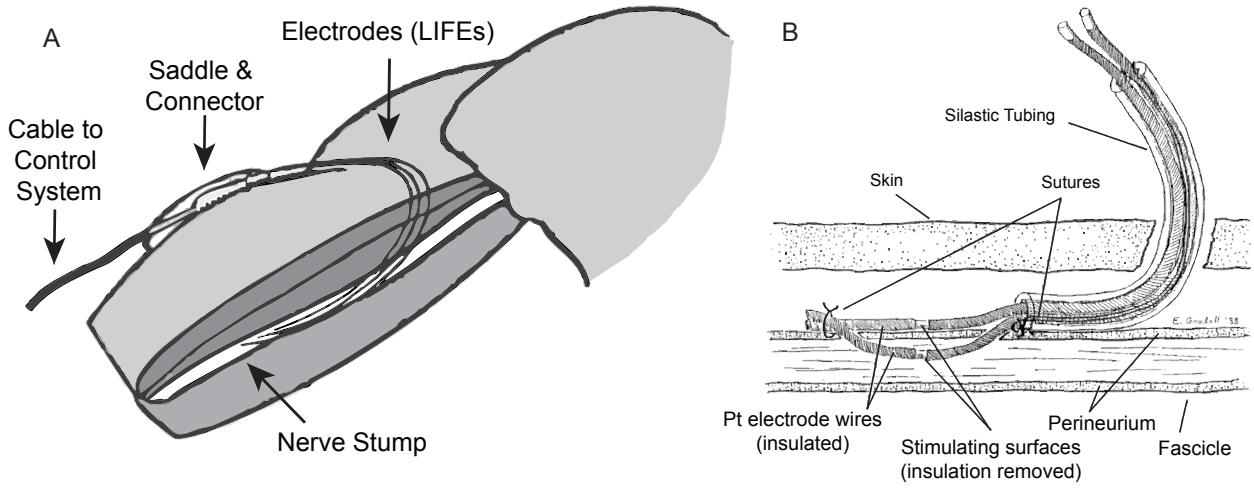

Figure 1.2: Illustration of longitudinal intrafascicular electrodes (LIFEs). (A) View of system as implanted in an amputee. (B) Close up of the electrode. The electrodes themselves consist of fine wires with 1 mm of exposed contact. These electrodes are individually inserted into fascicles. These electrodes have been placed in amputees on a short term basis and can be removed by gently pulling without anesthetic. For more details see original texts. (Images based on Dhillon et al. 2004, Nannini and Horch 1991)

Another approach for providing artificial sensory feedback that has been recently developed is that of getting nerve to regrow into different host tissue. This process, known as targeted reinnervation, has been pioneered largely by Dr. Todd Kuiken. As an example, in a 2007 publication Kuiken and colleagues report on a set of patients whose brachial plexus nerves have been transferred to upper arm and chest muscles. When sensory neurons reinnervate the

muscle tissue, touching the muscle evokes sensations that are referred to the missing limb (Kuiken et al. 2007). Although this approach is promising, it will not be the focus of this thesis.

1.2.2 The Stimulation Paradigm/Protocol

The ultimate goal of this work is to restore somatosensory feedback to people that currently lack or have less than normal somatosensation. The approach that we are pursuing as part of this study relies on artificial sensors which are placed on an artificial limb to transduce external (and internal) sensations. These sensors would detect limb movement, such as finger flexion, as well as touch, temperature, etc. These sensors would than transmit this data to some interface that artificially activates intact neural pathways, leading to sensation.

One of the primary focuses of this thesis is in trying to answer how the nervous system should be stimulated (activated) to transmit somatosensory information to the brain. Approaches can be specific to limb state input, such as a change in elbow angle by a particular amount, or can be more generalized, such as never exceeding a particular stimulus amplitude or using a particular type of stimulus waveform. These rules or approaches to stimulation to accomplish the specified task, such as somatosensory feedback, are what are known as stimulation paradigms and/or protocols.

Since this concept is so important, let us briefly examine at least one well established stimulation paradigm that is being used clinically. One fairly well known stimulation paradigm is called continuous-interleaved-stimulation or CIS, which has been used in cochlear implants (Wilson et al. 1991). Like all other cochlear implant stimulation paradigms, CIS maps a set of input frequencies to stimulation on a set of channels. Put another way, the spectral content of sound is mapped to a place of stimulation in the cochlea. To transmit this information to the

brain, each channel modulates its amplitude relative to the magnitude of the spectral content it is representing. One of the things that made CIS unique was the decision to use discrete stimulus pulses, instead of a continuous waveform. This decision, in conjunction with interleaving neighboring channels, allowed CIS to avoid interactions from simultaneous stimulation on neighboring channels. The avoidance of simultaneous stimulation is thought to improve the ability to perceive speech. Simultaneous stimulation will be explored further in Chapter 6.

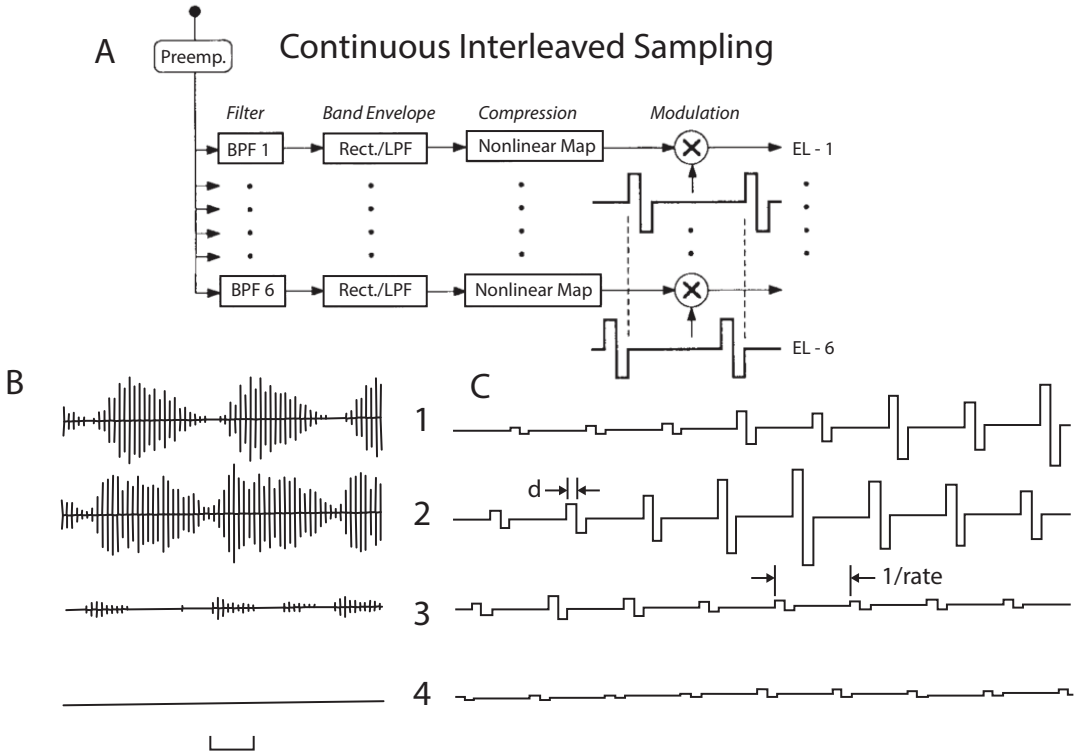

Figure 1.3: Continuous Interleaved Stimulation protocol. (A) Incoming sound is separated into different channels by band-pass filtering after a preemphasis filter which attenuates low frequency components. Other processing follows, see original text for details. (B) Demonstration of modulation of stimulus amplitude given speech sound ('aw'). Stimulus amplitude is modulated and the stimulus rate is constant. (C) Zoom in of the bracketed interval in (B). An important update of CIS compared to previous stimulation paradigms was the use of non-overlapping pulsatile stimuli. Ignoring unspecified filtering parameters, the details in this figure are sufficient specification of a stimulation protocol to take incoming audio and deliver stimulation on a set of channels. A similar type of design approach is needed for somatosensory feedback. (Figure is from Figures 1 and 2, Wilson et al. 1991)

Unlike CIS and other cochlear-implant stimulation paradigms, sensory feedback paradigms in the peripheral nervous system tend to modulate the stimulus rate (also referred to as stimulus frequency) instead of the stimulus amplitude, because stimulus frequency is known to modulate perceived intensity (Adrian and Zotterman 1926). The stimulation paradigm used by Dr. Horch has been to stimulate on each electrode at a constant stimulus amplitude that is midway between stimulus threshold and a stimulus amplitude which causes a change in elementary sensation (from those at lower stimulus amplitudes) or discomfort. At the chosen stimulus amplitude the stimulation rate is modulated according to a psychometric curve which is generated from user input (Dhillon et al. 2004), relating stimulation rate to some perceived sensory input (e.g. touch or proprioception, Figure 1.4). Currently each implanted electrode is treated as an individual feedback channel. Given the coarse nature of the implant, one electrode per fascicle, this is probably a valid assumption.

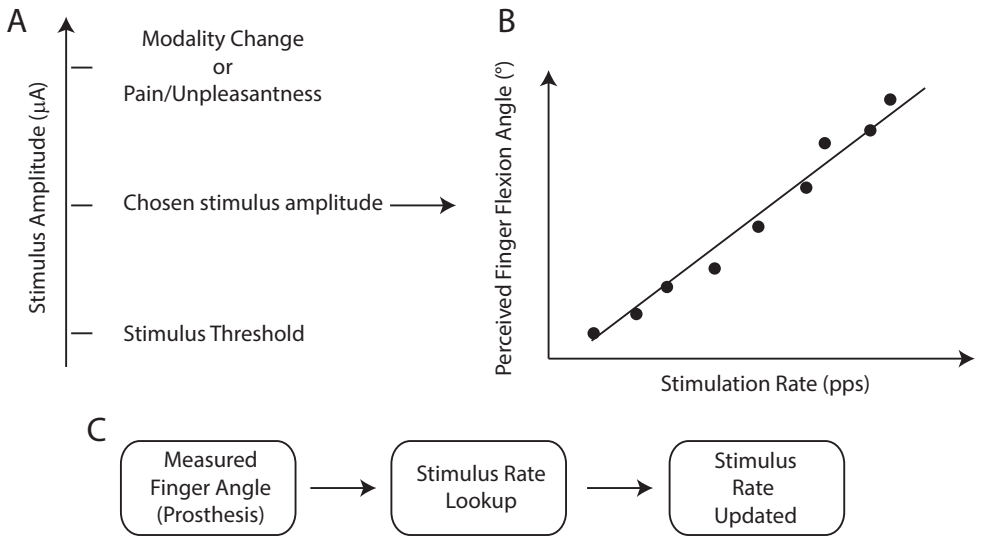

Figure 1.4 Design of a single-channel stimulation protocol for somatosensory feedback. (A) Stimulus amplitude is determined. At some stimulus amplitude above threshold, the feedback modality is determined (in this case finger flexion). A maximum stimulus amplitude is determined, which occurs when the stimulus amplitude elicits an unpleasant response, or when the type of feedback changes modality. A stimulus amplitude between threshold and this maximum is chosen for further testing. (B) As the stimulus rate is changed, the subject is asked to indicate the perceived angle of finger flexion, either on an open-ended scale, or via matching the angle on the opposite, intact limb. (C) Implementation of the stimulus paradigm. Once the relationship between stimulus rate and perceived angle has been obtained, the stimulus design is finalized. As the prosthesis measures a change in finger angle, via some sensor, the necessary stimulus rate required to elicit the measured angle is determined. Finally the stimulation rate is updated.

For this study, we wanted to know how current somatosensory stimulation paradigms, such as the one illustrated in Figure 1.4, might change if instead of using only a few electrodes we started using many tens or eventually even hundreds. Also, microstimulation in general is a relatively nascent field. Current clinical devices such as a cochlear prosthesis or an electrode for deep brain stimulation use feature sizes on the order of millimeters rather than microns (Volkmann et al. 2002, Saunders et al. 2002). What considerations in development of a stimulation paradigm are necessary due to the small nature and high density of the electrodes?

Ultimately our work is trying to determine how we can develop a stimulation paradigm that provides feedback that is as natural as possible. When considering this goal, it is important to realize that there are many ways to manipulate the stimulus on each electrode to activate neural tissue. When taking into account multiple electrodes, the relative timing between stimuli on these electrodes, and the dependence of these results on the location of the tissue with respect to the electrode, the number of options for stimulation parameters can quickly become overwhelming. Methods are needed to reduce this parameter space and to learn what works, and what doesn't work, so that the design of stimulation paradigms in a clinical setting is tractable and more useful than naïve approaches.

1.2.3 Performance Assessment

When providing artificial somatosensory feedback, it is important to have some metric to determine how well the stimulation paradigm being employed works. Put another way, there are many alternative approaches to providing artificial feedback. In order to choose the appropriate approach, one must be able to compare the relative performance of each.

Since the earliest studies on the topic, one of the most popular ways of assessing the ability to provide sensory feedback is to measure motor performance with and without the stimulus (Mann 1970, Reswick 1975). Unfortunately for prosthesis users, this approach simultaneously tests sensory feedback performance and motor performance. Improvements to sensory feedback stimulation paradigms may be masked by poor motor performance occurring from the inability to extract decent control signals. Additionally, motor skills that incorporate somatosensory feedback may take some time to learn. Learning may make it difficult to properly assess eventual performance outcomes from a quick testing session.

An additional approach used for stimulation paradigm design is psychometric interrogation. As a person receives different stimuli they are asked to make relative comparisons. For example, for a stimulus channel which elicits a sensation of elbow flexion, the person might be asked how different stimulus rates relate to the perceived elbow angle (Dhillon and Horch 2005). Alternatively, someone might be asked to describe the pleasantness of a stimulus to determine the appropriate stimulus amplitude or whether or not an electrode should be used. Although this approach is extremely useful, it is unclear to what extent this approach can be extended to more complicated stimuli which may be difficult to describe. Additionally, testing multiple different stimulus paradigms may not be possible given how long the subject is willing to participate in testing.

In addition to behavioral assessment and psychophysical interrogation, there exists a third approach for assessing performance; electrophysiological measurements. This approach is based upon the assumption that neural activation is an indicator of functional outcome. Thus, if we can record activation of a neuron during a stimulus, and from previous experimental work have some idea as to how activation of that neuron contributes to somatosensation, then we can use the recording as an assay of the stimulation performance in restoring somatosensation. In many ways this is a novel approach. As such, the questions being asked of this approach are largely methodological more so than outcome based. In other words, one of the goals of this thesis is to try and develop this as a valid experimental approach for use in further investigations of stimulus performance. This approach is used twice in my thesis, first to examine neural activation of primary afferent neurons (Chapter 2), and second, to examine activation of somatosensory cortical neurons (Chapters 4 and 5). If successful, electrophysiological measurements have the potential to increase quantitative measurement outcomes.

Learning and neural plasticity are significant potential confounding factors when assessing performance outcomes. This topic is beyond the scope of this thesis, although eventually it will need to be addressed in the field. It is likely that important lessons can be learned from the field cochlear implants, which has had to deal with the problem of comparing different stimulation paradigms, where users tend to come to testing sessions biased by the previous experience and learning they have done with a previous system.

With an implanted feedback system, electrode stability may also play an important role in the assessment of performance. There is generally a reaction from the tissue to the implanted system which changes the relationship between electrode stimuli and activated neural tissue (Branner et al. 2004, Fisher et al. 2013). If the relationship between a delivered stimulus and the tissue it activates changes it will likely lead to a change in the relationship between a stimulus and the functional outcome. Importantly, this means that results obtained in an acute setting may be different than those obtained after the passage of time with a chronic implant, even if neural plasticity, in the traditional sense, has yet to occur. This also has the potential to complicate assessment measures. Again, this is beyond the scope of this thesis.

1.3 MICROELECTRODES

For the purposes of this thesis, a microelectrode refers to an electrode with features on the order of microns. Although microelectrodes have existed for a long time (e.g. Hubel 1957), their use in neuroprosthetic research is relatively new. Typically these electrodes have been used for making single-unit recordings or for microstimulation, both for scientific research purposes, but not for clinical devices. For example, researchers have inserted microelectrodes through the skin into

peripheral nerves, a technique known as microneurography, to record the response of single neurons to touch (Hagbarth and Vallbo 1967). In addition the same electrodes can be used to determine the type of sensation evoked from activation of a single primary afferent (Torebjörk and Ochoa, 1980).

For neuroprosthetic research however, there are at least two factors that have contributed to the limited use of microelectrodes. The first factor deals with technology. Working with and semi-permanently implanting microelectrodes, particularly arrays of microelectrodes, is often much more difficult than doing the same with surface electrodes or larger wires. Although there have been instances of self-manufactured sets of electrodes for decades (Loeb et al. 1977), recent technology developments (Branner et al. 2001, Wise et al. 2004, Musallam et al. 2007) have led to significant improvements in both device quality and ease of manufacturing.

Another significant factor which has made recent microelectrode work relatively novel is the relative invasiveness of microelectrodes relative to other approaches. Microelectrodes are typically designed to penetrate tissue so that they are in close proximity with nervous tissue. This invasiveness has the potential to lead to a more aggressive inflammatory response, as well as to cause electrode failure, and ultimately, could lead to device failure. Although a functioning microelectrode array may perform better than a macroelectrode array, in terms of increased SNR for recordings and increased selectivity for stimulation, a clinical device must not fail and this has led to the use macroelectrodes for clinical devices.

Even with the potential pitfalls of microelectrodes, they offer significantly improved access to sub-populations of neural tissue. As such, they have recently been used in areas where it is unclear if larger electrodes will provide sufficient specificity of neural activation. In motor stimulation applications, for years researchers have tried to restore functional movement to

paralyzed people by stimulating muscles and motor neurons. This technique has typically been done using electrodes on the surface of the skin, muscle, or by using electrodes that wrap around the outside of a nerve. To improve performance researchers have recently started implanting microelectrode arrays directly into the nerve (Branner et al. 2001). A similar situation has occurred with researchers that are trying to restore vision by stimulating the surface of the visual cortex. Initial attempts using electrodes on the surface of the brain (e.g. Dobelle et al. 1974) did not work as well as hoped and thus researchers have begun examining cortical stimulation using penetrating microelectrodes (Davis et al. 2012).

Importantly, the transition to the microelectrode scale and the associated change in proximity between electrode and tissue brings changes in the way the electrode will interact with the tissue. Given the close proximity to the tissue, the ability to target a sub-population of neural tissue is increased. The electrode density however is not high enough such that there is a 1-to-1 pairing between electrodes and neurons. Thus a question exists as to whether it is better to activate only a small subset of neurons with a tight relationship between electrode and activated neural tissue, while at the same time not being able to activate a significant portion of the population because of the relatively low density, or whether is it better to activate more tissue, with potentially less fidelity. In other words, even though microelectrodes offer the possibility of having less electrode activation overlap, there is still a significant sampling issue that needs to be addressed by the stimulation paradigm. Most chapters in this thesis will have issues that arise or are of interest because of the use of microelectrodes.

1.4 MULTICHANNEL ELECTRODE ARRAYS

Somatosensory feedback has traditionally used one, or perhaps two feedback channels. In a review of cochlear implants, one of the primary events identified as leading to a significant change in performance was the transition from a single electrode to a multi-electrode array (NIH 1995). Due to the spacing between electrodes and tissue only 4 – 8 independent sites are available for stimulation in the cochlea, even with more electrodes present (Wilson and Dorman 2008). This limitation is unfortunate as it is significantly less than the number of auditory neurons that could be targeted. In a healthy auditory nerve, it is estimated that there are roughly 30,000 myelinated nerve fibers (Spoendlin and Schrott, 1989), although these numbers decrease by a variable amount in cases of deafness.

The limitation to less than ten effective electrodes does not exist for an array of penetrating microelectrodes in tissue, where tissue proximity means more electrodes are likely to improve performance. The microelectrode arrays that are currently available have upwards of 100 channels (Branner et al. 2001). Recent changes in the design have led to a 4x increase in channel density (Wark et al. 2013), which could soon mean placing even more electrodes in the same tissue space. Thus the number of potential electrode channels is increasing. It is unclear however, what changes if any should be made to stimulation paradigms to fully take advantage of these new high-channel count arrays. The arrays used during some of our experiments are shown in Figure 1.5.

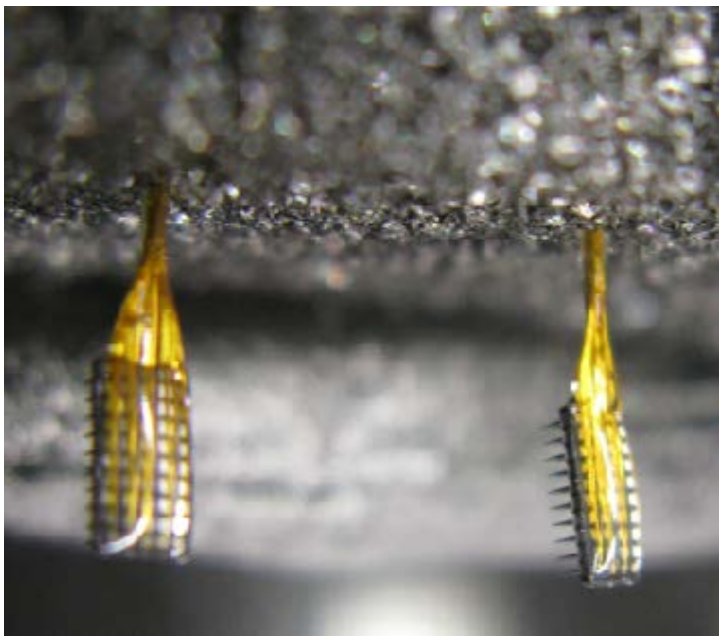

Figure 1.5: Split Utah Array. The electrodes created are generated by taking a traditional 10x10 Utah Electrode Array and cutting it into two pieces. The resulting two arrays are more appropriately sized for placement in dorsal root ganglia. Even these arrays are relatively large, prompting the design of higher density arrays which for the same channel counts can be much smaller (Wark et al. 2013).

This is especially true given the anatomy of the peripheral nervous system. One of the advantages of cochlear implant stimulation is the well-organized tonotopic map of the cochlea. Different parts of the cochlea are more sensitive to different frequencies of mechanical displacement (and thus neural activation), with the base being more sensitive to high frequencies and the apex to low frequencies (for review see Robles and Ruggero, 2001). In addition, this innervation is relatively compact. A somewhat similar setup occurs in the retina, where there is a spatial organization of the incoming visual stimulus in a relatively compact location. Given the close proximity that electrodes can take relative to retinal cells (Zrenner 2002), it is easy to see how dense arrays could lead to improved spatial resolution for prostheses that are trying to restore vision. The input to the somatosensory system, however, is spread throughout the limb.

Electrodes that are placed in the peripheral nerve, especially at more proximal locations, sacrifice a clear organization in order to minimize implant locations. Although gross level organization of fibers by type and projection area are known and acknowledged, especially in more distal locations (Stewart 2003), knowledge of organization that would be relevant for somatosensory feedback is still lacking. Given the unclear fine-scale organization, it is less clear what approaches should be taken when using more stimulation channels to provide somatosensory feedback.

1.5 SOMATOSENSORY ANATOMY AND PHYSIOLOGY

The following is a brief overview of relevant anatomy and physiology as related to this thesis. Although the word "sensory" may be commonly used to describe the type of feedback being provided, somatosensory is more accurate, referring specifically to sensations derived from the limbs and excluding other senses such as vision, audition, or olfaction. Somatosensation involves many different sensory modalities including the sense of limb temperature, pain, itch, touch, proprioception (and/or kinesthesia) and possibly pleasure (McGlone and Reilly 2010).

1.5.1 Peripheral Receptors

The basis for somatosensation starts at the periphery in specialized receptors. The receptors are each sensitive to a specific type of stimulus input, such as pressure, skin stretch, or temperature. For example, the muscle spindles are stretch receptors located within muscles that respond to muscle stretch. Different components of the spindle are sensitive to static and dynamic stretches,

which can be thought of roughly as sensing muscle length and velocity. Given the strong correlation between muscle length and limb position, these receptors are thought to provide proprioceptive feedback (Proske and Gandevia 2012). Other types of receptors include Meisnner corpuscles, Pacianian corpuscles, Ruffini endings, Merkel cells, free nerve endings, muscle spindles, Golgi-tendon organs, and joint receptors (Kandel et al. 2000). Each of these receptors is uniquely positioned and designed to capture a particular element of limb state which ultimately gives rise to limb perception.

1.5.2 Primary Afferents

Neurons are connected to each of these sensory receptors in order to transmit their activity to the brain. Neurons in the peripheral nervous system that are connected to these receptors are known as primary afferents, indicating that they are the first (primary) sensory (afferent) neurons in the pathway of transmitting receptor activity to the brain for sensation. The primary afferent consists of a peripheral axon branch which extends to sensory receptors, and a central branch which projects to targets in the spinal cord. At the junction of these two branches is a third branch, or stem, which connects to the soma. Primary afferents inherit similar characteristics, such as axon diameter and projection location in the spinal cord, based on the type of receptor that they receive input from. The difference in axon diameter between different primary afferent types has important implications for stimulating and recording from these neurons.

1.5.3 Dorsal Root Ganglia

The cell bodies of primary afferents group together in a structure that is known as the dorsal root ganglion (DRG). Due to the size of the cell bodies relative to the axons of the afferents, each DRG exhibits a slight bulge relative to the tissue nearby. The DRG are located close to the spinal cord, at which point sensory and motor fibers have divided into separate components. An illustration of the primary afferent and its relationship to other tissue structures is shown in Figure 1.6. DRGs are shown in Figure 1.7 to further orient the reader as to their layout in the body and structure. The cell bodies are the trophic center of the cell (Devor 1999). When damage occurs to the peripheral nerve, the cell body is still able to support a portion of the cell, even though it is not attached to the receptor. This allows for the potential therapeutic interventions that are considered in this thesis.

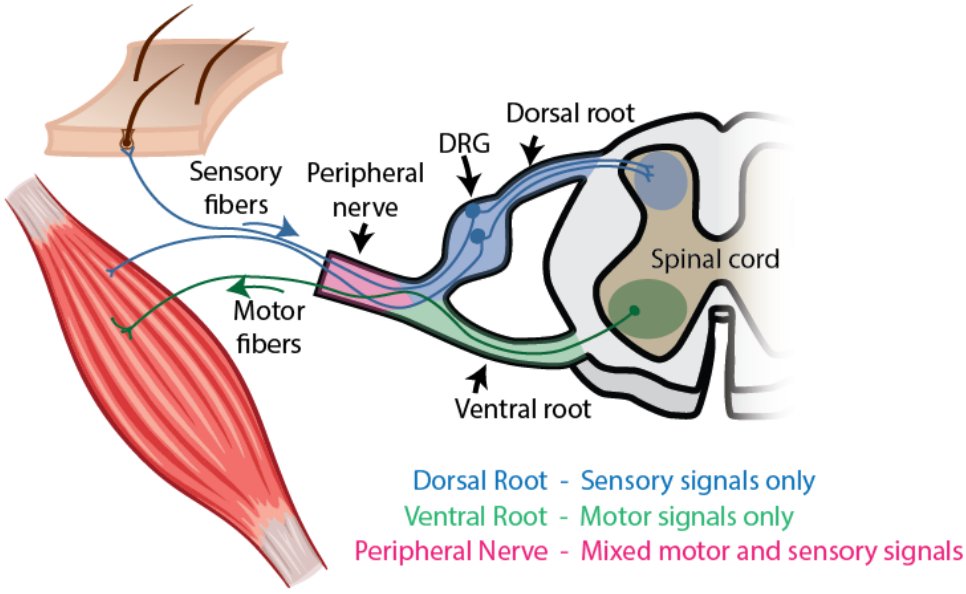

Figure 1.6: Primary afferents. Illustration of primary afferents in the context of sensory receptors, the peripheral nerve, and spinal cord. Two primary afferents are shown, one which receives its input from a hair follicle and another from a muscle spindle. Primary afferents project to the spinal cord and their cell bodies are in a structure known as the dorsal root ganglia (DRG).

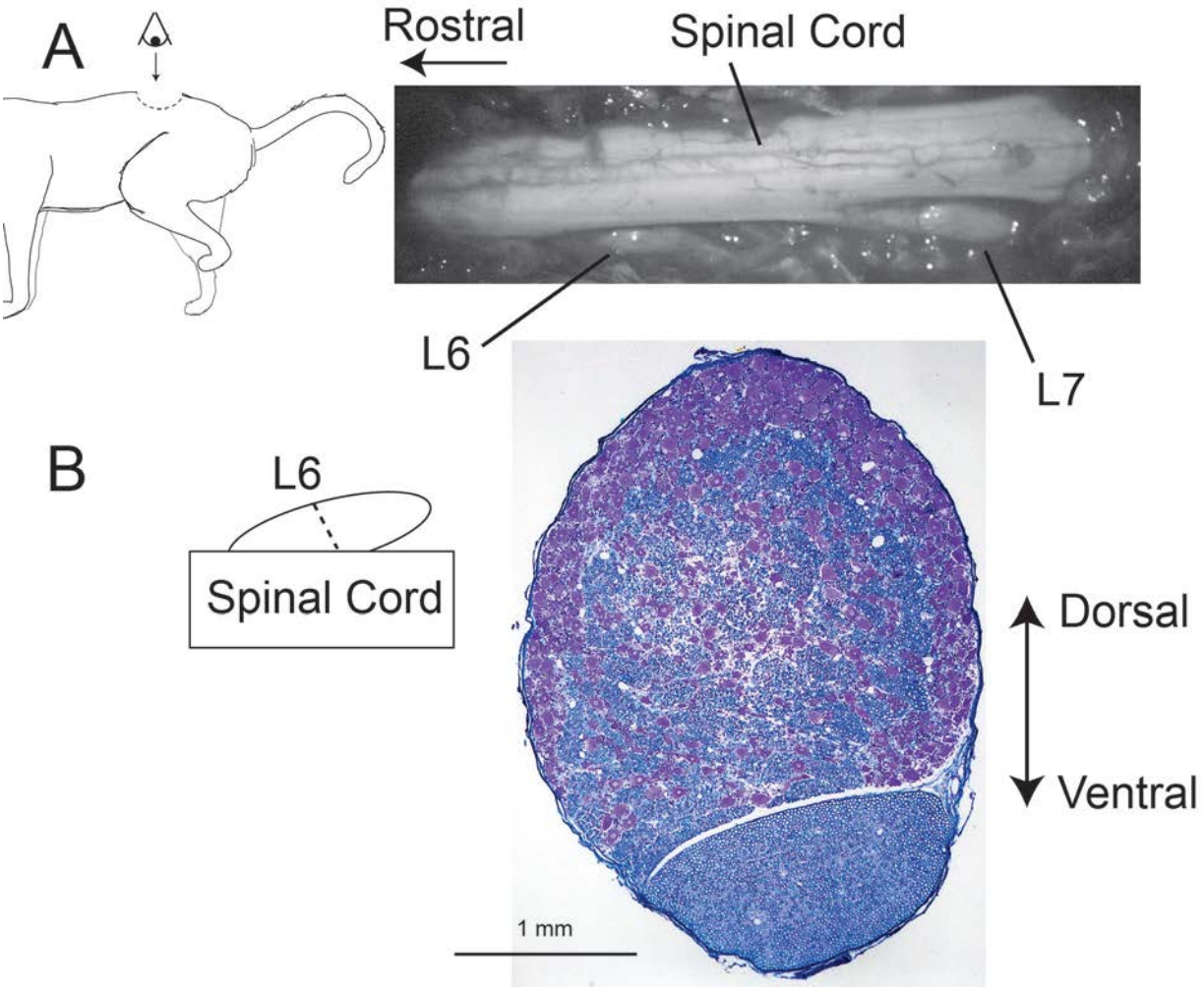

Figure 1.7: In vivo DRG layout and structure. (A) View of the exposed spinal cord and L6 and L7 DRG. The width of the spinal cord is roughly 7 mm. (B) Cross section of the right L6 DRG. Tissue has been stained using Nissl (violet, cell bodies) and Luxol fast blue (myelin). Given the dorsal approach to access the ganglia, electrodes would be inserted from the top of the cross section. The bottom of the tissue slice shows the ventral root.

1.5.4 Higher Order Sensory Processing

The details of the processing between primary afferents and somatosensory cortex are beyond the scope of this thesis, other than to acknowledge that sensory processing does occur at multiple

synapses. Synaptic processing first occurs at the spinal cord, then at higher order brain centers. Although there are certainly projections via interneurons to motor neurons, as well as to other areas of the brain, our primary interest will be in projections to primary somatosensory cortex.

1.5.5 Primary Somatosensory Cortex

Primary somatosensory cortex is located just posterior of motor cortex. In monkeys, the primary somatosensory cortex is typically broken up into four areas, 3a, 3b, 1, and 2 (Kaas 1983). The numeric distinctions of 1, 2, and 3 are Brodmann areas, which were derived from cytoarchitecture studies. Further examination of area 3 led to the split of this area into 3a and 3b (Jones and Porter 1980).

As outlined by Kaas these areas each have their own representation of the body and show different recording characteristics in response to stimuli. In general, areas 3a and 2 tend to respond to deep body tissues, joints and muscles whereas 3b and 1 respond to cutaneous stimuli. Of these areas, 3b is considered to be the primary input, showing the least processing of sensory inputs (Mountcastle 1997).

Often the monkey primary somatosensory cortex serves as the reference starting point when trying to understand sensory cortices of other animals, such as cats. The cat is thought to have similar sensory areas, although 3a can be found on the gyrus (postcruciate), unlike area 3a in monkeys which is located in the central sulcus (Kaas 1983). This makes access to the area 3a with electrodes potentially much easier in cats than in monkeys. See Figure 1.8 for more on cat somatosensory cortex.

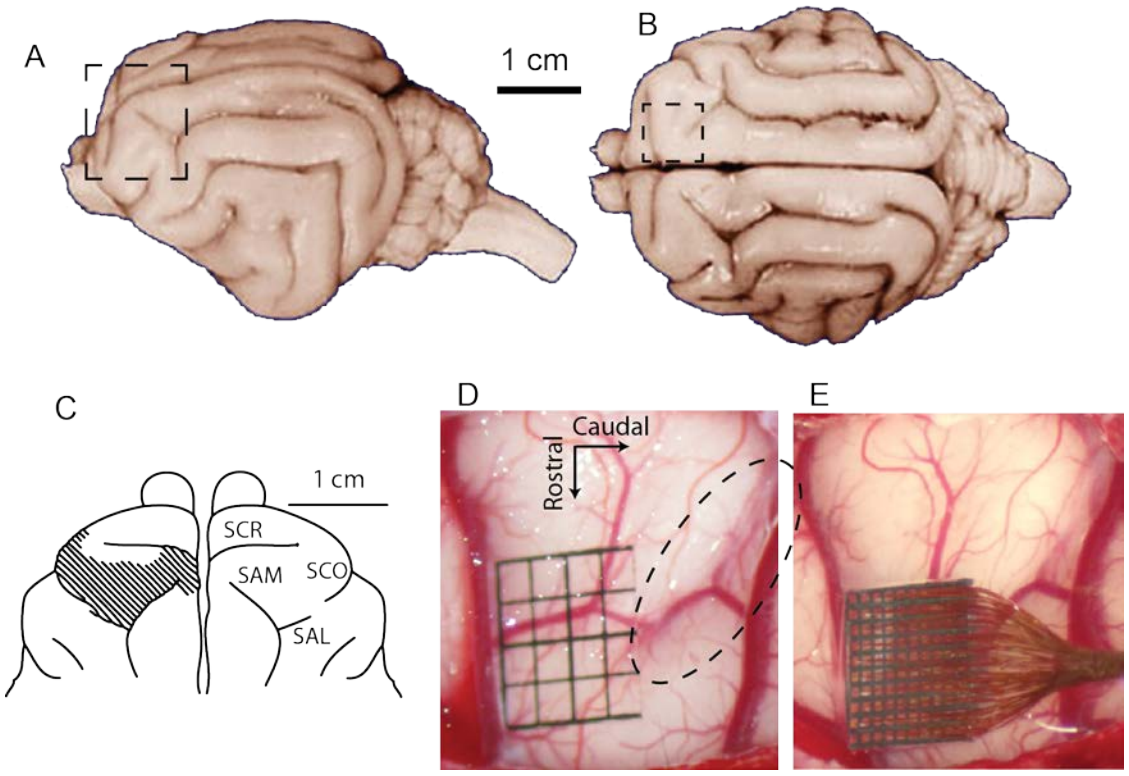

Figure 1.8: Cat somatosensory cortex. (A) View of cat brain with dura removed so sulci are clearly visible. The box encompasses sensorimotor cortex. Given the small size of frontal cortex the brain starts to tilt downward in this area. (B) Rotation of the brain to better show somatosensory cortex. (C) A stylized view of cortex, with diagonal hashing showing somatosensory cortex. Relevant sulci include the cruciate sulcus (SCR), medial ansate (SAM), coronal sulcus (SCO), and lateral ansate (SAL). (D) Surgical exposure of right somatosensory cortex. Each square in the transparency grid is 1x1 mm. Small blood vessels identify the medial ansate (circled), which terminates at the right edge of the transparency. The cruciate sulcus is covered by a large blood vessel (left), which has been seen in all of our surgeries. (E) Implant of 10x10 electrode array measuring 4.2x4.2 mm. Orientation is the same as in (D) The box in (B) roughly corresponds to the view seen in (D) and (E). (Photos in (A) (B) from brainmuseum.org, see Fobbs and Johnson 2011, (C) modified from Myasnikov et al. 1997)

1.6 RESEARCH OBJECTIVES AND CHAPTER SUMMARIES

Given the current lack of prostheses with sensory feedback, and the questionable performance of previous devices, it is likely that high channel count multielectrode arrays may be useful in providing more natural sensory feedback. Given the complexity of such an endeavor, it will likely be useful to create alternative techniques for exploring artificial sensory feedback that go beyond psychophysical interrogation and performance assessment. Both of these methods are likely to be very important, however they may not be well suited for exploring a large stimulus parameter space and many different stimulation paradigms.

To this end, this thesis will explore new mathematical and experimental models for studying somatosensory feedback. To provide artificial somatosensory feedback, I will be examining peripheral nerve stimulation, primarily in dorsal root ganglia of a cat model. In most cases however, the conclusions drawn from this approach can apply to other stimulus locations and models.

Chapter 2 describes an experimental technique in which we record antidromic propagation of action potentials using a nerve-cuff placed around the sciatic nerve. Action potentials are initiated by single channel stimulation in the L7 dorsal root ganglion. Microstimulation of dorsal root ganglia had yet to be described when these experiments were conducted. Unlike motor neuron stimulation, thresholds for stimulation of sensory afferents cannot be determined by electromyography (EMG) or force recordings, which have significantly higher signal-to-noise ratios as compared to nerve-cuff recordings.

The technique described in Chapter 2 is well suited for determining stimulus thresholds, but not for examining recruitment of multiple fibers. In **Chapter 3** a computational model is developed to examine recruitment of primary afferents at higher stimulus amplitudes.

Given a better understanding of the relationship between stimulus amplitude and number and types of neurons recruited, **Chapter 4** examines the use of cortical recordings as a guide for determining the ability to transmit information into the brain by varying stimulus channel location, amplitude, and rate.

Chapter 5 extends the approach used in Chapter 4 to multiple stimulus channels by use of a paradigm known as replay stimulation. As this is the only chapter in the thesis not currently published or submitted for publication there is extra discussion on the difficulties encountered with the approach and its merits in informing design of sensory feedback paradigms.

Chapter 6 returns to computational modeling to try and explore a phenomenon observed in Chapter 5, that simultaneous stimulation seemed to significantly impact transmission of information to cortex.

2.0 MICROSTIMULATION OF PRIMARY AFFERENT NEURONS IN THE L7 DORAL ROOT GANGLIA USING MICROELECTRODE ARRAYS IN ANESTHETIZED CATS

The contents of this chapter are published as: *Gaunt RA, Hokanson JA, Weber DJ (2009) Microstimulation of primary afferent neurons in the L7 dorsal root ganglia using multielectrode arrays in anesthetized cats: thresholds and recruitment properties. J Neural Eng 6:55009*. I was responsible for designing the experimental infrastructure necessary to collect the data, data collection and analysis, and contributed to the overall design of the paper.

2.1 INTRODUCTION

In recent decades the feasibility and utility of neural prostheses and functional electrical stimulation (FES) has been widely demonstrated in both animal models and humans. Brain-computer-interfaces offer the possibility of expressing motor command signals via decoded neural signals (Fetz 1969, Hochberg et al. 2006, Schwartz et al. 2006, Velliste et al. 2008), enabling direct neural control of prosthetic limbs (Velliste et al. 2008) or control over the reanimation of paralyzed muscles in a native limb by FES (Moritz et al. 2008). Despite these successful interfaces with the motor system, there remains a need to develop a somatosensory

neural interface (SSNI) that can provide the nervous system with high-dimensional artificial somatosensory feedback in a manner that could be functionally relevant for prosthetic control.

A SSNI could improve the performance and user-acceptance of a neural prosthesis, because limb-state feedback is vital for achieving stable and adaptive motor control, particularly for grasp and manipulation tasks where visual feedback alone is insufficient. Loss of somatic sensation is a major cause of disability, not only because it diminishes the ability to touch and manipulate objects, but also because it is associated with other problems such as chronic pain and damage to hands and feet. Lacking proprioceptive feedback, patients with large-fiber sensory neuropathies exhibit severe impairments in the coordination of movements at multiple joints (Sainburg et al. 1993) and a degradation in the accuracy of movements performed without visual guidance (Sanes et al. 1984). Creating a neural interface that restores natural and complete tactile, proprioceptive, and thermal sensations will be extremely challenging, if not impossible. However, results from studies in animals (Romo et al. 1998) and humans (Dhillon and Horch 2005) support the feasibility of providing at least some level of meaningful sensation through electrical stimulation of somatosensory neurons located at central or peripheral sites in the nervous system.

Patterned electrical stimulation of sensory neurons can be used to introduce surrogate sensory signals into the nervous system, where information is encoded in the rate, number and type(s) of sensory fibers being activated. Microstimulation studies have shown that discrete and graded tactile sensations can be evoked through stimulation at either peripheral or central locations in the nervous system. For example, microstimulation of single peripheral afferents evokes conscious sensations of flutter-vibration and pressure in humans (Vallbo 1981, Ochoa and Torebjork 1983, Macefield et al. 1990). Similarly, studies in humans undergoing

neurosurgical treatments for tremor revealed that threshold microstimulation in the somatic sensory nucleus of the thalamus evokes sensations of touch, pressure, and body movement (Ohara et al. 2004). Primary somatosensory cortex is yet another central target for introducing somatosensory feedback as demonstrated by work in non-human primates (London et al. 2008). However, targeting first order neurons (i.e. primary afferents) may provide the most complete and natural scenario for transmitting somatosensory information, because activation of sensory neurons at the point of entry into the central nervous system ensures that the feedback is delivered to all of the central targets involved normally in sensory processing. These central targets include the cerebellar and spinal circuits that are involved in coordinating movements among multiple joints and limbs (Thach 1998, Zehr and Duysens 2004).

Primary afferent neurons can be accessed directly by implanting electrodes in the peripheral nerve or dorsal roots, including the dorsal root ganglia (DRG) region containing the cell bodies for these neurons. Implanting microelectrode arrays in the dorsal roots and DRG offers some advantages in that afferent fibers from an entire limb are consolidated into a few adjacent roots containing purely sensory fibers. These fibers become more distributed and mixed with efferent fibers in the peripheral nerve. Also, the roots and DRG are protected by the spinal column and are less mobile than the peripheral nerve, offering better isolation from mechanical forces that may damage or dislodge the implant. Although accessing the spinal roots requires an invasive laminectomy, the mechanical protection afforded by the surrounding vertebral bone may prove beneficial to long-term stability of the neural interface. Long term recordings of afferent fibers in the DRG have been performed (Prochazka et al. 1976, Loeb et al. 1977) and recent work shows that these signals can be decoded to predict hindlimb kinematics in the cat

(Weber et al. 2007). However, the DRG has remained unexplored as a stimulation target for the development of a SSNI.

The primary aim of this paper is to characterize the recruitment of DRG neurons by single channel microstimulation applied through penetrating microelectrodes. This work provides a basic evaluation of the technical feasibility of DRG stimulation in preparation for investigation of the broader goal of using patterned multichannel microstimulation of primary afferent neurons in the DRG to transmit tactile and proprioceptive feedback to users of prosthetic limbs. The specific properties that we examined include: threshold stimulation amplitude, caliber of fibers activated at threshold and higher stimulation amplitudes, stimulation range for recruitment of responses with the same conduction velocity, and the effect of stimulation location within the DRG. Portions of this work have been published as abstracts (Hokanson et al. 2008).

2.2 METHODS

Acute experiments were performed in four anesthetized cats to measure the stimulation thresholds and recruitment properties of primary afferent neurons in the DRG using multichannel microstimulation. All procedures were approved by the University of Pittsburgh Institutional Animal Care and Use Committee.

2.2.1 Microelectrode array and nerve-cuff implant surgery

Adult cats (3–5 kg) were anesthetized with isoflurane throughout the experiment. A venous catheter was inserted into each of the forelimbs to administer fluids and drugs. At the beginning of surgery, atropine sulfate (0.15 mg/kg IV) was administered to reduce airway secretions. Blood pressure, ECG, core body temperature, oxygen saturation, and end tidal CO2 were monitored continuously throughout the experiment. An electric heat pad and ceramic heater were used to maintain body temperature near 37° C. At the conclusion of the experiment, the animal was euthanized with a 5 mg/kg dose of potassium chloride.

A 5-pole nerve cuff electrode array was placed around the sciatic nerve midway along the thigh (distal to the bifurcation of the muscular branch, but proximal to the separation of the common personal and tibial branches) to record activity in the electroneurogram (ENG) during DRG microstimulation. The central and outermost electrodes of the sciatic nerve cuff (SNC) were connected together to act as a common reference electrode against which the active (2nd and 4th) electrodes were recorded differentially (see Figure 2.1C) (Hoffer et al.., 1981). The active electrodes were spaced 8 mm apart. Spike-triggered averaging and stimulus-triggered averaging were used to isolate single-unit and compound action potentials in the ENG.

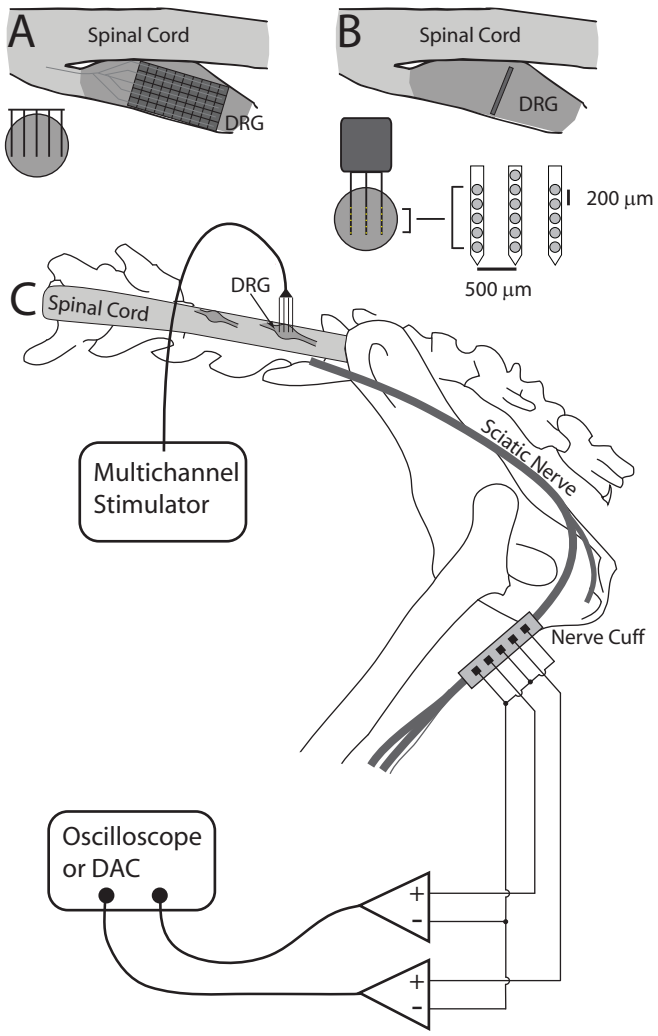

Figure 2.1: Schematic of experimental setup. (A) Illustration of the insertion of individual Cyberkinetics arrays in the DRG from above (dorsal view through transverse plane, upper right) and a cross section through the DRG (lower left). (B) Illustration of the insertion of NeuroNexus probes into the DRG. The array locations shown are estimates, but the arrays were generally inserted near the center of the ganglion. C) Overall experimental setup. A multichannel recording/stimulation system was connected to the multielectrode array inserted into the DRG. A 5-pole nerve cuff was placed around the sciatic nerve and attached to a digital oscilloscope (cats #1–3) or data acquisition system (cat #4)

A laminectomy was performed to expose the spinal cord and left dorsal roots at the 6th and 7th lumbar segments (L6 and L7). All microstimulation was performed in the L7 DRG and

some additional spike-triggered averaging data were collected in the L6 DRG. The cat was affixed in a spinal frame with the torso supported and hindlimbs extended freely. The head was fixed in a stereotaxic frame and a vertebrae clamp and hip pins were used to stabilize the spine and pelvis. Multichannel microelectrode arrays were inserted into the L6 and/or L7 DRGs. Two different array configurations were used in these experiments, but all were activated iridium microelectrodes with similar impedances of approximately 50 kΩ at 1 kHz. 16-channel "acute" arrays from NeuroNexus Technologies were used in cats #1–3 and were inserted into the L7 DRG and held in position with a micromanipulator. These arrays had 3 shanks, with 5 channels on the outer shanks and 6 on the center shank. The inter-shank spacing was 500 μm and inter-electrode spacing on each shank was 200 μm. Each electrode had a surface area of 625 μm2. In cat #4, a pair of Cyberkinetics arrays with 400 μm interelectrode distances, a shank length of 1.5 mm, and a surface area of 2000 μm2 per electrode were inserted into the L6 (4×10 array) and L7 (5×10 array) DRGs using a high-speed pneumatic inserter tool (Cyberkinetics, Foxborough, MA). The NeuroNexus and Cyberkinetics electrode arrays were used to access different planes of the DRG, providing a more thorough sampling of locations throughout the volume of the DRG. Figure 2.1 shows a diagram of the experimental setup including the electrode configurations.

2.2.2 Microstimulation and data acquisition protocols

An RX7 microstimulation system (Tucker-Davis Technologies, Alachua, FL) was used to deliver biphasic current pulses consisting of a leading 200 μs cathodic phase, followed by a 400 μs anodic phase of half amplitude to maintain charge balance. Reference and ground electrodes were placed in the epidural space along the spinal cord. The stimulation intensities reported

herein represent the amplitude of the cathodic phase. Stimulation pulses were delivered at 10–20 Hz to allow a high number of trials to be tested quickly. Several trials were repeated at 2 Hz yielding the same results.

In cats #1–3, stimulus intensities above and below threshold were tested repeatedly in order to resolve the threshold level to approximately 0.1 μA. Following threshold determination for cat #3, a series of stimulus intensities were tested in increasing order (3, 4, 5, 7.5, 10 and 15 μA). In cat #4, fixed stimulus intensities (1–3 μA in 0.2 μA steps, 3.5–6 μA in 0.5 μA steps, and 7–10 μA in1 μA steps) were tested in random order.

Microstimulation within the DRG elicited antidromically propagating action potentials in the sciatic nerve. These ENG signals were amplified with a gain of 10,000–20,000 and bandpass filtered (100–20,000 Hz) using a CWE BMA-400 bioamplifier (CWE Inc., Ardmore, PA). ENG signals from cats #1–3 were sampled and averaged based on the stimulus trigger using a Tektronix 3014-B oscilloscope at a frequency of 1–2.5 MHz. (Tektronix, Beaverton, OR). For cat #4, raw ENG was sampled at a rate of 300 KHz using a digital-to-analog converter (NI-USB 6259, National Instruments, Austin, TX) and stored on a computer. These data were filtered from 1–10 KHz using a 2nd order Butterworth zero-phase filter, aligned each sweep to the stimulus trigger or recorded spike in the DRG, and averaged. Data sampled on the oscilloscope were also filtered using the same parameters. 500 individual sweeps were used to generate stimulus-triggered averages.

2.2.3 ENG analysis techniques

Stimulation-triggered averaging was used to identify neural responses in the SNC evoked by microstimulation applied through a single electrode in the DRG. The microstimulation threshold

for activating neurons in the DRG was determined by finding the lowest stimulation intensity (i.e. threshold amplitude) where an identifiable response was observed in the nerve-cuff after stimulation-triggered averaging. Action potentials propagating through the cuff appear with similar shape but different latencies. Two different cross-correlation analyses were used to identify both the occurrence of activity in the SNC and the signal propagation delay between the proximal and distal electrodes in the SNC. The propagation delay was used to measure the CV of the evoked response(s) and estimate the caliber of the recruited fiber(s). These methods are described in detail in the following paragraphs.

2.2.3.1 Automated detection of evoked responses

An algorithm for robustly identifying the presence of one or more evoked responses in the averaged ENG was developed based on the application of a sliding-window, 'local' cross-correlation (LCC) analysis. LCCs were performed by selecting a 0.5 ms window (about the width of a typical waveform) from the distal of the two ENG channels and cross-correlating it with data from the proximal channel over a range of possible delays corresponding to CVs from 10–150 m/s. The maximum value for this LCC was extracted as shown in Figure 2.2A. The window was then moved over the entire data set for the distal channel in steps of 50 μs, generating a time-series of maximum LCC values spanning the entire sweep (bottom half of Figure 2.2B). The caption for Figure 2.2 contains additional information about this approach.

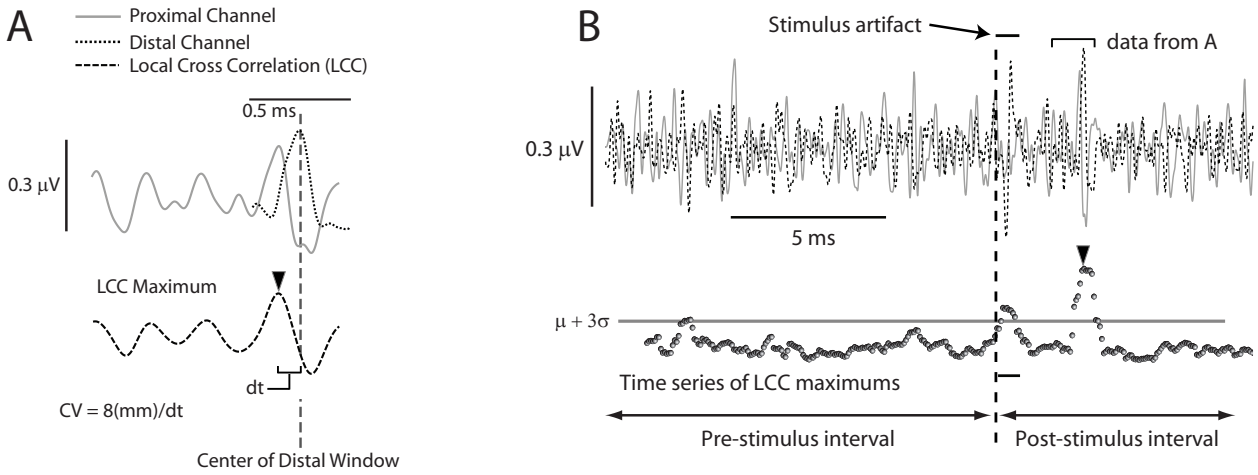

Figure 2.2: Illustration of the method used to determine the first significant response in the averaged ENG recordings. (A) Example of a LCC. Data not within the appropriate local windows (see text) have been zeroed. The maximum value of the cross-correlation (arrow) is used later for determining significant responses. (B) The process was repeated for the entire sweep with the distal window shifting in 50 μs increments. Shown in the lower portion of this panel are the maximum values from the LCCs. LCC values in the pre-stimulus interval were used to calculate the mean and standard deviation of the signal.

Significant responses in the ENG were determined by comparing the values in the pre- and post-stimulus LCC time series. The threshold for detecting a significant response was defined as the mean+3 standard deviations of the LCC values measured in the pre-stimulus interval (see Figure 2.2B). Points in the post-stimulus time interval where the LCC time series rose above the threshold were considered for further analysis (see the bottom half of Figure 2.2B for an example). To reduce false-positive detections, two additional criteria were applied before a response was considered significant. The criteria were: 1) the LCC time series must exceed and remain above the threshold for at least two consecutive time points, and 2) the same time points must also exceed the threshold at the next highest stimulus amplitude. As a check of the accuracy of this algorithm, false positive detections occurred during the baseline period in just two of over 900 trials; however the noise in these two trials was abnormally high.

2.2.3.2 Determining conduction velocity for evoked responses

The CV for each evoked response identified in the previous analysis was determined by measuring the propagation delay (Δt) between the proximal and distal electrodes in the SNC. The propagation delay was measured by cross-correlation analysis, applied to the negative-slope regions of the averaged ENG signals on each electrode. The time lag corresponding to the peak of the cross-correlation function was taken to be the propagation delay (Δt). The CV was calculated using the following equation, $CV = d/\Delta t$, where d was the distance between the two electrodes in the SNC (d = 8 mm).

For small fibers, determining the intracuff propagation delay using cross-correlation became unreliable due the low amplitude of these slow responses and the noise in the system. We therefore categorized all responses with CVs less than 30 m/s as 'slow responses' and did not report their actual CVs. Slow responses were identified when significant activity, as measured by the LCC, occurred after a DRG-to-SNC delay appropriate for a CV of 30 m/s. Accurate determination of this cutoff latency required accurate knowledge of the DRG-to-SNC distance. This distance was found using a linear regression analysis. The known intracuff CV measurements (e.g. those obtained from large-diameter fibers) and associated DRG-to-SNC propagation delays (t) for each animal were fit to the regression model, $CV = D/t + bias + N(0,\sigma)$, where D was the DRG-to-SNC distance and $N(0, \sigma)$ was a zero mean Gaussian random variable with variance to represent noise. The bias term helped account for time delays and measurement error. Using the estimates for DRG-to-SNC distance obtained from this regression analysis, the time at which a response with a CV of 30 m/s would occur was calculated. Significant responses occurring after this calculated time are reported as 'slow' responses.

2.2.3.3 Spike-triggered averaging of ENG signals

Occasionally, spike-triggered averaging was used to isolate afferent responses propagating through the SNC during manual manipulation of the hindlimb. Isolated spikes recorded in the DRG were used to trigger and align ENG recordings and a modification of the previously described method was used to determine the presence of significant activity and the associated CV. For each trial, 75% of the available sweeps were selected at random and maximum LCC time series were constructed as described above. In addition, the propagation delays from the LCC analyses were also recorded. This random selection and analysis process was repeated 100 times. The set of 100 maximum LCC time series were averaged and the standard deviation of the delays at each time point were computed and normalized by the maximum. If a point in the averaged maximum LCC time series was greater than its mean+3 standard deviations and the normalized standard deviation of the delay at this time was less than 0.1, the point was considered a potential response. Eight such contiguous points were required in order for these points to be considered significant. Qualitatively this algorithm selected significant responses based on high values of the LCC and consistent estimates of the intracuff delay. This algorithm reliably detected only one response per channel, which was always at a physiologically reasonable time.

2.3 RESULTS

The primary aim of this study was to characterize the recruitment of primary afferent fibers in response to electrical microstimulation applied through penetrating microelectrode arrays in the DRG of anesthetized cats. Stimulation was applied, one electrode at a time, at multiple sites in the L7 DRG via a 16-channel (cats #1–3) or 50-channel (cat #4) microelectrode array. In cats #1 and #3, all 16 electrodes were tested while in cat #2, 5 electrodes were tested and in cat #4, 32 electrodes were tested. Evoked responses were measured in the sciatic nerve with a nerve cuff electrode.

2.3.1 Stimulus threshold

Across all cats, the average microstimulation threshold for detecting ENG activity in the nerve cuff was 2.7 ± 1.3 μA. The lowest stimulus amplitude that elicited a response was 1.1 μA and in 76% of the cases, the threshold stimulus amplitude was less than or equal to 3 μA. There was no significant difference ($p = 0.16$) in recruitment thresholds between the animals with the mean threshold stimulus amplitude in each animal being 2.2 ± 0.5 μA, 3.4 ± 2.3 μA, 2.6 ± 1.6 μA, and 2.9 ± 1.1 μA. Of all the electrodes, stimulation through only five electrodes failed to elicit activity in the nerve cuff up to the maximum tested stimulation amplitude. In every case where the stimulus threshold was determined, the CV of the response was also measured. In most cases, a single response was detected at the stimulus threshold. However, on 18 electrodes, responses at multiple CVs were detected at threshold. Among all responses detected at threshold, it was found that the CVs were distributed from 38 m/s to 118 m/s with the average CV at threshold across all animals being 72 ± 17 m/s.

Figure 2.3 summarizes these results in terms of the threshold stimulation amplitude and the CVs measured at threshold for each electrode. Figure 2.3A shows a scatter plot of CVs and stimulus amplitudes for all threshold responses. The scatter plot demonstrates the independence of stimulus amplitude and fiber size at threshold, as there was no significant relationship between the stimulus threshold and the CV of the fiber recruited at threshold in any animal or in the grouped data. For example, in cat #3 ('x' symbols in Figure 2.3A), one electrode had a threshold of 1.1 μA with an associated CV of 118 m/s while another electrode had a threshold of 1.3 μA and CV of 57 m/s. In cat #4 ('◇' symbols in Figure 2.3A), one electrode had a threshold of 1.2 μA and a CV of 44 m/s while another electrode had a threshold of 1.6 μA and a CV of 104 m/s.

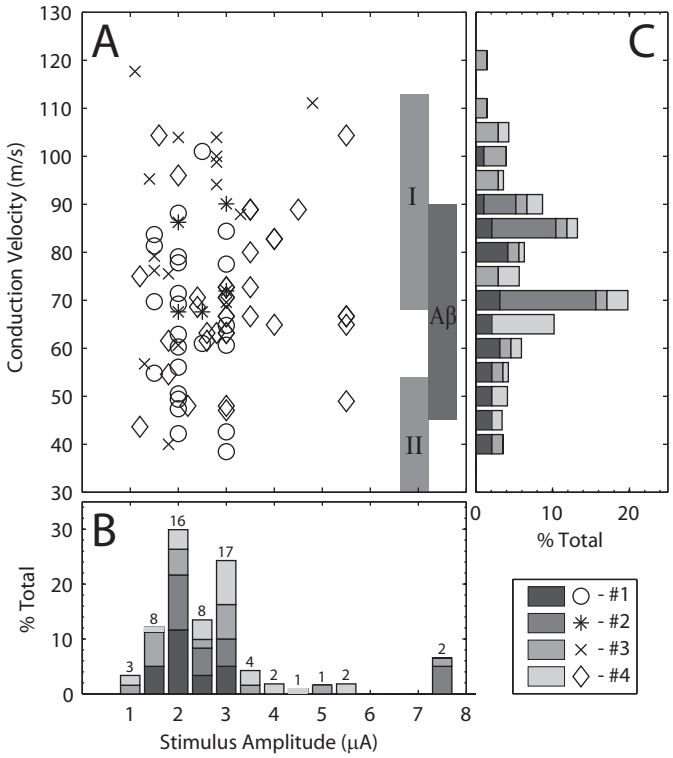

Figure 2.3: Threshold stimulus amplitudes and the CV of the nerve cuff response at threshold. (A) Scatter plot of CV for evoked responses versus the corresponding stimulus amplitude. The abscissas for panels A and B are the same. The vertical gray bars in A indicate the range of CVs corresponding to group I, group II and Aβ fibers (Lloyd and Chang 1948, Boyd and Kalu 1979). (B) The stacked histogram shows the channel count of the stimulus amplitudes at threshold, normalized by the total count for each animal. Normalization was performed to account for the unequal numbers of electrodes tested in different animals. The total number of electrodes tested in each animal account for 25% of the total values in the histogram. The numbers above each bar indicate the number of stimulation channels in each bin. Each bar spans a 0.5 μA range centered on the value indicated below each bar. (C) Distribution of CVs for responses evoked at threshold normalized by the total count for each animal. In some cases, responses at multiple CVs were evoked at threshold, indicating recruitment of multiple fiber types. Each bar spans a 5 m/s range centered on the value indicated to the left of each bar. The ordinates for panel C are the same as for panel A.

The stacked histogram in Figure 2.3B shows the normalized distribution of stimulus thresholds for each animal. In this figure, the stimulation amplitude represents the lowest amplitude that generated a response in the nerve cuff. Separate peaks in the histogram were

observed at approximately 2 μA and 3 μA. The presence of multiple peaks in this distribution may be a result of undersampling the stimulus amplitude range, especially in the first 3 animals where the stimulus amplitude was not incremented systematically. However, given that in these animals threshold responses were recorded at lower stimulus amplitudes on some electrodes, this is unlikely. As noted previously, the majority of the threshold responses occurred at or below 3 μA and only 2 channels had thresholds higher than 6 μA.

The stacked histogram in Figure 2.3C shows the normalized distribution of CVs measured at the threshold stimulus amplitude for each electrode. Two distinct peaks in the measured CVs at threshold were observed at approximately 85 m/s and 70 m/s. These correspond to the median CV of axons in the group I range (~85 m/s) and Aβ range (~72 m/s). Fibers recruited at threshold with CVs greater than the minimum CV for group I fibers (70 m/s) accounted for 50% of the responses. If this range is expanded to include fibers with CVs greater than 60 m/s, which includes the peak of the Aβ fibers, then 81% of the threshold responses were accounted for.

2.3.2 Multiple responses

After the threshold microstimulation amplitude was determined, the amplitude was increased incrementally to investigate the recruitment of additional afferent fibers within the DRG. It was frequently observed that stimulation at higher amplitudes recruited fibers with distinctly different CVs and latencies than the fiber or fibers recruited at threshold. In these cases, stimulus amplitudes and CVs were determined for this secondary response. The secondary response, in general does not represent the recruitment of the second afferent, but rather the recruitment of

one or more afferents having a distinctly different CV. An example of such a secondary response is shown in Figure 4 where the threshold response (CV = 63 m/s, Aβ range) occurred at an amplitude of 3 μA and a secondary response (CV = 83 m/s, group I range) occurred at an amplitude of 5.5 μA. Of the 64 electrodes where responses were recorded in the nerve cuff, 34 exhibited a pattern where the secondary response occurred at an earlier latency than the threshold response. In a further 18 electrodes the secondary response occurred at a longer latency than the threshold response and in the remaining 12 electrodes, no clear secondary response was observed up to the maximum tested stimulation amplitude.

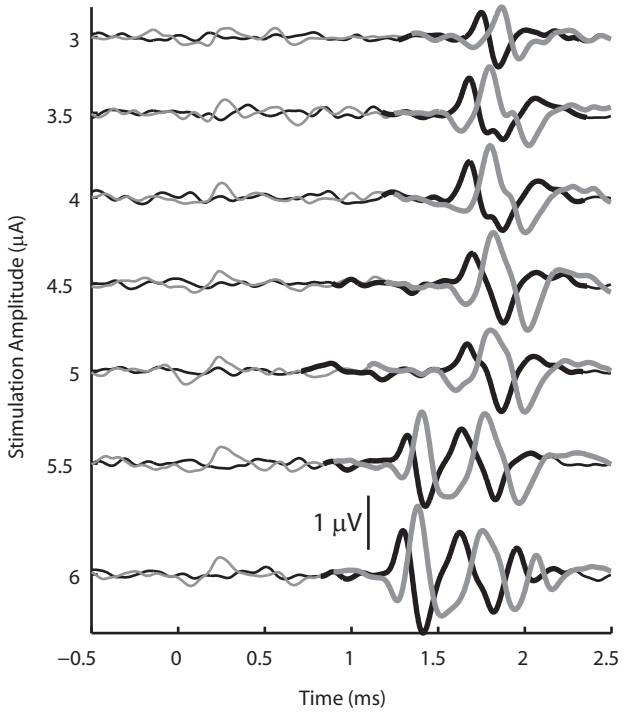

Figure 2.4: Example of slow fiber recruitment prior to the recruitment of faster fibers at a higher stimulation amplitude. The CV measured at threshold was 63 m/s, and the CV of the secondary response, which first appeared at a stimulus amplitude of 5.5 μA, was 83 m/s. The signal from the proximal nerve cuff electrode is shown in black and the signal from the distal electrode is shown in gray. Thick lines indicate portions of the signal where the response was found to be significant.

From the perspective of implementing a somatosensory neuroprosthesis based on DRG stimulation, it is desirable to achieve selective stimulation of one or only a few afferents. Thus, the range of microstimulation amplitudes from threshold to the appearance of a secondary response is of interest and provides a measure of the range in which recruitment of similar caliber fibers occurs. Figure 2.5A shows a histogram of the difference in the stimulation amplitude between the threshold and secondary responses. There was an approximately uniform distribution of stimulation amplitude differences from 0–3.5 μA. Only 8% of the electrodes had differences larger than 3.5 μA, however, 48% of the electrodes tested had amplitude differences greater than 2 μA. In addition, Figure 2.5A includes only those electrodes where a secondary response was recorded. In an additional 12 electrodes (19% of the total number of electrodes), no secondary response was observed up to the maximum stimulation amplitude tested.

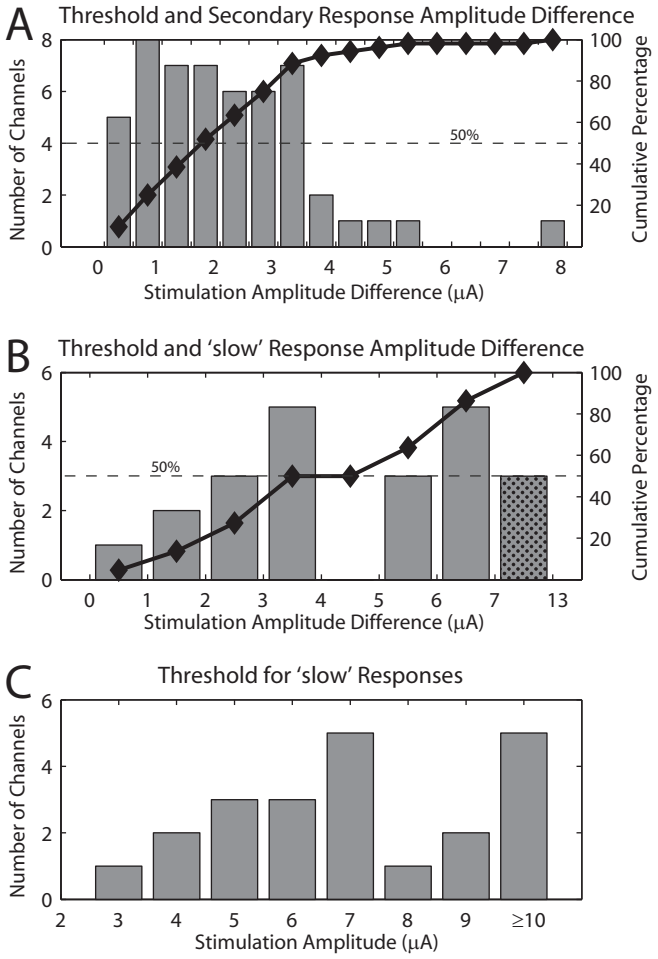

Figure 2.5: Difference in stimulation amplitudes between different classes of responses. (A) Histogram of the difference in stimulus intensity at threshold and the stimulus intensity required to recruit a secondary response identified by activity at a different CV. The cumulative percentage of the distribution is plotted by the black line and markers. 100% is calculated based on the 52 electrodes that exhibited a secondary response at higher stimulus amplitudes. (B) Histogram of the difference in stimulus intensity at threshold and the stimulus intensity required to recruit a response with a CV less than 30 m/s. The smallest difference was 0.5 μA (n = 1). Significant responses with CVs less than 30 m/s were found on 22 of the 51 electrodes considered. The black line and markers show the cumulative percentage of the histogram. (C) Histogram of the stimulus amplitude required to elicit significant responses at latencies appropriate for a CV of less than 30 m/s. 25 channels in which a response was detected showed no response from 'slow' fibers even at the maximum possible threshold stimulus amplitude (15 channels at 9 μA and 10 channels at 10 μA).

Responses with CVs below the group II and Aβ range were never observed at threshold. However, stimulation on 22 of the 69 electrodes evoked responses with CVs less than 30 m/s at stimulus amplitudes higher than the threshold amplitude. Figure 2.5B shows a histogram of the difference in stimulus amplitude between the threshold and that required to recruit a response with a CV < 30 m/s. Figure 2.5C show the distribution of the actual stimulus amplitudes required to recruit these slow fiber responses. These figures indicate that in over half the cases, a 3 μA or greater increase in simulation intensity above threshold is required to activate afferents in the group III/Aδ range.

2.3.3 Early small fiber recruitment

As mentioned earlier, it was frequently observed that the CV of the response at threshold was slower than the CVs of responses that appeared at higher stimulation levels. In fact, in 53% of the electrodes that evoked responses in the nerve cuff, smaller diameter fibers were recruited at a lower threshold than larger diameter fibers. Figure 2.4 shows an example of a channel where a slower conducting fiber was recruited before a faster conducting fiber. In this example a single response with a CV of 64 m/s was present for stimulation amplitudes from 3–5 μA. As the stimulation amplitude increased, the magnitude of the response grew, but not until 6 μA was a new response detected at a different latency. This second response had a faster CV of 83 m/s. Overall, the CVs for the initial slow responses were 69 ± 13 m/s and the CVs for the later, fast responses were 93 ± 13 m/s. The average threshold for the initial slow response was 2.9 ± 1.5 μA while the difference in the simulation amplitude between the threshold and secondary response was 1.8 ± 1.5 μA. This pattern of responses in which axon size has very little impact on recruitment order is consistent with previous reports of intrafascicular microelectrode stimulation

where the small electrode-to-axon distances dominate recruitment order (Veltink et al. 1988, Veltink et al. 1989b).

2.3.4 Spike-triggered averaging results

Spike-triggered averaging was used to isolate the occurrence of action potentials in the nerve cuff associated with single-unit activation in the DRG. Nerve cuff responses to spike-triggered averaging were obtained for 10 neurons in 2 cats. The average peak-to-peak amplitude of the responses in these cases was 0.68 ± 0.16 μV. As a comparison, the average peak-to-peak amplitude of responses evoked by DRG stimulation at threshold was 0.69 ± 0.28 μV at threshold in the same two animals. This value was not significantly different than the spike-triggered average responses ($p = 0.72$, Wilcoxon rank sum test). Figure 2.6 summarizes the peak-to-peak amplitudes of the nerve cuff responses recorded under these two conditions. The amplitude of the response measured during spike-triggered averaging represents the magnitude of a single fiber response and is consistent with the magnitude of the response evoked by microstimulation at threshold.

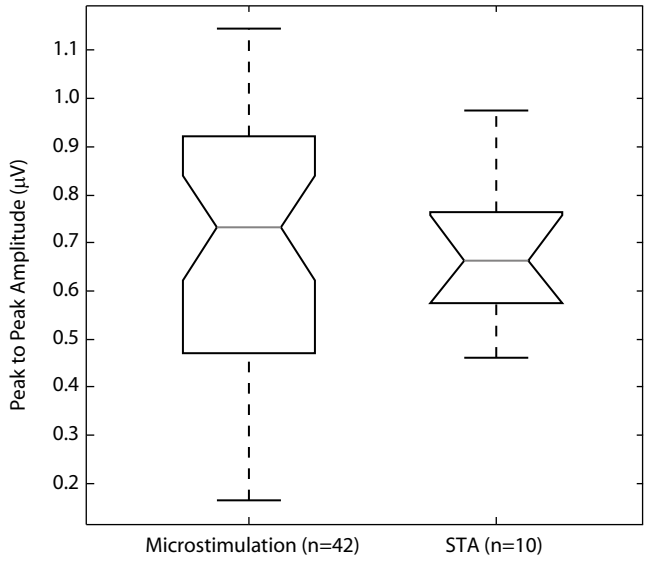

Figure 2.6: Peak-to-peak response amplitudes for microstimulation trials at threshold and spike-triggered average trials in the two cats (#3 and #4) in which spike-triggered averaging trials were performed. In both cases, the mean of the proximal and distal channel were used to calculate the peak-to-peak amplitude. In cases where multiple responses were observed at the microstimulation threshold, the largest amplitude was used (n = 8 of 42 cases). The average peak-to-peak responses in the microstimulation trials and spike-triggered average trials were 0.69 ± 0.28 μV and 0.68 ± 0.16 μV respectively. No significant difference between these two groups was found (p = 0.72, Wilcoxon rank sum test). The number of trials contributing to the box plot are indicated in the abscissa labels.

2.3.5 Location effects

The use of multielectrode arrays allowed the examination of stimulus location within the DRG as a potential source of variation in the recruitment of afferent fibers. Figure 2.7 shows the relationship between the location of the stimulating electrode and the threshold amplitude for activating fibers in two different CV ranges. The electrodes shown in Figure 2.7A–C were three shank NeuroNexus probes with 16 stimulation sites distributed in the transverse plane. The electrodes used in Figure 2.7D and E were on a Cyberkinetics array (5×10 configuration) in which all the electrodes were at a uniform depth (~1 mm) within the DRG. Two different planes

in the DRG were sampled by the two array configurations and no evidence was found for the presence of a relationship between stimulation threshold and the physical location of the electrodes. However, it was noted in several cases that electrodes that were likely located near the edge of the DRG had higher thresholds than other electrodes. For example, in Figure 2.7B the electrodes with the highest threshold were located at the bottom right edge of the array (medial side of the DRG) and may have been at the border or even slightly outside the DRG. Similarly in Figure 2.7D, several electrodes along the lateral edge of the array had high thresholds or elicited no response up to the maximum amplitude tested. Again, it is possible that these electrodes were located at the border, or perhaps even outside the DRG.

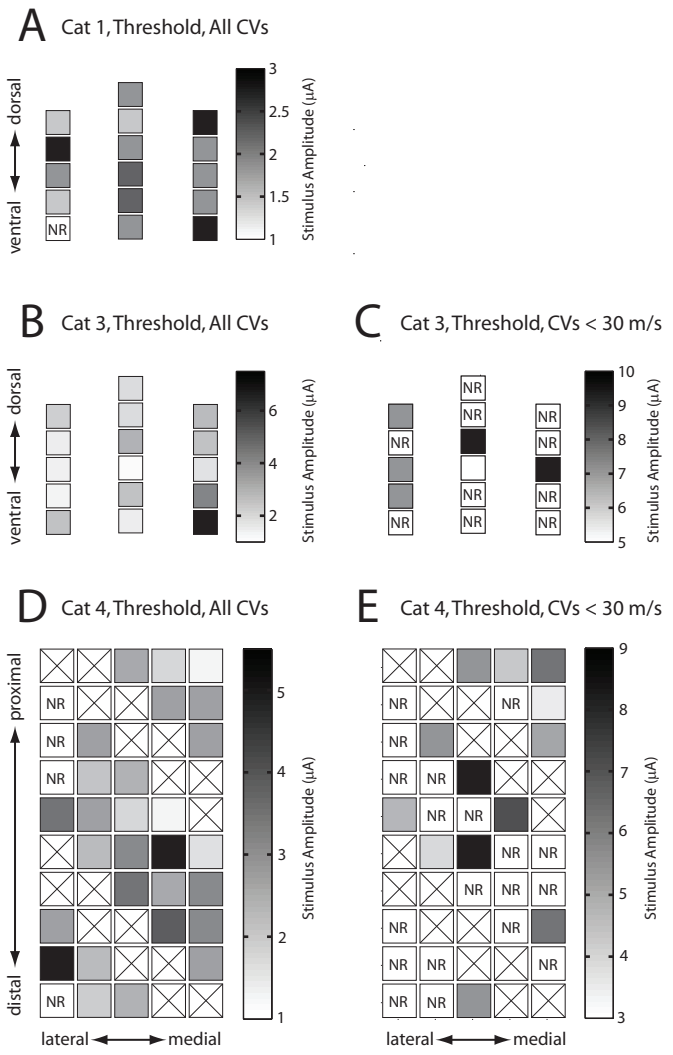

Figure 2.7: Stimulus amplitude plotted by electrode location within the DRG for the threshold response in cats #1, #3, and #4 (parts A, B, and D respectively) and for the first response with a CV of less than 30 m/s in cats #3 and #4 (parts C and E respectively). Data from cat #2 was not included because only five electrodes were tested. The orientations of the electrodes within the DRG are indicated in each panel. Note that the scale bars are different for each panel. The highest thresholds shown in panel B were observed in the lower right region of the array (4.8 μA and 7.5 μA). It is possible that these electrodes were at or near the edge of the DRG perhaps accounting for their high thresholds. In addition, four electrodes on the lateral edge of the array shown in panel D did not evoke a response up to the maximum tested stimulus amplitude of 10 μA. An additional electrode on this edge had a threshold greater than 5 μA. Boxes marked with an 'X' indicate electrodes that were not tested. Boxes marked by 'NR' indicate electrodes that did not elicit a response up to the maximum tested stimulus amplitude.

2.4 DISCUSSION

The primary result from this study is that microelectrode arrays implanted in the DRG can be used to selectively stimulate small groups of afferent fibers throughout the DRG, typically at stimulation currents less than 3 μA. Prior studies investigating microstimulation thresholds in the nervous system have reported stimulus thresholds at similarly low stimulus amplitudes in the range of 0.1–5 μA (Jankowska and Roberts 1972). More specifically, a study of intraneural microstimulation of afferent axons to examine electrically evoked sensations reported stimulus thresholds in the similarly low range of 1–2μA (Ochoa and Torebjork 1983). In this study, the charge per phase injected at threshold was 0.6 nC/phase and increased up to 3 nC/phase at the maximum stimulation amplitude. This corresponds to a maximum charge density of 480 μC/cm2 and 150 μC/cm2 for the NeuroNexus and Cyberkinetics electrodes respectively. These stimulation parameters were below the safe charge per phase limits of approximately 150 nC/phase (McCreery et al. 1992) and below the charge density limits for activated iridium electrodes of approximately 1–3 mC/cm2 (Beebe and Rose 1988, Cogan et al. 2005).

In addition to recruiting somatosensory afferents at low thresholds, on over half of the electrodes tested, the CVs of fibers recruited at threshold were slower than the CVs of fibers recruited at subsequently higher stimulus amplitudes. Generally, recruitment of neurons by electrical stimulation is biased toward the activation of large diameter fibers at lower stimulus amplitudes than smaller diameter fibers (Durand et al. 2004). However, this large-to-small recruitment order is primarily a concern for extraneural stimulation using cuff electrodes. Mathematical modeling (Veltink et al. 1988) and experimental work (Veltink et al. 1989a, Yoshida and Horch 1993) demonstrate that for intraneural microelectrodes, the recruitment order is essentially neutral with no preference for either large or small diameter axons. In this study,

53% of the electrodes recruited ‘slow’ fibers prior to recruiting ‘faster’ fibers, which agrees with these previous conclusions. From the perspective of a somatosensory neural prosthesis, this pattern of recruitment is significant because it demonstrates that the location of the stimulus electrode relative to surrounding fibers within the DRG is a critical factor, and that microstimulation within the DRG is capable of selectively activating the afferent fibers for a wide range of sensory modalities.

Two results argue for the point that in many cases the responses observed at or near threshold were the result of activation of a single or just a few fibers of similar caliber. Among the 64 electrodes on which nerve cuff responses were observed, the threshold response of 46 of these electrodes contained a response at just a single CV. These CVs spanned a range that includes group I and group II muscle afferents and Aβ cutaneous fibers. If multiple axons were recruited at threshold, it is likely that the nerve cuff activity would contain responses at multiple CVs. As discussed however, this was not the observed result. Additional evidence suggesting that just a few or even a single fiber was recruited at threshold comes from the magnitude of the nerve cuff response at threshold. It was found that there was no statistical difference between the peak-to-peak amplitude of the response at threshold and the peak-to-peak amplitude of the response measured during spike-triggered averaging, which contains only the measured response to activity in a single axon. While this does not guarantee that the responses to microstimulation were also from a single fiber, our results are consistent with this possibility.

2.4.1 Considerations for the development of a SSNI

There are several issues that are relevant to the development of a microstimulation based SSNI. Stimulation should selectively activate one or more fibers having similar receptive fields and

modalities, and increasing the intensity of stimulation should recruit additional fibers with similar properties. Also, the device should be capable of activating a wide range of sensory modalities. Previous discussion addressed the ability of microstimulation to recruit one or a small number of fibers. Our results for electrical microstimulation thresholds and recruitment within the DRG are the same as those reported for intraneural stimulation of peripheral nerve. Although microstimulation in the DRG activates a different portion of the axon than stimulation in peripheral nerve does, the sensory percepts evoked by both methods of stimulation should be similar. Intraneural stimulation has been shown to elicit very localized and finely graded responses (Dhillon and Horch 2005), including responses of different modalities through a single electrode (Ochoa and Torebjork 1983). It is likely that stimulation within the DRG would be similarly effective in eliciting punctate and meaningful sensations.

Stimulus amplitude modulation was used in the present study to examine changes in the peak-to-peak amplitude of the compound action potential measured in the sciatic nerve. In many cases, increases in the peak-to-peak amplitude were observed without changes in the latency or CV of the response. This suggests the recruitment of additional fibers of similar caliber and may point in some cases to localized structure in terms of axon modality within the DRG. Although the issue of somatotopy or other structural organization within the DRG is not fully understood, evidence of weak somatotopic organization exists (Burton and McFarlane 1973, Wessels et al. 1990, Prats-Galino et al. 1999, Aoyagi et al. 2003). Furthermore, experiments in cats have shown that nerve fibers in the dorsal roots are organized in “microbundles” in which small groups of fibers from contiguous skin areas tend to run together (Wall, 1960). Such results make it plausible to achieve graded recruitment of multiple afferents having similar modality and receptive field. Such fibers would have similar diameters, leading to the observed result.

In these experiments, it was not determined whether the receptive fields of the afferents recruited at increasing stimulus amplitudes were co-localized. Since the somatotopy of the DRG may be weak, increases in stimulus amplitude or small changes in electrode location could change the perceived stimulus location. This particular issue would be mitigated with stimulation applied in distal portions of the peripheral nerve where the fascicular organization may be stronger. The practical trade-off however is that peripheral nerve approaches would require multiple, widely distributed implant sites to cover the muscle groups and dermatomes accessible through a single DRG. In addition, the higher mobility of peripheral nerve presents a more challenging environment in which to achieve a stable, long-term interface with high-density electrode arrays.

A further necessity for a somatosensory neuroprosthetic implant is that the device should be able to activate fibers for different sensory modalities, including muscle and cutaneous afferents that subserve proprioception and tactile sensations. This seems to be possible with the present approach. Direct evidence for this comes from examination of the CVs of the responses measured at threshold. Afferents with CVs ranging from 38–118 m/s were recruited at threshold and Figure 2.3C shows the distribution of CVs observed at threshold. The distribution of CVs was bimodal in nature with peaks at 70 m/s and 85 m/s. This range of CVs is consistent with measurements made using spike-triggered averaging based on recordings from microelectrode arrays in the L7 ganglia (Aoyagi et al. 2003). Different CVs are closely associated with activity in specific sensory modalities. Group I, group II and Aβ axon diameter ranges along with scaling factors to convert diameter to CV (5.7 for group I and Aβ axons and 4.6 for group II axons) were used to estimate CV ranges appropriate for responses in each fiber class (Lloyd and Chang 1948, Boyd and Kalu 1979). Axons in these CV ranges include afferents from muscle spindles, Golgi

tendon organs, and a variety of cutaneous and joint receptors (Boyd and Davey 1968). Thus, we conclude that low intensity microstimulation through penetrating microelectrodes in the DRG is capable of activating a range of sensory modalities sufficient to elicit sensations of proprioception and touch.

A final consideration for this work, as well as all work involving the development of permanent interfaces with neural tissue is that of electrode design and stability. Chronic implants of the Cyberkinetics array in the cortex of non-human primates have shown stable recordings for 1.5 years (Suner et al. 2005), but in the DRG, stable recordings have persisted for at most several weeks (Weber et al. 2007). Arrays of individual microwires implanted in the lumbar spinal cord can maintain stable stimulation thresholds for months (Mushahwar et al. 2000). However, the development of electrode arrays suitable for implantation on the order of years is a necessary requirement before these technologies could be implemented in clinical practice.

2.4.2 Limitations

A potential limitation of the experimental setup concerns the presence of L7 DRG axons in the sciatic nerve, particularly in the region covered by the SNC. Proximal to the location of the nerve cuff, the sciatic nerve bifurcates and innervates the hamstrings through the muscular branch. If many of the axons in the L7 DRG do not pass through the SNC, stimulus threshold estimates could be overestimated. However, several lines of evidence suggest that this potential source of error is not likely to have significantly affected our results. First, it is known that the cutaneous afferents contained in the L7 DRG have receptive fields exclusively in the distal leg (Brown and Koerber 1978). Second, in studies involving multielectrode recordings in the L7 DRG where unit identification was performed, very few afferents are reported as having receptive fields in

regions that would not have been sampled by our nerve cuff (Aoyagi et al. 2003, Weber et al. 2006).

Examination of the data itself also suggests that this potential source of error did not substantially affect our results. Of the 69 electrodes tested, nerve cuff responses went undetected on only 5 channels over the range of stimulation amplitudes tested. This could be attributed to the afferent fibers travelling in the hamstrings nerve. Alternatively, as mentioned earlier and shown in Figure 2.7, these 5 electrodes were all located at the perimeter of the electrode arrays, making it plausible that the electrodes tips were not actually positioned inside the DRG. In an additional two cases, the stimulation threshold was greater than 6 μA. However, these electrodes were also located at the border of the electrode arrays. The lowest threshold measured was 1.1 μA and 76% of the electrodes had thresholds less than 3 μA. Given these points and that most of the L7 afferents travel through the sciatic nerve, it is reasonable to conclude that the sciatic nerve activity recorded at stimulation amplitudes less than 3 μA represent the activity of the first fiber recruited by DRG stimulation. Claims about the average threshold are therefore unlikely to be significantly affected by having some percentage of L7 axons not passing though the cuff. If anything, L7 fibers not passing through the nerve cuff lead to an overestimation of stimulation thresholds. This is most problematic when considering the range of stimulation amplitudes at which fibers of similar caliber are recruited (see Figure 2.5A). In these cases, the difference between the threshold for the first recruited response and the second recruited response could become smaller.

Another potential source of error is that stimulation within the DRG could lead to reflex activation of α-motor axons whose efferent signals would contribute to the ENG signal in the SNC. This is particularly true for the monosynaptic Ia reflex since a single primary afferent may

make synaptic contact with the majority of the motoneurons within the pool (Mendell and Henneman 1971). Nevertheless, it was felt that the low stimulation amplitudes combined with isoflurane anesthesia would be sufficient to prevent activation of spinal reflexes (Rampil and King 1996, Zhou et al. 1997, Antognini et al. 1999). In addition, the hindlimb was monitored throughout the procedures and no movement was ever observed at the low intensities of stimulation that were tested. Finally, even had reflexes occurred, the latency at which action potentials from efferent fibers would have appeared in the nerve cuff would be noticeably later than those of afferent fibers. This point was examined by comparing the measured CVs of every identified response with the latency at which the response occurred in the SNC. Since the distance from the DRG to the SNC was known, and given a minimum additional 1 ms to account for synaptic delay and conduction to and from the spinal cord from the DRG, the latencies for expected efferent responses were calculated. For example, in cat #4, the DRG-to-SNC distance was 126 mm. For an identified response with a measured CV of 70 m/s, the latency of an efferent response would have to be at least 2.8 ms as compared to the 1.8 ms latency expected for an afferent axon. In no case did the identified responses have latencies appropriate for efferent rather than afferent activity.

Another limitation of this study is the inability to accurately measure the CVs from the SNC recordings for small diameter fibers. In spite of averaging the ENG signals approximately 500 times per stimulus amplitude, the low signal-to-noise ratio for SNC recordings limited the reliable detection of responses from the smallest fibers. Since the magnitude of the ENG signal is proportional to the size of the fiber (Gasser 1928), slower fibers were difficult to detect. Based on the relative amplitudes of detectable responses and typical noise level, we estimate that the minimum CV detectable at thresholds similar to those found for the first response was 20 m/s.

Determining recruitment properties of small fibers within the DRG is an important practical consideration in terms of the potential for eliciting the full range of sensory responses including noxious responses, but is outside the scope of the present work.

2.4.3 Further investigation

No obvious structure was observed in terms of recruitment thresholds within the DRG although the DRG is known to consist of an inhomogeneous distribution of cell bodies and axon bundles with uncertain somatotopic organization. Histological examination of electrode locations would provide a more solid anatomical basis for interpreting differences in the response to stimulation at certain locations. For example, several electrodes exhibited very little change in the peak-to-peak response amplitude despite a four-fold increase in the stimulus amplitude, while the response on other electrodes increased by a factor of 20 or more. These differences are likely related to the varying composition and density of fibers and cell bodies surrounding each electrode in the DRG.

Another issue to examine is whether or not there is a relationship between the type of unit recorded on a given electrode and fiber type recruited at threshold. In other words, if a particular electrode records isolated spikes from a neuron with an identified modality, receptive field and CV, does the fiber recruited at the stimulation threshold have similar properties.

2.4.4 Conclusion

In this study we demonstrated that stimulation within the DRG is able to recruit afferent fibers at stimulation intensities similar to those described for intraneural stimulation in the peripheral nerve. These intraneural microstimulation studies in humans demonstrated that psychophysiologically relevant sensations were evoked and that these responses were somatotopically and modality specific and had graded responses to changing stimulus parameters (Vallbo 1981, Ochoa and Torebjork 1983). Since stimulation in the DRG accesses these same fibers, albeit at a different location, we believe that stimulation within the DRG has the potential to provide similar subjective responses to these reports, but with an additional benefit of being able to recruit a greater range of afferent fibers with different properties at the same physical location. The DRG therefore is an attractive target site for microstimulation to introduce surrogate somatosensory information into the nervous system.

3.0 A COMPUTATIONAL MODEL FOR ESTIMATING RECRUITMENT OF PRIMARY AFFERENT FIBERS BY INTRANEURAL STIMULATION IN THE DORSAL ROOT GANGLIA

The contents of this chapter are published as: *Bourbeau DJ, Hokanson JA, Rubin JE, Weber DJ (2011) A computational model for estimating recruitment of primary afferent fibers by intraneural stimulation in the dorsal root ganglia. J Neural Eng 8:056009*. I was responsible for implementing the code used to run the neuron recruitment models. I also contributed significantly to the analysis code, mathematical/statistical analysis, and figure development.

3.1 INTRODUCTION

Electrical stimulation of peripheral nerve fibers holds great potential for developing motor and sensory neural prostheses; for review see (Navarro et al. 2005). Extraneural peripheral nerve interfaces (i.e., positioned outside the epineurium) are currently being used in a variety of clinical applications, including cochlear implants (House and Urban 1973, Clark et al. 1975) and for functional electrical stimulation of paralyzed muscles (McNeal et al. 1977, Peckham et al. 1980, Creasey et al. 1996). However, electrical stimulation via extraneural electrodes tends to preferentially activate larger myelinated fibers (Veltink et al. 1989, Micera and Navarro 2009), making extraneural stimulation

unsuitable for applications requiring selective activation of smaller fibers. By comparison, intraneural interfaces (i.e., electrodes that penetrate the epineurium) offer greater selectivity and can be arranged in high-density arrays to provide a large number of independent sites for activating motor (McDonnall et al. 2004b) or sensory (Middlebrooks and Snyder 2010) nerve fibers. Investigation of the recruitment of sensory fibers from intraneural stimulation in the dorsal root ganglia (DRG) is what drove the development of this model, although the approach generalizes to microstimulation in other areas of the peripheral nervous system.

Selective activation of different sensory fiber types is important for the development of a somatosensory neural interface for restoring tactile and proprioceptive sensations for neuroprosthetic limbs. Specifically, microstimulation of primary afferent fibers in the DRG is being explored as a means of providing tactile and proprioceptive feedback. A sensory neural interface comprising electrodes in a few DRGs could provide access to the full range of somatosensory fibers covering large portions of a limb in a compact and mechanically stable structure. Previously, we performed primary afferent microstimulation studies with penetrating microelectrodes in the DRG to determine the electrical current thresholds for activating primary afferent fibers. The conduction velocities of fibers that were recruited at the lowest thresholds varied from 38–118 ms^{-1}, indicating that a wide range of fiber diameters were recruited in isolation. The thresholds for all of these fibers were similar, typically 1–3 μA (Gaunt et al. 2009). This pattern of neutral recruitment order has also been observed with intrafascicular electrodes in the peripheral nerve (Yoshida and Horch 1993), and suggests that at low intensities, fibers located nearest the electrode can be recruited selectively, independent of fiber diameter. Such selective recruitment would be particularly advantageous for

creating a somatosensory neural interface, where it is desirable to activate fibers of various types to transmit specific modes (e.g. tactile and proprioceptive) of somatosensory feedback. However, these electrophysiology experiments were limited in their ability to answer questions regarding the recruitment patterns of fibers by size in response to microstimulation.

Computational models have provided valuable insight into the effects of electrical stimulation on fiber recruitment in peripheral nerves. Veltink and colleagues (Veltink et al. 1989) developed a model that simulated peripheral nerve geometries and conductivities, and then applied electric fields corresponding to stimulation. They used the McNeal model (McNeal 1976) for nerve fiber excitation to determine the neural response to stimulation and concluded that intraneural or even intrafascicular stimulation was necessary to selectively stimulate fascicles below the surface of a peripheral nerve. Subsequent work by (Veraart et al. 1993, Tyler and Durand 2002, Schiefer et al. 2008), however, has shown that stimulus current steering methods and nerve reshaping can be used to increase selectivity for even deep fascicles, though there still exist limitations in activating smaller diameter fibers. Meier and colleagues (Meier et al. 1992) modeled electric field distributions in a nerve bundle and the response of single nerve fibers to arbitrary electric fields. They used these models to predict the response of bundles of peripheral nerve fibers to electric fields created from either monopolar or tripolar intrafascicular electrode configurations and found that tripolar stimulation achieved better spatial selectivity and yielded a more physiologically appropriate recruitment order. Recently, Butson and colleagues (Butson et al. 2011) used nerve slices to build a model for simulating intraneural stimulation of a sciatic nerve fascicle. The focus of that work was to examine recruitment as a function of

electrode position and stimulation paradigm. They explored such factors as the current density within axons of different sizes, myelination as a barrier to fiber activation, and the spacing between electrode sites of a microelectrode array.

The models developed in these previous studies were based on specific geometries for the fiber bundles and do not generalize easily to other structures. In particular, the irregular and variable arrangement of fibers and cell bodies in the DRG makes it impractical to define a specific geometry to model the various electrode-fiber configurations that are possible. An alternative approach, which has been used for modeling the recruitment of fibers by deep brain stimulation, is to estimate the volume of tissue activated (VTA) by a given stimulus current (McIntyre et al. 2004, Butson and McIntyre 2005). Those investigators determined the VTA for a stimulus based on which neuronal fibers around an electrode were activated in response to that stimulus. A larger VTA meant that neurons further away from the electrode had been activated.

We used a similar approach to predict the activation of primary afferent fibers of various sizes as a function of stimulus intensity. We started by estimating the current-distance relationship, which determines the activation threshold as a function of the distance between the current source and nearest node of Ranvier. This distance then defines a volume around the electrode, which we term the volume of influence (VoI). Our model simplifies the electric field calculation by assuming a homogeneous, isotropic extracellular medium in a local volume surrounding the electrode, similar to the approach taken in (McIntyre and Grill 2000). We adapted the multi-compartment neuron model in (McIntyre and Grill 2000) to determine the current-distance relationship for primary afferent neurons comprising a range of fiber diameters.

Given the assumption that the node of Ranvier is the site of activation, all fibers having a node within the VoI will be activated. Thus, a given stimulus will activate all fibers having at least one node within the boundary of the VoI. We used an analytical approach to determine the probability of finding a node of Ranvier inside the VoI. This probability depends on the internodal distance; smaller fibers have shorter internodal distances and therefore more nodes per unit length. It is not necessary to assume a specific electrode-node geometry because we integrate the probabilities over all possible configurations within the VoI (see Appendix A for details). We implemented this "likelihood of activation" approach to estimate the recruitment of primary afferent fibers by microstimulation in the DRG. This approach assumes that the distribution of fibers follows published data for the number and distribution of fibers of various diameters in the DRG. Given the current-distance relationship for each fiber diameter, the model provides a likelihood estimate of the number and types of fibers recruited based on the density and distribution of fibers by size. These features lead to a flexible model that can simulate various stimulation scenarios and electrode-fiber geometries, including the inhomogeneous distribution of fibers in the DRG.

3.2 METHODS

A computational model has been developed in two parts. In the first part we simulated activation of single axons by a point source current using NEURON (Hines and Carnevale 2001). This single-fiber model was used to determine the current-distance relationships of primary afferent fibers having diameters in the range 7.3 – 16 μm. These current-distance relationships predict,

for a given stimulus intensity and fiber size, the maximum distance an electrode can be from a node of Ranvier and still activate that fiber. In the second part of the model, we used the predictions from the current-distance relationships to estimate the likelihood of recruiting specific numbers of fibers of a given size within a normative population of DRG neurons. The population model was based on published data for the distribution of fiber sizes in feline L7 DRG (Risling et al. 1983).

3.2.1 Single-fiber model

Electrical excitability for a single fiber was represented with the double cable model published by McIntyre, Richardson and Grill, referred to as the MRG model and built in the NEURON environment (McIntyre et al. 2002). Although cell bodies are present in the DRG tissue, we assumed that they were not directly excitable in the range of low amplitude (0 – 6 μA) stimulation currents that were simulated and so did not include them in our single-fiber model (see discussion). This single-fiber model uses

$$V_x = \frac{I*\rho_{ext}}{4\pi d_x} \qquad (3.1)$$

taken from (McIntyre and Grill 2000) to describe the extracellular potential (V_x) acting on the fiber. Equation 3.1 is evaluated at each discrete compartmental location (x) along the length of the multi-compartmental fiber model to determine if, taken over the entire length of the fiber, the stimulus was sufficient to evoke an action potential in the simulated fiber. This expression is a function of the distance between the stimulating electrode and the segment of the fiber (d_x) as well as the current amplitude (I) applied through the resistivity of the extracellular medium (ρ_{ext}).

This current-distance relation was computed for fibers of various discrete diameters (see Table 3.1). These fiber sizes were then included in simulations of heterogeneous populations of fibers.

Table 3.1: Model parameters. For each fiber diameter included in the model, the table lists the number of fibers (N_{fD}) found in the feline L7 DRG based on (Risling, Aldskogius et al. 1983), as well as the fractional area of the fibers of interest occupied by each fiber size (R_{fD}), and the intermodal lengths (L_{int}) based on (Nilsson and Berthold 1988).

fD (μm)	7.3	8.7	10	11.5	12.8	14	15	16+
N_{fD}	1780	1730	1160	1920	1270	1370	630	990
R_{fD}	0.06	0.09	0.08	0.17	0.14	0.18	0.10	0.17
L_{int} (μm)	750	1000	1150	1250	1350	1400	1450	1500

While the MRG model was validated originally for peripheral motor axons, we used the model to predict activation of sensory fibers in this paper. Although studies have demonstrated that there are differences in the excitability of motor fibers and sensory fibers as a function of stimulus pulsewidth (Veale et al. 1973, Panizza et al. 1998, Panizza et al. 1994), Erlanger and Blair (Erlanger and Blair 1938) showed that the difference was insignificant at pulsewidths near 200 μs. For these simulations, we used biphasic, charge-balanced stimulus waveforms (200 μs cathodal, 400 μs anodal phases).

We used the single-fiber model to determine the maximum distance a monopolar, point source electrode could be from a fiber's node of Ranvier and still elicit an action potential from that neuron, for a given stimulus current amplitude and fiber diameter. In addition, we assumed an isotropic homogeneous extracellular medium with ρ_{ext} equal to 500 Ω-cm (McIntyre and Grill 2000). This assumption leads to a spherical VoI, with the radius defined as that maximum distance of activation determined from the current distance relationship (Figure 3.1A). Note that

this assumption of isotropy may have significantly affected our results. However, we ran additional simulations assuming anisotropy, with resistivity values published for spinal cord (Ranck and Bement 1965). Using a longitudinal resistivity of 300 Ω-cm and a transverse resistivity of 1200 Ω-cm, we found similar results as when assuming isotropy (see Discussion).

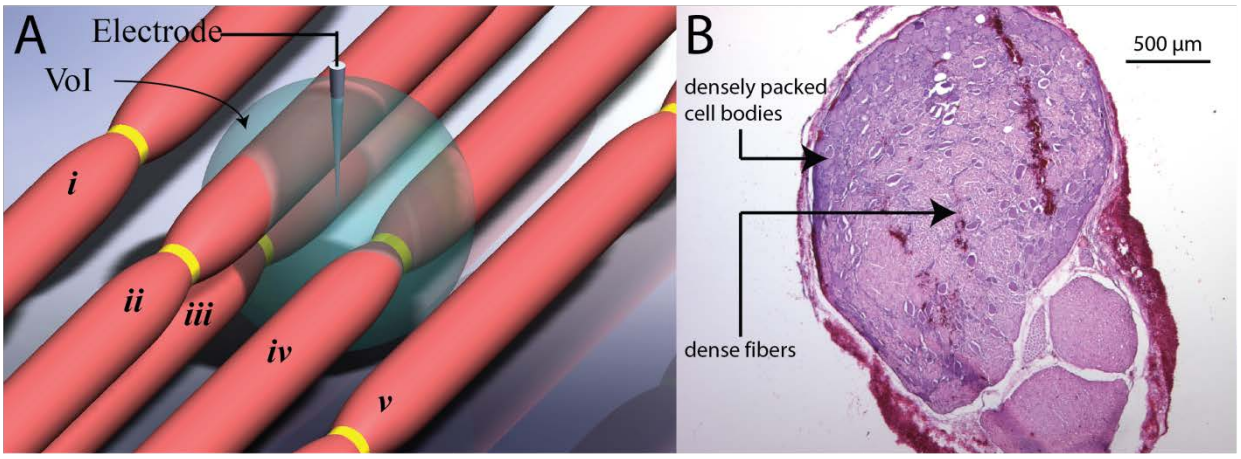

Figure 3.1: Sphere representing the volume of influence (VoI) created by a point-source current stimulus delivered by a microelectrode. (A) The radius of the sphere increases with stimulus amplitude and also varies with fiber diameter. The radius is determined by the current-distance relationship calculated with the single-fiber model for neuronal excitation. Fibers iii and iv, having a node of Ranvier within the VoI, will be activated. Fiber ii, though it passes through the VoI, does not have a node of Ranvier within the sphere and thus will not be activated. Fibers i and v, likewise, will not be activated. (B) Transverse section of feline L7 DRG (top) and ventral root (bottom), hematoxylin and eosin (H&E) stained. Cell bodies are predominantly located along the perimeter of the DRG, but are also sparsely distributed in the center among fibers of passage creating a heterogeneous tissue structure.

We used the MRG model to simulate eight discrete fiber sizes (see Table 3.1). For each fiber size, we used the single-fiber model to determine the extent of the VoI (i.e. the radius) given variations in the stimulus amplitude. The current-distance relationships for the different

fibers were then used as inputs to a population model to examine the probability of recruitment in a normative population of axons in the DRG.

3.2.1.1 Population model

A computational model was developed in MATLAB (The Mathworks, Inc., Natick, MA) to determine the probability of recruiting a given number of fibers of a specified diameter, based on the likelihood of capturing a node of Ranvier within the VoI. This probability depends on two factors: 1) the density of axons packed in the VoI (i.e., the number of axons of a given diameter per cross-sectional area of the VoI), and 2) the inter-nodal distance of a given fiber diameter. In the simplest case, we could assume a uniform distribution of fibers in the DRG and compute the number of fibers of a given diameter packed in the VoI (N_{VoI}) to get

$$N_{VoI} = N_{fD} * \frac{A_{VoI}}{A_{DRG}} \qquad (3.2)$$

In (3.2), N_{fD} is the total number of fibers of a particular fiber diameter (*fD*) present in the DRG and is based on published data for fiber size distributions in the L7 DRG of cat (see Table 3.1). A_{VoI} and A_{DRG} are the cross-sectional areas of the VoI and DRG tissue, respectively. For each fiber size, the radius of the VoI increases with the intensity of the stimulus current, and is taken from the current-distance relationship obtained with the single-fiber model. Note that in this work, we focus on the set of fiber sizes (*{fD}*) corresponding to medium and larger diameter fibers, representing the cutaneous and muscle afferent neurons that are the primary targets of microstimulation in our studies. Equation 3.2 assumes that the fibers are distributed uniformly throughout the tissue. However, to account for the non-uniform distribution of fibers, cell bodies, and other tissue in the DRG (Figure 3.1B), we modified (3.2) by

$$N_{VoI} = R_{DRG} * R_{fD} * \frac{A_{VoI}}{A_{fD}} \qquad (3.3)$$

In Equation 3.3, the number of fibers having diameter *fD* passing through the VoI includes two additional scaling factors to account for the non-uniform distribution of fibers in the DRG. The first term, R_{DRG} represents the fraction of the VoI cross-section that is occupied by the fibers of interest, and we refer to this term as the *packing ratio*. The second term, R_{fD}, is the fractional fiber area and it represents the fraction of the fibers of interest comprising fibers of a specific diameter. A conceptual illustration of these parameters is provided in Figure 3.2. As shown in Figure 3.2B, only a portion of the VoI contains fibers of interest, due to the presence of other tissues (e.g. cell bodies, blood vessels, and smaller fibers).

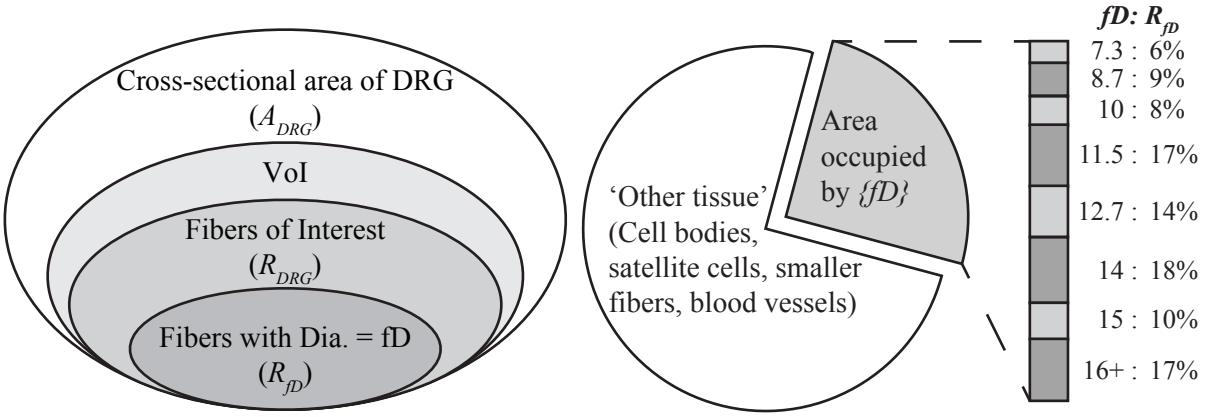

Figure 3.2: Conceptual illustration of model parameters associated with the distribution of fibers in the VoI (not drawn to scale). (**A**) The VoI comprises a small portion of the total area of the DRG, a fraction of which is in turn composed of the fibers of interest (R_{DRG}). The area associated with fibers of interest is further divided into portions associated with specific fiber diameters (R_{fD}). (**B**) Pie chart illustrating fractional areas of DRG composed of 'other tissue' and the fibers of interest. The *packing ratio* comprises fiber diameters 7.3 μm and larger, each having a fractional fiber area (R_{fD}) based on the number of fibers of each diameter found in the DRG. The percent area associated with each fiber diameter is shown by the stacked bar plot at the right of the pie chart.

An average value for the packing ratio (R_{DRG}) can be calculated based on fiber counts and cross sectional area for each of the fibers of interest, expressed as

$$R_{DRG} = \frac{\sum_i N_{fD_i} * A_{fD_i}}{A_{DRG}} \qquad (3.4)$$

However, the actual value may vary substantially throughout the DRG, being higher in areas densely packed with fibers and lower in areas containing more cell bodies (see Figure 3.1B). To examine the effects of this variation on the model, we performed simulations to predict the probability of recruiting at least one fiber, varying the stimulus intensity from 1 – 6 μA and the packing ratio from 0.1 to 1.0. The simulation results were compared with recruitment threshold data from (Gaunt et al. 2009) to determine an appropriate range of values for R_{DRG} (see discussion).

Published data for the distribution of fibers of various sizes in the L7 dorsal roots of cats is provided in (Risling, Aldskogius et al. 1983). These data were used in

$$R_{fD} = \frac{N_{fD} * A_{fD}}{\sum_i N_{fD_i} * A_{fD_i}} \qquad (3.5)$$

to calculate the fractional area of the fibers of interest that is occupied by fibers of a specific diameter (R_{fD}; see Table 3.1 and Figure 3.2B). Note that the data reported in (Risling et al. 1983) is for fibers in the dorsal roots. To account for the ~30% decrease in fiber diameter that occurs between the DRG and dorsal roots (Suh et al. 1984), we scaled the fiber diameters listed in the Risling data by a factor of 1.4 to represent fiber diameters in the DRG. For example, Risling found that there are approximately 1780 fibers in the dorsal roots with diameter equal to 5.1 μm, corresponding to the group of 7.3 μm fibers in the DRG (see Table 3.1). Lastly, we grouped all fibers having diameters equal to or greater than 16 μm into one group of "16+" μm fibers.

In Equation 3.3, we estimated the number of fibers of a given diameter that pass through the VoI (N_{VoI}). This equation was evaluated for each specified fiber size, for a given stimulus amplitude. To determine which of these fibers would become activated, we must evaluate the probability of each fiber having a node of Ranvier within the boundary defined by the radius of the VoI (r_{VoI}). The probability that a fiber of a given diameter has a node of Ranvier within the VoI depends on the ratio of the length of fiber captured by the VoI (L_f) over the internodal length of the fiber (L_{int}). If a fiber passes through the VoI at a known radial distance (r_f) from the center, the probability that a node is captured within the VoI is given by

$$P\left(node\middle|I,fD,r_f\right)=\begin{cases}\dfrac{L_f}{inL_{fD}}=\dfrac{2\sqrt{r_{VoI}^2-r_f^2}}{inL_{fD}} & inL_{fD}>2r_{VoI}\\ \min\left(1,\dfrac{L_f}{inL_{fD}}\right) & inL_{fD}\leq 2r_{VoI}\end{cases} \quad (3.6)$$

In cases in which the VoI is sufficiently large such that the length of the fiber encapsulated in the VoI is greater than the internodal length of the fiber, this equation would evaluate to 1. For example, a fiber passing through the center of a large VoI (i.e., $L_{int} < 2r_{VoI}$) will be guaranteed to have a node of Ranvier within the VoI. However, for stimulation intensities in the range 1 – 6 μA, the diameter of the VoI is ~40 – 240 μm. The range of internodal lengths for the fibers we examined was from 750 – 1500 μm, and thus (3.6) evaluates to much less than 1 at all values of r_f for this range of low intensity of stimuli.

Since the location of the fiber (r_f) is not known a priori, we computed an average value of the probability by integrating over all possible locations of the fiber within the VoI and normalizing by the cross sectional area of the VoI as shown in

$$P(node|I,fD,inL_{fD}>2r_{VoI})=\frac{\int_0^{r_{VoI}}L_f*2\pi r_f*dr_f}{inL_{fD}*\pi r_{VoI}^2} \quad (3.7)$$

Equation 3.7 applies only when the diameter of the VoI is less than the internodal length of the specified fiber (i.e., at low current amplitudes), as is the case for the 1–6 μA range of stimulation current examined here. However, for a higher current amplitude that results in a VoI whose diameter is larger than the internodal length, (3.7) is insufficient and an alternate equation is required (see Appendix A).

Next, the probability mass function for a binomial distribution is used to compute the probability of recruiting a given number of fibers of a particular diameter (N_{act}) from the number of fibers packed in the VoI (N_{VoI}) to get

$$P(N_{act}|I,fD) = \binom{N_{VoI}}{N_{act}} P(node|I,fD)^{N_{act}}[1 - P(node|I,fD)]^{N_{VoI}-N_{act}}. \quad (3.8)$$

This calculation was performed for each fiber size and depends on the current amplitude and fiber size, which determine the size of the VoI and hence the number of fibers that can be captured in the VoI as shown in (3.3).

Finally, we combined the probabilities for activating different fiber sizes to determine the probability of recruiting a particular number of fibers at specific current amplitudes. To get this total probability, we needed to account for all possible combinations of fiber recruitment that yielded the specified total number of fibers (N_{rec}) as in

$$P(N_{rec}|I,\{fD\}) = \sum_i \prod_j P\left(\boldsymbol{C}_{i,j}\middle|I,\{fD\}\right). \quad (3.9)$$

We began by defining a matrix of possible combinations ($\boldsymbol{C}$) that has j columns corresponding to the number of different fiber diameters. Each of the i rows of $\boldsymbol{C}$ is a possible combination of fiber sizes from the set $\{fD\}$, such that the sum across the row is equal to N_{rec}. The set of fiber diameters $\{fD\}$ to include may be specified as any subset of the fiber diameters listed in Table 3.1. The maximum possible value of N_{rec} is equal to the sum of N_{VoI} values for the fiber diameters in the set $\{fD\}$; that is, one cannot recruit more fibers than could be packed into

the VoI. Using (3.9) we were able to estimate the probability of recruiting specific combinations of fibers (e.g. one medium fiber and one large fiber or two medium fibers and one large fiber) (see Appendix A for further details).

3.2.2 Electrophysiology

Data reported from a previous in vivo study were used for comparison with model predictions. For details on the methods used to collect these data refer to (Gaunt et al. 2009). The University of Pittsburgh Institutional Animal Care and Use Committee approved all procedures. To summarize, adult cats were implanted with penetrating microelectrode arrays in the L7 DRG for stimulation and a 5-pole nerve cuff electrode around the sciatic nerve for recording elicited antidromic action potentials. Single channel microstimulation in the dorsal root ganglia was performed to determine the threshold stimulus amplitude at which a response could be recorded in the nerve cuff using stimulus-triggered averaging. A charge-balanced biphasic, cathodic-leading 200 μs pulse followed by a 400 μs anodic pulse was used for stimulation. Thresholds were typically between 1 and 3 μA and approximately 97% of the observed thresholds were less than or equal to 6 μA (Gaunt et al. 2009). We therefore chose this value as an upper limit on stimulus amplitude for simulations in the present paper.

The nerve cuff had two recording sites at a fixed separation distance (8 mm). The propagation delay was measured within the nerve cuff as the time it took for an action potential to propagate between the two recording sites. The electrode separation distance divided by this propagation delay yielded the conduction velocity for an activated unit. An estimate of the fiber diameter was obtained by dividing the conduction velocity by 5.66 based on (Boyd and Kalu

1979). Fiber diameters detected in the in vivo study ranged from 7.3 – 16 μm, which drove the selection of the fiber sizes tested in our model.

3.3 RESULTS

In this study, we used the single-fiber model to compute current-distance relationships for each of 8 different fiber sizes (see Table 3.1). We used these relationships to compare the probabilities of recruiting each of these fiber sizes as a function of the number of fibers that could fit within the resulting VoI and their internodal lengths. Finally, we used the population model to predict recruitment in a heterogeneous population of fibers in the DRG. Simulations were run to determine the number of fibers, by size, that would be activated in response to a given stimulus intensity. We verified these results against primary afferent microstimulation recruitment data reported previously (Gaunt et al. 2009).

3.3.1 Current-distance relationship

Activation of a neural fiber depends on several factors, including stimulus waveform and amplitude, fiber size, and distance from the stimulating electrode. For example, the inverse relationship between the extracellular voltage and the distance between the electrode and a node of Ranvier drives the nonlinear behavior of the current-distance relation as expressed in (3.1). Figure 3.3A illustrates the effect of increasing fiber diameter on the current-distance relation, as predicted by the single-fiber model. In general, the electrode-to-node distance increases with the stimulus amplitude. At higher intensities, the larger diameter fibers can be

activated at much greater distances. This gives rise to the so-called 'reverse recruitment' phenomena that has been described for muscle activation with epineural electrodes (Veltink et al. 1989, Micera and Navarro 2009). However, for amplitudes below 10 μA (see inset in Figure 3.3A), there is little difference in the current-distance relationship for fibers of different diameters. Thus, at these low intensities, the radius of the VoI is effectively the same for all myelinated fibers within the range tested. Although the VoI is the same for these fibers, this does not mean that these different sized fibers have equal likelihood of being recruited in the 0–10 μA range. In order for a fiber to become activated, one of its nodes of Ranvier must be captured within the VoI.

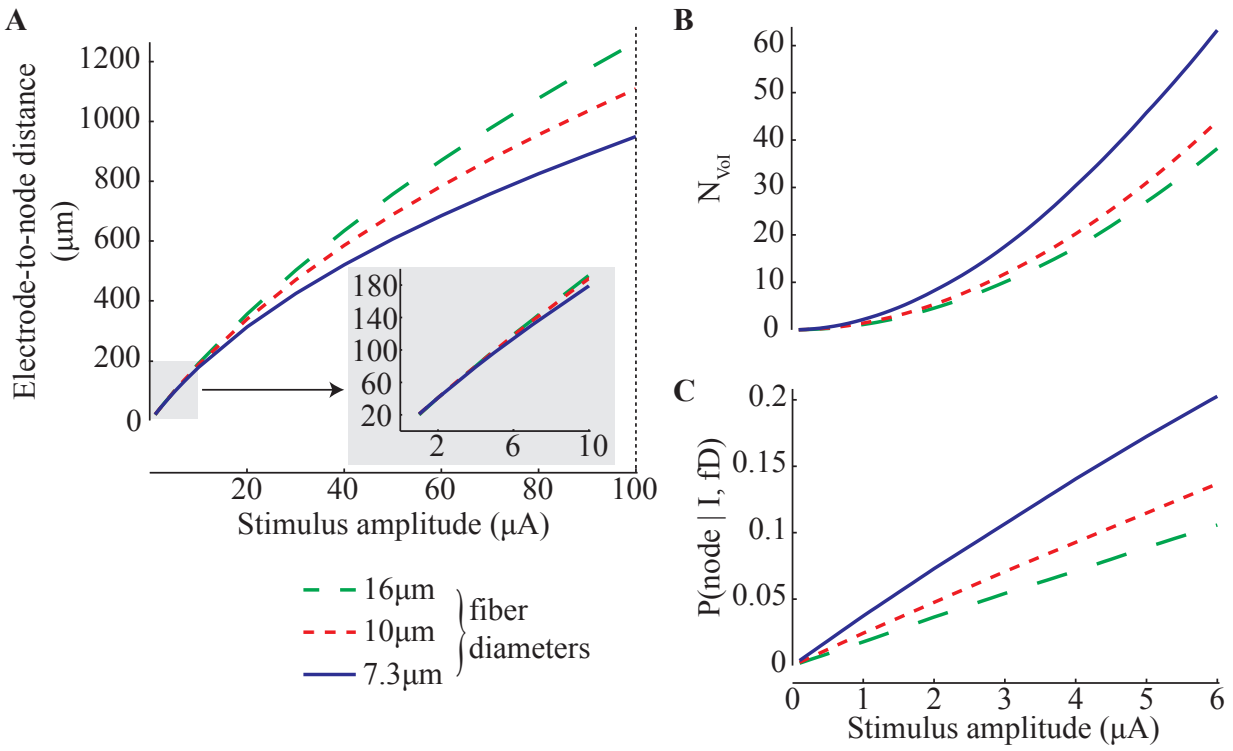

Figure 3.3: Effects of fiber diameter on current-distance relation, fiber packing and probability of having a node in the VoI. (**A**) Current-distance relationships from single-fiber model. Electrode-to-node distance corresponds to the radius of a spherical VoI centered about a stimulating electrode. (**B**) The number of fibers that can be packed into the VoI assuming a packing ratio equal to 1. (**C**) Probability of capturing a node of Ranvier in the VoI as predicted by (3.7). Fiber sizes of 7.3 µm, 10 µm and 16 µm were simulated.

To compare the likelihood of recruiting different fiber sizes, we simulated populations of neurons assuming a packing ratio (R_{DRG}) of 1 in (3.3) to estimate the number of fibers passing through the VoI. Figure 3.3B shows the number of fibers penetrating the VoI, which increases in size with the stimulation intensity (1–6 µA). Note that there are considerably more 7.3 µm diameter fibers penetrating the VoI. This is because there are nearly twice as many 7.3 µm diameter fibers as there are 10 and 16+ µm fibers in the DRG (see Table 3.1). In addition, there is a higher probability of capturing a node within the VoI (see Figure 3.3C) for the 7.3 µm

diameter fibers because the internodal length (L_{int}) is shorter (Table 3.1), as shown in (3.7). Thus, Figures 3.3B and 3.3C suggest a bias towards recruitment of smaller diameter fibers, due to the relatively greater number of 7.3 μm fibers and the higher number of nodes per unit length as compared to the larger fibers.

3.3.2 Thresholds for single-fiber recruitment in a population

Using the population model, we first explored the effects of the packing ratio on recruitment predictions based on (3.9). We ran simulations to predict the probability of recruiting at least one fiber, varying the stimulus intensity from 1–6 μA and the packing ratio from 0.1 to 1.0 in (3.3). The model predictions are shown in Figure 4. In general, the probability of recruiting at least one fiber is very low for stimulation amplitudes < 1 μA and increases with the stimulus amplitude. Note that the rate of increase is much faster when the packing ratio is high. We defined the recruitment 'threshold' as the stimulation amplitude that yields a 0.5 probability of recruiting at least one fiber, indicated by the dotted line in Figure 3.4. The recruitment threshold is ~1 μA when the packing ratio is 1, but increases to nearly 3 μA when the packing ratio is only 0.1. The series of '+' symbols indicate the cumulative probability of recruitment from subject 1 in our previous in vivo experiment (Gaunt et al. 2009). We found that for a packing ratio of 0.26, the population model provided an excellent fit ($R^2 > 0.9$) to those in vivo data. We also used the population model to fit recruitment data for subject 4 from the same published data and found a packing ratio of 0.11 yielded the best fit ($R^2 > 0.9$). The variability in the packing ratios for these two experiments is likely due to differences in the electrode placement between the two experiments; the density of fibers around the electrodes was apparently higher in subject 1 than in subject 4 as suggested by the higher packing ratio found for subject 1. Using the model to fit

the electrophysiology data across all four subjects, the best packing ratio was found to be 0.2 ($R^2 > 0.9$). Thus, despite the potential for large differences in fiber density throughout the DRG, the range of values for the packing ratio is fairly narrow (R_{DRG} = ~0.1 – 0.3) for the data obtained in our in vivo study.

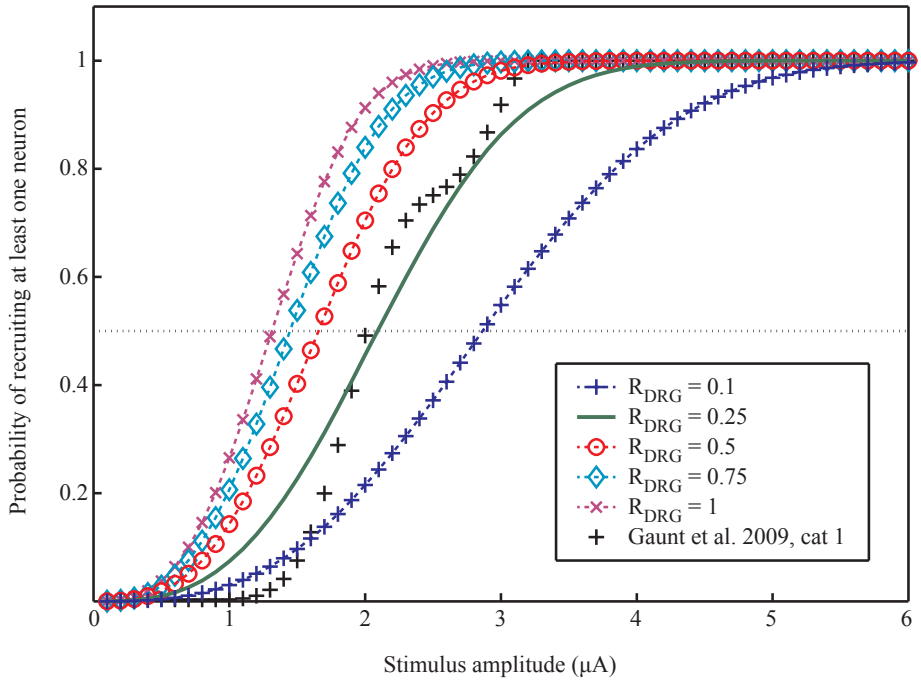

Figure 3.4: Sensitivity of population model to the packing ratio. The black markers represent published electrophysiology data for a single subject (Gaunt, Hokanson et al. 2009). The other traces represent model simulation results of recruiting at least one fiber for different packing ratios. The model best predicts the electrophysiology data for a packing ratio of approximately 0.26 (R^2>0.9) for cat 1, and 0.2 (R^2>0.9) across subjects.

Gaunt and colleagues also observed that in 53% of electrodes tested in 4 animals, medium-diameter fibers were recruited at lower current amplitudes than the larger fibers recruited with the same stimulating electrode (Gaunt et al. 2009). This result suggests a small bias favoring recruitment of medium-diameter fibers when stimulating at the lowest-intensity that yielded an identifiable response (i.e. a so-called threshold response). We examined this bias with the population model by calculating the probability of recruiting only one large

(i.e., $\{fD\}_{large}$ = 12.8 – 16+ μm) or one medium (i.e.$\{fD\}_{medium}$ = 7.3 – 11.5 μm) diameter fiber in isolation across a range of stimulation amplitudes. Recruitment of exactly one fiber in isolation corresponds to the threshold responses that were recorded in the previous in vivo study. For this analysis, we used a packing ratio of 0.26 to allow direct comparison of the model results to the data set for subject 1 in the in vivo study (see Figure 3.4).

Figure 3.5 shows the probability of recruiting only one large or medium fiber across stimulation amplitudes (0–6 μA). Both probability curves have a maximum at 2.3 μA and span a range of stimulation amplitudes from approximately 1–4 μA. In the in vivo study, 100% of the threshold responses were found at stimulation amplitudes between 1.5 and 3 μA. Furthermore, 13 of the 24 (54%) threshold responses were from medium diameter fibers. However, the probability curves in Figure 3.5 suggest an even stronger bias, with the probability of recruiting a medium diameter fiber at threshold more than twice that for large diameter fibers across nearly the entire range of stimulation amplitudes. The nature of this bias will be discussed later (see Discussion).

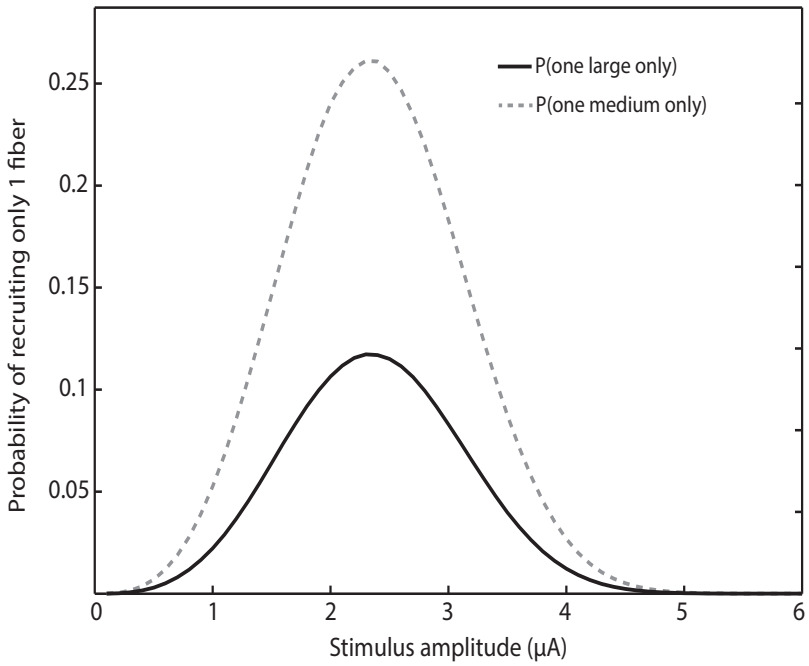

Figure 3.5: Model predictions for the probability of recruiting only 1 large or medium diameter fiber in isolation.

3.3.3 Multi-fiber recruitment in the DRG

The population model was used further to examine the probability of recruiting different numbers of fibers ranging in size from 7.3 – 16 μm, over a range of stimulus intensities (Figure 3.6A). We chose a packing ratio of 0.2 to represent the average packing ratio determined from fitting the model to in vivo data across all subjects reported by Gaunt and colleagues (Gaunt et al. 2009). Solid and dashed traces in Figure 3.6A show separate distributions for the recruitment of large and medium fibers, respectively. For these simulations, we determined the probability of getting N_{rec} larger fibers irrespective of the number of medium fibers recruited (solid traces), or vice versa (dashed traces). This plot demonstrates that medium fibers can be recruited at lower intensities than larger fibers even when multiple fibers are being recruited. Furthermore, this difference increases as the number of fibers being recruited increases. The maximum probability

for these curves decreases nonlinearly as the number of fibers recruited increases. In addition, the current at which the maximum probability is reached increases at a decaying rate as the number of fibers recruited increases. That is, as more fibers are recruited, there is a trend for the distribution to be flatter and shift less along the abscissa.

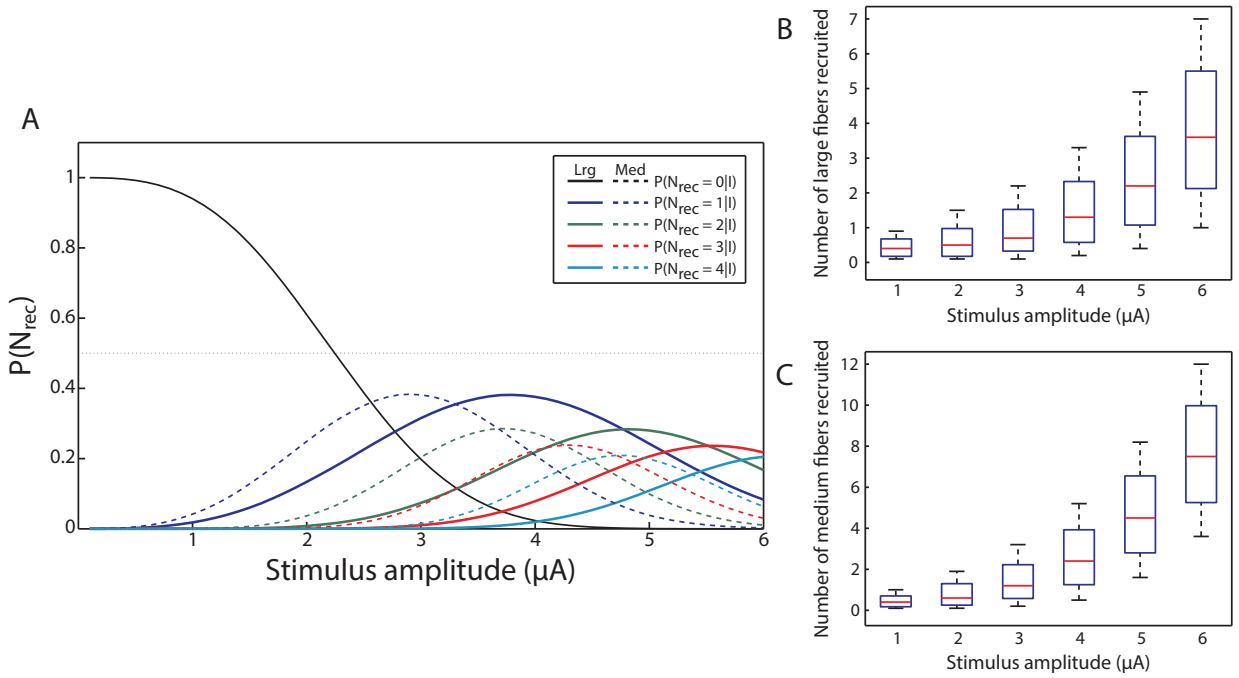

Figure 3.6: Recruitment of multiple fibers in a heterogeneous population across stimulation amplitudes in the range 1–6 μA. (**A**) Traces represent the probabilities of recruiting exactly zero, one, two, three, or four fibers. Solid traces represent recruitment of large fibers (12.8 to 16+ μm) while dashed traces represent recruitment of medium fibers (7.3 to 11.5 μm). (**B**) and (**C**) Range of numbers of large and medium fibers recruited, respectively, given stimulus amplitude.

Finally, we examined the number of fibers recruited in a typical population of medium and larger DRG fibers (≥ 7.3 μm). The boxplots in Figures 3.6B and 3.6C show the range for the number of fibers recruited in the large and medium diameter fiber sets, respectively. The boxplots show the 5th, 25th, 50th, 75th and 95th percentiles of the distributions of numbers of fibers

recruited. As the current is increased, the median increases exponentially, with growth rates of 0.47 μA^{-1} and 0.53 μA^{-1} for large and medium fibers, respectively. Thus, the rate at which additional fibers are recruited depends on the fiber size; as the VoI grows with stimulation intensity, the number of medium fibers having nodes of Ranvier captured within the VoI increases more quickly.

3.4 DISCUSSION

In developing this computational model, we sought to address questions about the number and sizes of primary afferent fibers recruited by primary afferent microstimulation in the DRG. Previously published computational models were designed to address recruitment in specific peripheral nerve structures using a deterministic approach. Here we specified the stimulus intensity and fiber sizes of interest to define a volume of tissue activated. The model uses a probabilistic approach to estimate recruitment of fibers in the DRG, but it can be adapted readily to model different tissue morphologies given information on the distribution of fiber sizes in the tissue. Finally, we compared model predictions to data collected from in vivo experiments and explored the factors accounting for the pattern of recruitment observed.

3.4.1 Recruitment order

We began by running simulations to explore the recruitment of fibers based on size, which suggested that smaller fibers were as likely or more likely to be recruited than larger fibers over the range of fiber sizes and stimulus intensities tested. At large stimulus intensities (i.e., $I > \sim 30$

μA), the electrode can activate larger fibers at a greater distance compared to smaller fibers, as demonstrated by the current-distance relationship (Li and Bak, 1976). However, at the stimulus intensities that we tested (less than 10 μA) the current-distance relationship was effectively the same for the different fiber diameters (Figure 3.3A).

The difference in probabilities of recruiting different-sized fibers was due to a combination of two main factors: 1) the number of fibers of a given size that are likely to be present in the VoI and 2) the likelihood of a fiber having a node of Ranvier in that VoI. Equation 3.3 and Figure 3.3b showed that as fiber diameter decreased, the number of fibers that were likely to be packed into a VoI increased. This behavior was influenced by the distribution of fibers by size (N_{fD}). In the case of feline L7 DRG, the distribution of fiber sizes is skewed toward medium size fibers over larger fibers. Equation 3.7 and Figure 3.3C showed that as fiber size decreased, and accordingly as internodal length decreased, the probability of those fibers having a node of Ranvier in the VoI increased. Because of these two factors, there was a greater likelihood of recruiting a smaller fiber before a larger fiber in our model.

3.4.2 Recruitment in a population

After examining recruitment order, we explored the contribution of the packing ratio to recruitment in a population. The impact of the packing ratio on predictions of recruitment with the population model is important because of the direct physiological implication of this parameter. We found that the model best fit the recruitment data observed in vivo for a packing ratio of 0.2 ($R^2 > 0.9$). To validate this parameter, we used (3.4) to calculate a value for the packing ratio based on measurements of A_{DRG}, which are approximately 4.9 – 7.1 mm^2 for DRG diameters measured to be 2.5 – 3 mm. Using the fiber diameter distribution data from Risling

and colleagues (Risling et al. 1983), the area occupied by fibers larger than or equal to 7.3 μm is approximately 1.15 mm^2; this is the value of the numerator in (3.4). Dividing this area by the cross-sectional area of feline DRG yields a packing ratio of 0.16 – 0.23. This packing ratio range corresponds closely to the range found in our simulations (0.11 – 0.26). Furthermore, using the 'best-fit' values for packing ratio and solving (3.4) for A_{DRG} yields DRG diameters in the range 2.4 – 3.6 mm, which again agrees well with our measured values.

The packing ratio was varied to evaluate the sensitivity of the model to this parameter. As the packing ratio increased, the likelihood of recruiting neurons at lower amplitudes increased because of the greater number of fibers passing through the VoI (Figure 3.4). DRG are heterogeneous structures and the packing ratio represents only an average value; the packing ratio may be higher or lower in different sections of the tissue (see Figure 3.1B). For example, the local volume around a stimulating electrode may have a high packing ratio if the electrode is surrounded by a bundle of fibers, or it may have a small packing ratio if there are cell bodies occupying a large portion of the VoI.

To explore the recruitment of different fiber sizes, we simulated a heterogeneous population of neurons, varying the fiber sizes included in the population. Figure 3.5 demonstrates the different contributions of medium fibers (7.3 μm – 11.5 μm) versus large fibers (12.8 μm – 16+ μm) to the probability of recruiting a fiber in this population. This figure shows that when stimulating at low intensities, the chance of recruiting a single medium fiber is more than twice that of recruiting a single large fiber. Thus, the population model suggests a much stronger bias favoring recruitment of medium fibers than was observed in vivo. One likely source of this discrepancy stems from the differences in the ability to record propagating action potentials from large and medium fibers in a nerve cuff, as was used in our in vivo study. The recorded voltage

of an extracellular signal increases in a power law fashion with increasing conduction velocity, which is closely related to fiber size (Milner et al. 1981). Thus, action potentials from smaller fibers are more difficult to detect and it is possible that some active medium fibers may have gone undetected in the nerve cuff recordings used to identify thresholds in the in vivo study.

3.4.3 Assumptions and limitations

In this paper, we assumed that the extracellular medium was infinite, homogeneous and isotropic (McIntyre and Grill 2000). Ranck and Bement showed that the extracellular medium of the spinal cord dorsal columns in cat is anisotropic, with a longitudinal resistivity of approximately 300 Ω-cm and a transverse resistivity of approximately 1200 Ω-cm (Ranck and Bement 1965). This anisotropy would change the shape of the VoI from spherical to ellipsoidal by altering the resistivity parameter (ρ_{ext}) to have a longitudinal and a transverse component, rather than being direction-insensitive. We altered the model to assume an ellipsoidal VoI with these extracellular resistivity parameters and found no significant difference in the probability of recruiting one or a few fibers (data not shown). For the simulation conditions that we tested and presented in this paper, we felt that this simplifying assumption using a spherical VoI was justified.

We did not include cell bodies in the model, assuming that the site of activation would always occur at the nodes of Ranvier rather than at the soma. Amir and Devor (Amir and Devor 2003) developed a model for frog DRG neurons to explore the soma's role in propagating an action potential. We used their model to test the DRG neuron's response to extracellular stimulation as a function of current amplitude and electrode placement (data not shown). We found that, regardless of current amplitude or electrode position, we could not activate the neuron by stimulating the cell body. In addition, previous work has shown that the site of action

potential generation is always at a node of Ranvier and not the cell body (Ranck 1975, Gustafsson and Jankowska 1976, Lu et al. 2008). This work led us to assume that only nodes of Ranvier were potential sites for activation in response to extracellular stimulation within the ranges of stimulus parameters tested.

Only stimulus amplitudes less than 100 μA were tested with the single-fiber model and less than 10 μA were tested for the population model. The larger amplitude range (0 – 100 μA) was tested with the single-fiber model to explore the current-distance relationship over a wide range of currents. The smaller current range, less than 10 μA, was of particular interest here because intraneural microstimulation experiments have demonstrated that this lower current range is sufficient to elicit neuronal responses (McDonnall et al. 2004a, Gaunt et al. 2009). In addition, stimulation currents less than 6 μA accounted for 97% of the threshold responses reported for in vivo experiments (Gaunt et al. 2009). Of equal relevance, the single-fiber model predicts that as the current intensity is increased above 10 μA, the distance an electrode can be from the fiber to achieve recruitment increases beyond 200 μm (Figure 3.3A). Commercially available electrode arrays have inter-electrode spacing ranging from 200–400 μm (Mushahwar et al. 2007, Gaunt et al. 2009). This spacing appears to be appropriate based on the model's results for recruiting small numbers of neurons at stimulus amplitudes below 10 μA, though different recruitment circumstances may require that this spacing be altered.

3.5 CONCLUSIONS

We have developed a model that predicts recruitment of sensory fibers in the DRG in response to extracellular microstimulation. The model offers some insights into the factors governing

recruitment in a mixed population of fibers. Our results indicate that at low intensities (< 10 μA), smaller fibers are more likely to be recruited as compared to larger fibers over the ranges of fiber sizes and distributions considered here. Furthermore, the results from these simulations suggest that previous in vivo studies may have underestimated the chance of recruiting medium diameter fibers with primary afferent microstimulation in the DRG. The model was also able to simulate the recruitment of multiple fibers, which can be used to predict, for a given stimulus condition, the most likely number of fibers, by size, that will be recruited.

The model has a number of potential applications. This model could be used to aid the design of microelectrode arrays, taking advantage of the model's ability to predict the number and size of axons recruited as a function of stimulus intensity. The model is able to provide information on the size of the VoI and thus the geometry of an array could be designed to minimize overlap between adjacent VoIs while maximizing specificity for target fibers. Besides stimulus intensity, other stimulus parameters may be tested, such as pulsewidth or polarity, on the effects of recruiting neurons in a population. In addition, other fiber sizes (less than 7.3 μm) may be incorporated into the model to represent other sensory modalities, such as nociceptors, thermal receptors, or other primary afferent fibers. For example, it is currently difficult to ascertain the degree to which we are recruiting pain fibers in these primary afferent microstimulation paradigms. Given the distribution of nociceptive fibers, the population model could offer some insight into the probability of activating these other fiber types.

4.0 EFFECTS OF SPATIAL AND TEMPORAL PARAMETERS OF PRIMARY AFFERENT MICROSTIMULATION ON NEURAL RESPONSES EVOKED IN PRIMARY SOMATOSENSORY CORTEX OF AN ANESTHETIZED CAT.

The contents of this chapter are published as: *Hokanson JA, Ayers CA, Gaunt RA, Bruns TM, Weber DJ (2011) Effects of spatial and temporal parameters of primary afferent microstimulation on neural responses evoked in primary somatosensory cortex of an anesthetized cat. Conf Proc IEEE Eng Med Biol Soc 2011:7533–7536.*

4.1 INTRODUCTION

Acceptance and usefulness of modern prosthetics is limited by their lack of sensory feedback (Mooney 1976, Atkins 1996). To overcome this limitation, patterned microstimulation of primary afferent neurons is being explored as a way to transmit sensory information into the central nervous system (CNS). Recent work in amputee patients has already shown that electrical stimulation with intrafascicular electrodes in peripheral nerves evokes painless sensations of touch and joint movement that were perceived to originate in the phantom limb (Dhillon et al. 2004).

The dorsal root ganglia (DRG) provide a compact target for accessing large populations of somatosensory fibers with high density arrays of microelectrodes. Previous studies have

shown that penetrating microelectrodes in the DRG can provide selective activation of various types of muscle and cutaneous afferents (Gaunt et al. 2009). A challenging problem is how to create effective patterns of stimulation in the array of inputs provided by the electrodes. The amplitude and rate of stimulation can be varied independently on each electrode, resulting in an extremely large parameter space for creating feedback patterns.

The goal of this study was to examine how variations in the basic parameters that define a multichannel pattern affect both the threshold for evoking a response and the range over which the response is readily distinguished from other inputs. Various patterns of primary afferent microstimulation (PAMS) were applied via penetrating microelectrodes in the lumbar DRG of anesthetized cats. We quantified the response to stimulation using the firing rates of neurons recorded on an array of microelectrodes in primary somatosensory cortex (S1).

Although it is not possible to know what type of sensation (if any) is represented by each S1 response, our goal was to examine the extent to which these responses differ across variations in the stimulus parameters. Stimuli that evoke similar responses in S1 are presumed to carry similar information. However, if variation in a particular stimulus parameter (e.g., pulse rate) leads to a large modulation in the cortical response, then variation of that parameter is viewed as an effective mode of conveying information to the brain (e.g., see Anani et al. 1977).

This paper presents some initial results regarding threshold and discriminability as a function of the following stimulus parameters: pulse amplitude, rate, and electrode location. Interactions between these parameters are observed in determining stimulus threshold. High classification accuracy between independently activated stimulus locations suggests they can be used as separate pathways for providing feedback. Results also demonstrate interesting interactions in the neural response evoked by multichannel stimulation.

4.2 METHODS

Results shown are from a single experiment. Experimental procedures were performed in accordance with the University of Pittsburgh IACUC.

4.2.1 Experimental Procedures

Isoflurane (1-2%) was used to maintain the cat in a surgical anesthetic plane, and after some preliminary surgery to expose the DRG, the cat was placed in a stereotaxic frame. Vitals were monitored continuously and kept within normal ranges. Electrode arrays (Blackrock Microsystems) were placed in the L6 and L7 DRGs as well as hindlimb area of S1 cortex (post-cruciate gyrus). Stimulation was conducted on 30 channels, 14 in L6 and 16 in L7 (see Figure 4.1A), one or two at a time using an MS-16 stimulus isolator (TDT). Cortical recordings (48 channels) were sampled at 25 kHz using an RZ system (TDT) and manually thresholded to determine times of multi-unit spiking activity.

Stimulation pulses were biphasic with a 200 μs cathodic phase followed by a half amplitude 400 μs anodic phase with a distant return electrode. Discrete stimulation patterns were applied to 1 of 30 electrodes at a time and consisted of a 300 ms train of pulses having a fixed amplitude and pulse rate, followed by a 700 ms quiescent period without stimulation. A total of 360 different patterns were tested (3 intensities [5, 10, 20 μA] and 4 pulse rates [10, 100, 300, and 1000 pulses per second; pps] at 30 different electrode locations) with 10 repetitions for each pattern. Single repetitions of each pattern were tested in random order.

We also tested a limited number of 2-channel stimulation patterns using the same stimulus pulse rates and amplitudes as described above. In each 2-channel trial, the same

stimulus pattern was applied synchronously to both electrodes in the pair. The S1 response to 2-channel stimulation was compared to the responses evoked by single channel stimulation on each electrode in the pair. This test was done to examine interactions in the neural responses evoked by the inputs applied at two different locations.

4.2.2 Data Analysis

The cortical response was evaluated as the spike count in a 50 ms bin starting 10 ms after the onset of a stimulation train. We used a Naive Bayes classifier with leave-one-out cross validation to determine differences in the S1 responses evoked by different stimulus patterns. Differences were considered significant if they exceeded a 99% confidence interval on chance (> 78% classification accuracy over the 20 total repetitions, 10 from each pattern). The cortical population was used for classification with the exception of Figure 4.1B in which single cortical channels were used.

4.3 RESULTS

4.3.1 Thresholds for evoking S1 responses

Figure 4.1A shows the electrode locations that were tested in each DRG. The numbers indicate the lowest stimulation amplitude at each site that evoked a significant response in S1 as compared to baseline. Over 30% of channels (11 of 30) evoked a response at the lowest amplitude (5 μA; at least one pulse rate). A similar percentage of channels (10 of 30) required

much higher currents (20 μA) to evoke a response. A small number of channels did not evoke a response at any of the levels tested, although those electrodes may have been outside the ganglia. Note that the differences are unlikely to reflect variability in the thresholds for recruiting neurons in the DRG (Gaunt et al. 2009), but may instead reflect differences in the pattern of connectivity from the DRG to S1. Also note that some clustering of thresholds is apparent in both arrays, which may indicate a certain level of somatotopic organization of sensory fibers within each DRG (Wessels 1993).

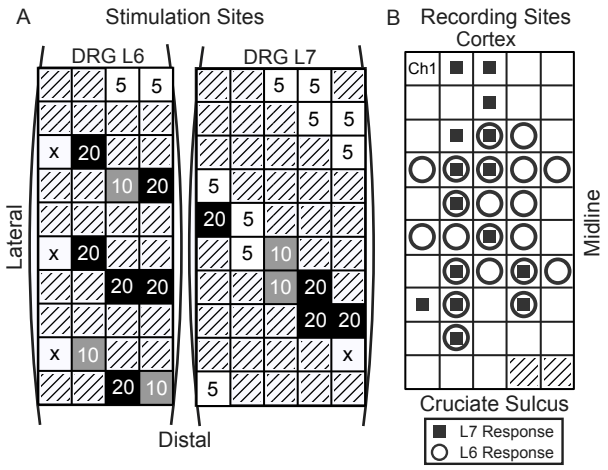

Figure 4.1: Spatial Effects. A: Spatial layout of the stimulus amplitude threshold (μA) for evoking a significant cortical response (vs. baseline) on each tested stimulus channel for the L6 and L7 DRGs. Threshold at any stimulus rate counted as being at threshold for the reported stimulus amplitude. An 'x' indicates that no stimulus amplitude/rate pair was sufficient to elicit a cortical response. Gray boxes represent disconnected channels. B: Spatial pattern of responses in S1 to 5 μA stimulation. Circles and squares indicate that a response was elicited by at least one electrode in the L6 or L7 DRG, respectively.

Of the 48 channels in S1, 26 showed significant responses vs. baseline from stimulation at 5 μA on at least one stimulus channel (see Figure 4.1B). Eleven of these channels were

responsive only to stimulation in L6, 5 were responsive only to L7, and 10 channels recorded responses evoked by stimulation in both locations.

Figure 4.2 illustrates the interaction between stimulation pulse rate and amplitude on the threshold for evoking a cortical response vs. baseline. With 5 μA stimulation applied at 10 pps, only 4 DRG electrodes evoked a significant response in S1. More than twice as many stimulation channels evoked a response at 5 μA when higher pulse rates were used. A similar but smaller effect was observed for 10 μA stimulation pulses, whereas no effect was observed at 20 μA. Although higher amplitude stimulation was most effective in surpassing the threshold needed to evoke an S1 response, it is clear that high pulse rate stimulation is also effective at facilitating stronger responses in S1.

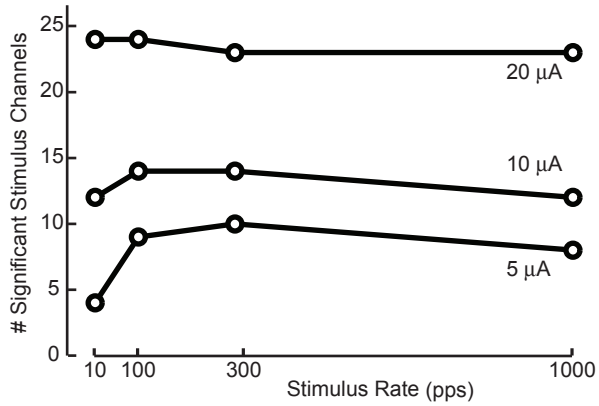

Figure 4.2: Interaction between stimulation pulse rate and amplitude on threshold for evoking a response in S1. Number of stimulus channels that evoked a discriminable response in cortex as a function of stimulus pulse rate for 5, 10, and 20 μA pulses.

4.3.2 Effects of stimulation location

We examined how the discriminability of the S1 response varied with the relative location of two stimulation sites in the DRG arrays. Figure 4.3A shows examples of the neural response averaged for stimulus patterns (10 repetitions each) that were applied at channels 1 and 3 (566

μm apart) in the L7 DRG. The averaged responses appear qualitatively similar but were discriminated reliably by a Naive Bayes classifier with 90% accuracy (18/20).

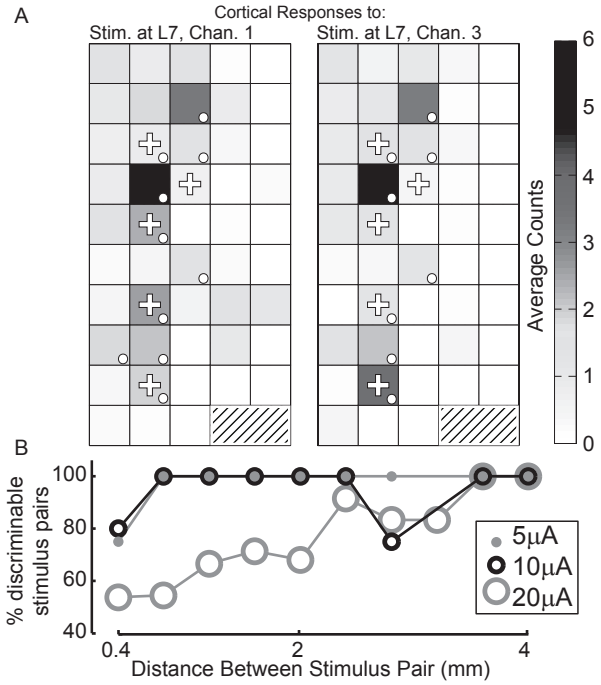

Figure 4.3: Discriminability of S1 responses evoked by stimulation at different locations, pulse rates, and amplitudes. A: Examples of the average cortical response to stimulation on channels 1 (left) and 3 (right) in the L7 DRG at 5 μA and 100 pps. Shown is the average spike count observed 10 – 60 ms following stimulus onset. Dots denote channels showing a significant response; plus symbols (+) indicate channels used for classification. Although they have similar average responses, they can be classified with 90% accuracy. B: Percentage of channel pairs that evoked discriminable S1 responses as a function of the separation distance between the 2 stimulation sites (rate = 100 pps). Only stimulus electrodes that evoked significant responses vs. baseline were included. Pairings were kept within arrays. Distances have been grouped to nearest 0.4 mm.

Figure 4.3B shows the percentage of stimulation pairs that evoked discriminable responses in S1 as a function of the distance separating the two stimulation sites (rate = 100 pps in all cases). At 5 and 10 μA, the cortical response was sufficient to discriminate between the stimulus pairs at most distances, with a slight decrease for adjacent stimulus sites as well as one

outlier pair separated by 2.8 mm at 10 μA. At 20 μA, the recruitment of a much larger number of primary afferent neurons resulted in S1 response patterns that were difficult to distinguish from each other when coming from nearby stimulus electrodes. For discriminable stimulus pairs, and across all distances, the average classification accuracies were 97%, 93%, and 90%, for stimulation amplitudes 5, 10, and 20 μA, respectively.

4.3.3 2-channel stimulation effects

Figure 4.4 shows examples of responses evoked on two S1 channels during single and 2-channel stimulation. The S1 channel in Figure 4.4A did not respond to stimulation on either of the channels independently, but responded strongly when the same two channels were stimulated together. This type of response suggests a convergence of excitatory inputs activated by channels 3 and 6 (1.44 mm apart), such that the combined activation was sufficient to evoke a response in S1. In Figure 4.4B, a response was evoked by stimulation on channel 3, but the response disappeared when paired with stimulation on channel 25. This pattern of responses suggests an inhibitory effect of channel 25 on the response evoked by channel 3. In total, 5.5% of the responses to 2-channel stimulation were similar to Figure 4.4A and 14.8% of the responses were similar to Figure 4.4B.

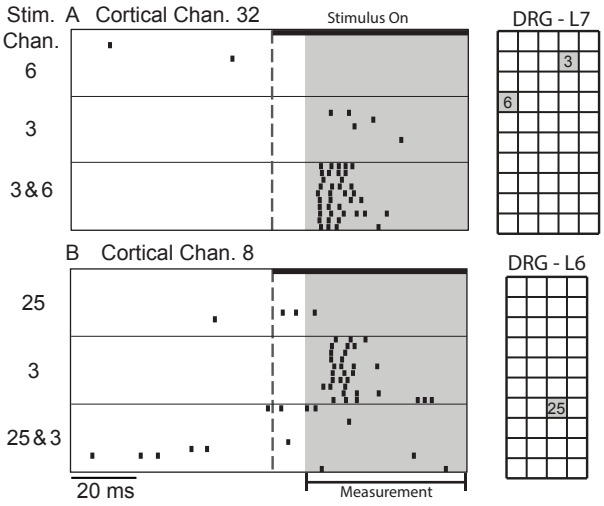

Figure 4.4: Two examples of S1 responses to single and 2-channel stimulation at 5μA. A: This S1 channel did not respond to stimulation at channel 6 or 3; concurrent stimulation on channels 3 and 6 evoked a vigorous response (rate = 1000 pps). B: This S1 channel responded to stimulation on channel 3, but not 25. When both channels were stimulated, the response was nearly eliminated (rate = 100 pps).

4.4 DISCUSSION

4.4.1 Providing Sensory Feedback

The primary aim of this work was to investigate means of providing sensory feedback to the nervous system through patterned microstimulation of primary afferent neurons. Although the response of most primary afferents to external stimuli is fairly well understood, details of how these afferent inputs are integrated in the CNS and their effects on higher-order neural networks are less clear. The manner in which these afferent inputs are integrated is a crucial determinant of the information conveyed by the combined activation of these inputs. Electrical microstimulation of primary afferents can yield insight into how to design stimulation patterns that are effective in conveying information to the CNS, even if they are not naturalistic.

The focus of this paper is on understanding how basic patterns of stimuli differentially activate a population of neurons in S1. We are assuming that if stimuli evoke similar cortical responses, then they convey similar information to the brain. Stimuli that evoke distinct responses, as determined by classification with machine learning algorithms, are presumably discernible by the brain as being different as well. At this point, we cannot conclude that distinct responses in S1 indicate differences in evoked percepts. Future studies will test for perceptual differences using psychophysical discrimination experiments.

4.4.2 Results: Implications for sensory neural prosthetics

One of the challenges with using multichannel microelectrode arrays to provide sensory feedback is figuring out how to encode information in the high dimensional input space that is available. The basic parameters of stimulation include pulse amplitude, pulse rate and electrode location and variations in each of these parameters affects the recruitment of neurons. Our results demonstrated that the threshold for evoking a response in S1 was highly dependent on these three parameters. Interactions among these parameters may greatly reduce the effective size of the input space. For example, interactions between stimulation amplitude and pulse-rate (Figure 4.2) indicate one mode of dimensionality reduction; at high stimulation amplitudes, variations in pulse rate are less effective in evoking distinct responses. Similarly, interactions between stimulus amplitude and electrode locations (Figure 4.3) indicate that the spatial resolution may be reduced as the stimulus amplitude is increased.

It is generally accepted that effective stimulation parameters will vary with stimulus location due to the recruitment of a different neural population. There may exist other

dependencies between our stimulus parameters which could be used to inform stimulus design. For example, stimulus channels that primarily activate muscle spindles may require spatial summation to sufficiently activate the cortex (Macefield et al. 1990). High threshold stimulus channels may be more effective if coactivated rather than simply increasing stimulus amplitude. With more data we plan on building statistical models that characterize these dependencies.

Rate/amplitude interactions suggest paradigms that model perceived intensity as a function of stimulus rate at a fixed amplitude (Dhillon et al. 2004) might not generalize to other amplitudes. A desire to selectively activate neurons means that lower stimulation amplitudes would be preferred. Low stimulus amplitudes, however, might limit the range of perceived intensities due to the decrease in responsiveness at high frequencies (Figure 4.2). This potential tradeoff is something that our experimental model would examine.

Results such as those shown in Figure 4.3 can be used to inform the design of electrode array geometries. Ochoa and Torebjörk (1983) mention that artificial stimulation almost never led to natural touch due to inappropriate or insufficient recruitment. This may be improved by maximizing the number of effective stimulus channels. In this experimental context, this would correspond to maximizing the number of discriminable stimulus channels for different arrays designs. Since we can discriminate between a majority of neighboring electrodes (Figure. 4.3) at low amplitudes, this suggests the need for denser arrays, or possibly more complicated stimulation paradigms such as current steering.

With some exceptions, the majority of somatosensory stimulation feedback studies have examined the use of single channels in isolation. Thoroughly examining groups of stimuli is difficult because of the staggering number of channel combinations. Figure 4.4 indicates that interactions between stimulus sites exist. Future work can elucidate to what degree these

interactions are at the site of recruitment versus convergence of inputs, the dependence of these interactions on the stimulus parameters, and ultimately how multiple channels can be used to increase the amount of deliverable feedback information.

5.0 CHAPTER 5: REPLAY STIMULATION

Parts of this chapter were published as: *Weber DJ, London BM, Hokanson JA, Ayers CA, Gaunt RA, Torres RR, Zaaimi B, Miller LE (2011) Limb-state information encoded by peripheral and central somatosensory neurons: implications for an afferent interface. IEEE Trans Neural Syst Rehabil Eng 19:501–513.* This publication was a joint effort between the Miller and Weber labs. Christopher Ayers and I were responsible for conducting the experiments and doing the data analysis for the Weber lab portions of the paper.

5.1 INTRODUCTION

In the previous chapter I introduced the concept of using cortical recordings to guide approaches to providing artificial somatosensory feedback. The stimuli used in that chapter were typical of most sensory feedback studies (Dhillon et al. 2004, London et al. 2008, O'Doherty et al. 2011, Koivuniemi and Otto 2011, Venkatraman and Carmena 2011), in that it was mostly single-channel stimulation at a predetermined amplitude and stimulus rate. Some studies have explored the use of aperiodic stimuli (O'Doherty et al. 2012), and others the use of multiple channels simultaneously (Fitzsimmons et al. 2007, Davis et al. 2012, Zaaimi et al. 2013) or in traveling waves (Fitzsimmons et al. 2007). However, without a physiological basis for these manipulations, scaling these approaches beyond a few channels is difficult. For example,

feedback could be provided by one stimulus channel stimulating at a rate of 30 pulses per second (pps), while another could stimulate at 50 pps. Both of these rates might be based on an optimal result obtained when each channel stimulates in isolation, but may not hold when stimulating on both channels at once. To investigate this, we might vary the rate of one channel while holding the other constant. In addition to various rate pairings, the stimulus amplitude, relative stimulus timings of the two channels, stimulus waveform shape, etc. could all have an effect on the outcome. Although these types of tests might be feasible in animal models, it is difficult for an experimenter to choose the appropriate set of tests to run, given the enormous stimulus parameter space.

Instead of choosing a spatio-temporal stimulus pattern de novo, one can be created by stimulating with a pattern based on recordings from primary afferents made during natural inputs (tactile and passive limb movement). This approach greatly simplifies the stimulus design and allows principled investigation of issues associated with multichannel stimulation. This approach, known as "replay" stimulation, attempts to provide a similar pattern of nervous system activation during stimulation as was delivered during the natural stimulus input.

5.2 STIMULATION APPROACH

5.2.1 Spatio-temporal Pattern Matching – Replay Stimulation

The first part of replay stimulation consists of stimulus design, which comes from recordings made in the dorsal root ganglia during natural (non-electrical) stimulus inputs. In these studies the inputs were limited to passive movement of the limb as well as any inadvertent cutaneous

stimulation that occurred from touching the limb to move it. Simultaneous recordings were made in DRG and in somatosensory cortex while manipulating the hind limb of the cat (Figure 5.1A). For the majority of data, hind limb movement was provided using a robot (VS6556E, DENSO Robotics, Long Beach, CA) to allow for averaging of responses by aligning the highly repeatable movement patterns that the robot created. A subset of spiking activity data was chosen from the DRG recordings to serve as the basis of the replay stimulus (for details see the next section).

Once neural recording trials were completed, a multichannel microstimulation system was connected to the DRG(s) to deliver stimulation patterns to the tissue. During the stimulus, each previously recorded action potential was replaced with a single stimulus pulse (Figure 5.1B). The stimulus was repeated multiple times to allow for averaging. Cortical recordings were made during stimulation to enable comparison of the cortical response during stimulation with the cortical response during the natural stimulus. During stimulation, the foot was held by the robot in a center position. During stimulation the leg was visually monitored to ensure that reflexive leg movements were not being evoked. Additionally, a force transducer (ATI Gamma SI-32-2.5) was used to collect hindlimb force for later analysis. Data with significant force measurements (relative to baseline) were excluded from the results shown. Evoked movements were minimized during stimulus trials by limiting the stimulus amplitude.

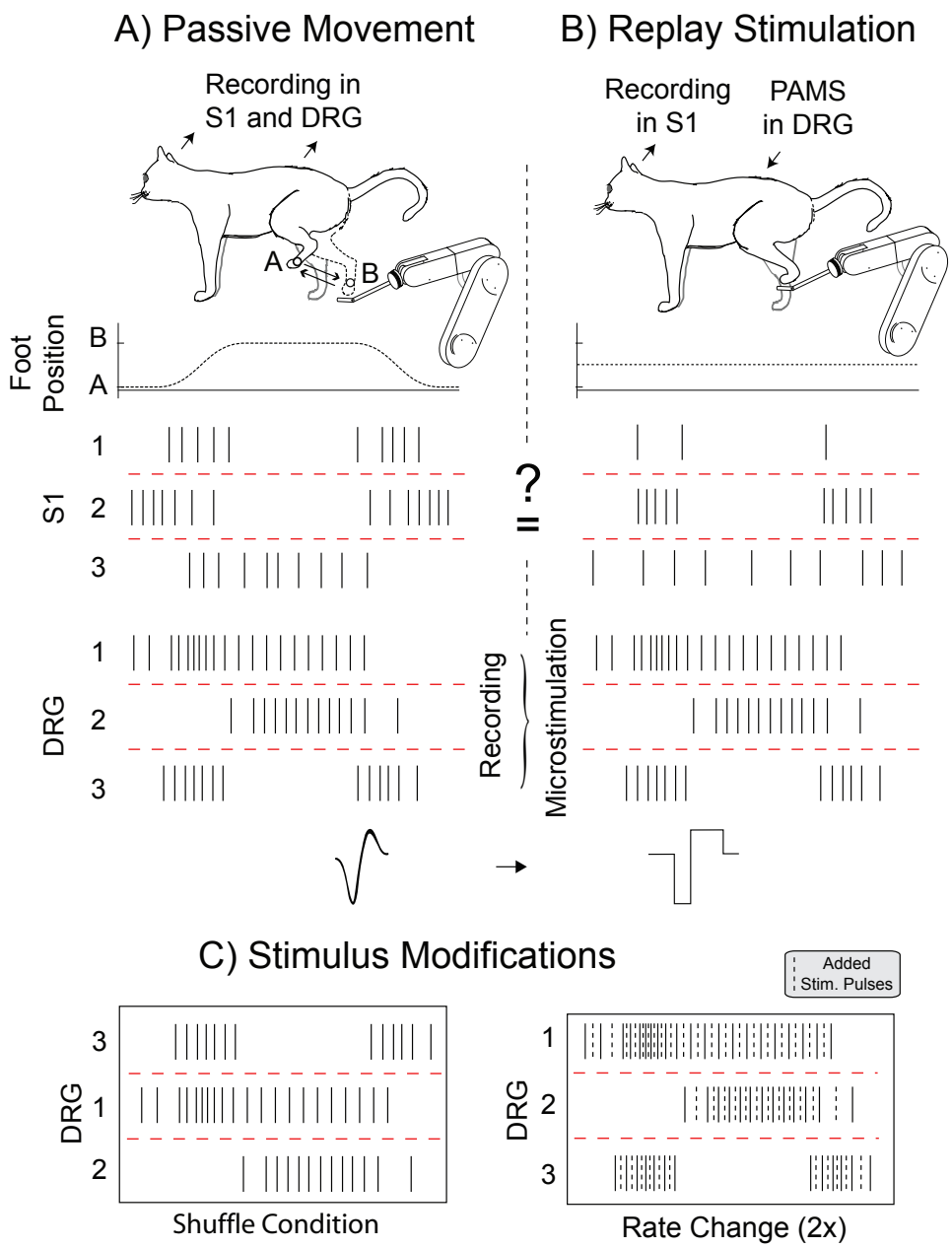

Figure 5.1: Illustration of the replay stimulation paradigm. (A) Simultaneous recordings are made in S1 cortex and DRGs during passive movement of the limb. (B) In another trial the recordings in the DRG are replaced with stimulus pulses which are meant to mimic the spatio-temporal pattern of activation that occurred during passive movement of the limb. (C) Modifications of the default replay stimulus serve as a basis for investigating this technique as an approach to studying somatosensory feedback.

5.2.2 Free Parameters

Use of the replay stimulation paradigm only controls the relative stimulus timings on each channel. Importantly, the stimulus waveform itself remains unspecified, both in terms of its general shape and its amplitude. For simplicity, all tests were done with equal stimulus amplitudes on all channels and using the same stimulus waveform for all stimulus pulses. The stimulus waveform consisted of a leading cathodic phase followed immediately by an anodic phase of half the amplitude and twice the duration. The width of the cathodic phase was held constant at 200 μs (thus a 400 μs anodic phase).

A more difficult free parameter that was not immediately obvious was spike thresholding and sorting. If each electrode were to record at most a single well isolated unit, then the replay stimulation paradigm is relatively straight forward. If however multiple neurons are recorded, replacing each action potential with a stimulus pulse confuses the interpretation of the paradigm. Another common issue that was faced was multi-unit recordings that were similar on many channels. It was initially unclear whether or not this type of multi-unit response should be included along with well-isolated single-unit responses, or perhaps even prioritized as it might be more indicative of the overall population response. The general approach taken was to set thresholds for units just above the noise level and to include all units as stimuli that crossed the threshold. Occasionally however the noise level of a channel would increase and the threshold would no longer be appropriate, as indicated by a very high average stimulus rate. In that case the channel was discarded (i.e. no stimuli were delivered on that channel during replay stimulation).

Additionally, the natural input to "replay" had to be chosen. Since a primary interest is in providing movement related feedback, we decided to use a passive movement input as the

'natural' input for replay trials. After testing several different movement types, including simulated walking patterns, it was decided to use a simple flexion-extension pattern. This choice also allowed for multiple repetitions within a short time period.

Another decision that had to be made was which subset of the natural input recordings were to be used as the basis for the stimulus. A single stimulation session which replicated a two to three minute recording session would ensure that all DRG recordings were presented as stimuli. This approach however would limit stimulus repetition due to time constraints. Instead, averaging would need to be done with an assumption that sets of passive movement elicited similar DRG recordings (thus similar DRG stimuli) and similar cortical responses, such that averaging across sets was appropriate. Alternatively, a subset of the session could be chosen. Ultimately this was the approach used; 10 – 20 second of data were chosen from the passive movement recordings for replay stimulation. This approach allowed for a consistent stimulus, and for examining variability in cortical responses to repetitions of the same stimulus. This allowed results like those seen in Figure 5.4, where the precise timing of the stimulus was important, which would not have been evident with slightly different stimuli. This decision however does mean that the subset chosen should be indicative of the typical DRG response. In at least one case the subset of time chosen had significant noise in DRG recordings. This non-typical stimulus was then used as the basis for a large set of trials, which was not desirable.

Given that we were able to record from 90 channels in the periphery but only stimulate on 32 (due to hardware limitations), we also needed to choose a subset of channels to use for stimulation. Due to the connectors between our stimulator and the electrode array it was not possible to choose any group of 32. Rather, we could choose from 2 out of 6 connectors of roughly 16 channels each. The averaged firing rate profiles of the DRG neurons were plotted on

a connector by connector basis and two connectors were visually chosen that appeared to have sufficient population variability.

5.2.3 Stimulus Modifications

The goal of the replay stimulation paradigm was not just to perform the basic replay stimulus. Additionally we desired to examine how stimulus manipulations to this base approached changed the evoked cortical responses. Importantly, using these manipulations we wanted to assess the extent to which this experimental paradigm could be used to learn general principles about artificial somatosensory feedback that could be applied to clinical cases in which replay stimulation is not possible.

The primary stimulus modifications examined were a stimulus channel shuffle condition and a stimulus rate change. During the shuffle condition, a Monte Carlo approach was taken to try and minimize the correlation in smoothed firing (stimulus) rates between an original DRG recording and the channel that would replace it during stimulation. In other words, the goal was to maximize the difference between the normal replay stimulation case and the shuffled condition (Figure 5.1C). The goal of this change was to examine the importance of the spatial accuracy of the stimulus locations, relative to the original cortical recordings.

Another modification to the stimulus involved inserting stimulus pulses between the original pulses in order to increase the instantaneous stimulus rate while maintaining the overall rate profile. For a rate increase of (X), (X-1) pulses were inserted at even spacing between every original stimulus pulse. For a 2x increase, this meant inserting one additional pulse halfway between each original stimulus pulse. For a 3x increase, 2 stimulus pulses would be inserted at 1/3 and 2/3 of the time between the original pulses. This process is shown in Figure 5.1C. No

stimulus pulses were inserted between a pair of original stimulus pulses when these original pulses were separated by more than 0.1s. This was done in an attempt to minimize spurious pulses between stimulus trains that were not functionally linked. The goal of this stimulus manipulation was to examine whether or not rate scaling could be used to increase the evoked cortical response, so as to be more similar to the response during passive movement. It is hypothesized that an increase in the stimulation rate could be used to increase propagation of information downstream through increased temporal summation at synapses in an attempt to overcome the lack of spatial summation.

Other modifications to the original replay stimulus are possible but were not explored systematically. One such modification is removal of a subset of stimulus channels, to gauge their importance in eliciting the overall response. This could be done using a number of criteria, such as location of the stimulus channel or type of stimulus input (e.g. velocity sensitive, position sensitive). Alternatively removal could be done randomly and with many different groups of channels removed in order to generate a parametric curve relating number of stimuli to the cortical response. Finally, another approach which was considered but was not tested was to add a baseline stimulus rate to each channel in an attempt to 'prime' the system (Priplata et al. 2002). These types of manipulations may also yield information as to how to best provide somatosensory feedback.

5.3 EXPERIMENTAL DETAILS

Results shown are from a single experiment, cat 1, with the exception of Figure 5.5 which is from cat 2.

5.3.1 Surgical Procedures:

The cat's head was supported by a stereotaxic frame and a second custom frame supported the torso, spine, and pelvis while allowing the hindlimb to move freely through its full range of motion. Surgical procedures for both cats, and experimental procedures for cat 1, were performed under isoflurane anesthesia (1%–2%). Blood pressure, core body temperature, respiration rate, end tidal CO_2 and oxygen saturation were measured continuously and maintained within normal, physiological ranges. Following surgery, cat 2 was allowed to recover. Experimental procedures for cat 2 were performed under dexmedetomidine (0.04 mg/kg).

An array of microelectrodes was inserted to a depth of 1.0–1.5 mm in the hindlimb region of S1 (Landgren and Silfvenius, 1969). A 5x10 channel array (Blackrock Microsystems, Salt Lake City, UT) was used for cat 1 and a 10x10 channel array was used for cat 2. We confirmed electrode placements in the hindlimb region by recording S1 neuronal responses evoked by electrical stimulation of the contralateral sciatic nerve via a bipolar nerve cuff electrode. The craniotomy performed on cat 2 was sealed using Kwik-Cast (WPI, Sarasota, FL) and a pedestal (Cererport, Blackrock Microsystems) was attached to the skull using bone screws for electrical access to the array.

DRG were exposed by laminectomy as described in Weber et al.. (2007). For cat 1, 4x10 and 5x10 arrays of sputtered iridium oxide film (SIROF) microelectrodes (Blackrock) were inserted into L6 and L7, respectively. For cat 2, both L6 and L7 were implanted with 32-channel floating microelectrode arrays (FMA, Microprobes Inc., Gaithersburg, MD). Typical impedance values for the SIROF electrodes were ~50kΩ at 1000 Hz. For cat 2, a custom electrical housing

unit was constructed which was placed above the skin and anchored to a baseplate that attached to the iliac crests.

5.3.2 Data Collection and Stimulation

Neuronal spiking data were sampled at 25 kHz using a multichannel neural recording system (RZ2, TDT) and digitally band-pass filtered between 300 and 3000 Hz. Thresholds were determined manually for each channel and spike events were defined whenever the signal exceeded this threshold. Hindlimb kinematics were recorded with high speed motion capture systems (IMPULSE, Phasespace) using markers placed on the iliac crest (IC), hip, knee, ankle, and metatarsophalangeal (MTP) joints. A robotic arm (VS6556E, DENSO Robotics, Long Beach, CA) was used to generate center-out-and-back displacements of the left foot in a parasagittal plane. For cat 2, movements were performed manually.

All stimulation was monopolar with respect to a large return electrode placed in the epidural space under the vertebrae. Stimulation was performed using MS-16 stimulators for cat 1 and an IZ-2 stimulator for cat 2 (Tucker Davis Technologies [TDT], Alachua, FL). Custom TDT Macros were written to support specific stimulus timing on each channel. Custom Labview code (National Instruments) provided a GUI interface for controlling the stimuli. Interfacing Labview with the TDT system was done using ActiveX components (OpenDeveloper, TDT).

For cat 1, six sets of data were collected during the experiment. Three electrode configurations were used, one in which electrodes spanned L6 and L7, and two others in which the electrodes were only in L6 or L7. For each of the three stimulus configurations two passive movement data sets were collected at two different robot movement speeds. During passive movement trials, ten sets with four flexion/extension repetitions each were conducted. One of the

ten sets was chosen as the basis for the replay stimulus. The replay stimulus was repeated seven times for each replay trial. Four different stimulus amplitudes (5, 7, 10, and 15 μA), three different stimulus rates (1x, 4x, and 8x), and an exact and shuffled condition were all tested for each data set (24 different trials). Each set was collected sequentially. For a single stimulus condition (unique amplitude, rate, and shuffle condition), all seven stimulus presentations were presented sequentially. During a set different stimulus conditions were interleaved randomly. Insufficient results were collected from cat 2 to be included in the analyses and the stimuli used are detailed when describing the results from that experiment.

5.3.3 Data Analysis

Firing rates were computed by convolving spike times with a non-causal Gaussian kernel and sampled at 32 ms intervals. Firing rates were computed on unsorted multiunit responses.

Average responses to passive movement and to replay stimulation were computed by averaging firing rates, aligned to the start of a flexion-extension movement. Correlation coefficients were computed for each cortical channel by correlating the averaged firing rate from a replay stimulus with the averaged firing rate during passive movement on the same cortical channel.

5.4 RESULTS

An example recording of a single somatosensory cortex (S1) channel during passive movement and replay stimulation is shown in Figure 5.2. Although the temporal profiles of the responses

are similar in this example (r = 0.48), the typical response to replay stimulation was noticeably different from the response to passive movement. This difference is reasonable given that a maximum of 32 stimulation channels across at most two ganglia were used to drive the cortical response. During passive movement, the entire population of hind limb afferents drives the cortical response.

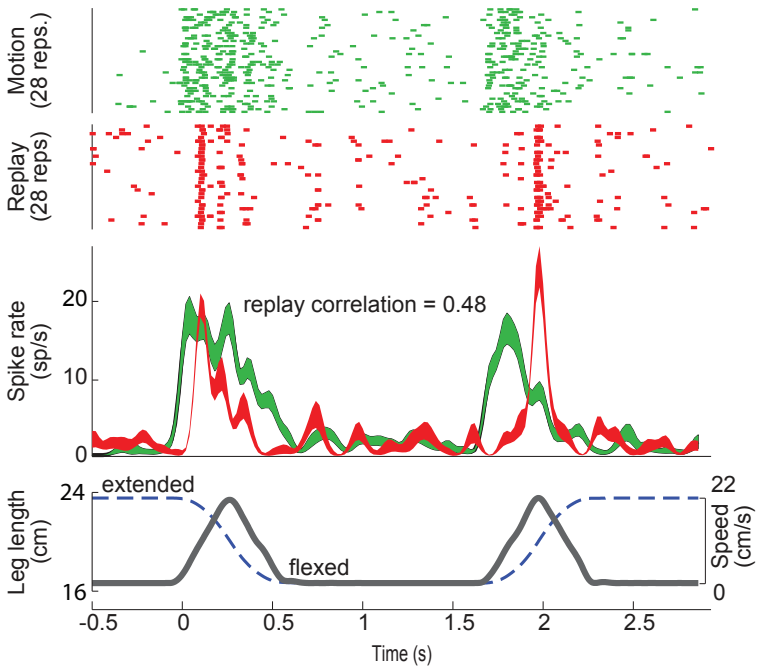

Figure 5.2: Example cortical responses to multiple presentations of a passive movement stimulus as well as an electrical stimulus using the replay stimulation paradigm (7 µA, 1x, 16 channels L7, 14 channels in L6). The stimulus movement was a simple flexion and extension of the leg. In total 40 different flexion/extension movements were presented (28 shown). Of these 40 movements, a continuous set of 4 was chosen to serve as the basis for replay stimulation. This stimulus was repeated 7 times.

5.4.1 Rate & Shuffle Effects

Two proposed manipulations to the replay stimulus trains were investigated to see if they could modify the cortical response in specific ways. The two modifications involved changing the instantaneous stimulation rate and changing the spatial patterning (shuffling) of the inputs.

Figure 5.3 shows the clearest example of the hypothesized effects of shuffling the stimulus inputs and changing the stimulus rates. The firing rates were averaged across movement sets (10 for the passive movement and 7 for the replay stimulus). Two of the four repetitions are shown. Shuffling the stimulus location dramatically changed the response consistent with the idea that spatial relationships are important in eliciting comparable cortical responses. In general, the results look closer to the original when not shuffled and with higher instantaneous stimulus rates. Correlation values are consistent with this observation. For the original replay case (exact match), correlation values were 0.60 (1x), 0.65 (4x), and 0.66 (8x) and for the shuffled stimulus the correlation values were 0.59 (1x), 0.58 (4x) and 0.41 (8x).

This example also highlights some important inconsistencies in these manipulations. In the original case, the peak response times are slightly offset from the peak response times to passive movement, particularly for extension movements (2^{nd} and 4^{th} peaks). In addition, the change in stimulus rate does not affect the entire response in the same way. As an example, there is relatively little increase in the first peak response when going from 1x to 4x. The same is not true of the second peak, where there is nearly a doubling in the response magnitude. These types of inconsistencies are important indicators that a stimulus model relating inputs to outputs might be necessary in order to match the cortical response to the stimulus with the response to passive movement.

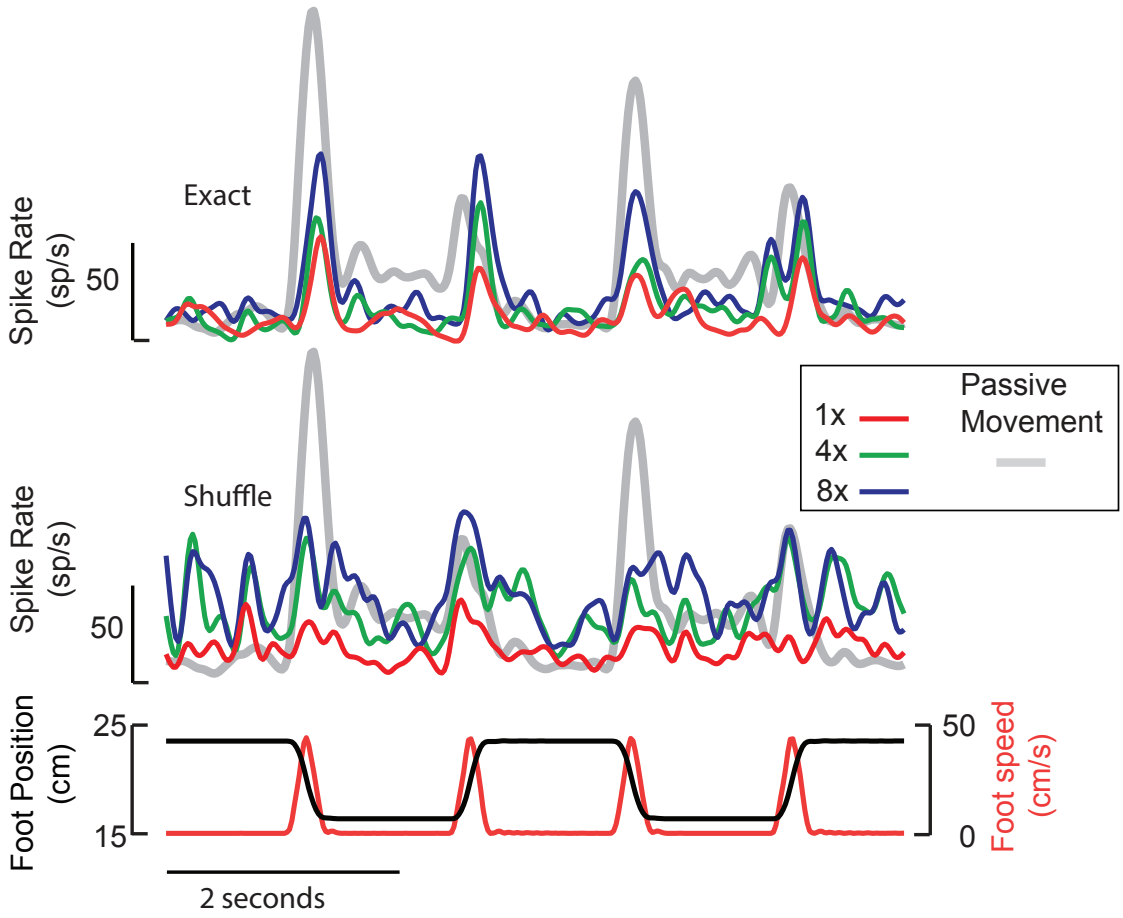

Figure 5.3: Rate and Shuffle Stimulus Manipulations. Example responses from a single cortical channel to passive movement, as well as various combinations of stimulus rates and shuffling conditions at 15 μA. Correlation values for the exact match case were 0.60 (1x), 0.65 (4x), and 0.66 (8x) and for the shuffled stimulus the correlation values were 0.59 (1x), 0.58 (4x) and 0.41 (8x).

A multi-way ANOVA with three factors (stimulus rate, stimulus amplitude, and the shuffle condition) was conducted to examine the impact of rate and shuffling across the entire population. Correlation between the firing rate of a cortical channel during replay stimulation and its original response to passive movement were used as the test values. From the ANOVA it was determined that the shuffle condition was not a significant explanatory variable, whereas stimulus amplitude and stimulus rate were.

Post-hoc analysis was done to compare the difference in correlation values as function of stimulus rate at each stimulus amplitude. On a channel-by-channel basis, differences in correlation values were computed between different stimulus rates at fixed stimulus amplitudes. Shuffle-condition responses were omitted. Using these values, paired t-tests were performed to test if the mean difference in these values was significantly different from zero. In total, 12 tests were performed. The average differences and significance values are shown in Table 5.1. A significance value of $p < 0.00083$ (0.01/12, Bonferroni correction) was used. For stimulus amplitudes of 7, 10, and 15 μA, increasing the stimulation rate from 1x to 4x led to an increase in the correlation between the firing rate of a cortical channel to the replay stimulus and the firing rate of the same cortical channel during passive limb movement. At 15 μA the difference between 1x and 8x became significant as well.

Table 5.1: Average difference in correlation values between stimulus rates at constant stimulus amplitudes. Significant values (average difference is not-zero) are indicated with an asterisk ($p < 0.00083$, paired t-test).

		Differences in Stimulus Rates		
		4x - 1x	8x - 1x	8x - 4x
Stimulus Amplitudes (μA)	5	0.014	0.011	-0.003
	7	0.116*	0.013	-0.052
	10	0.061*	0.038	-0.024
	15	0.097*	0.088*	-0.010

Difference in average correlation values

* $p < 0.00083$

The average correlation values for each stimulus rate and amplitude are shown in Table 5.2. Due to an error in data collection in one of the experimental sets which led to a missing stimulus condition, the paired differences are not equivalent to the difference in the means. The highest correlation value was observed at a stimulus amplitude of 15 μA and the rate multiplier was 4x.

No attempt was made to filter cortical channels based on their responsiveness to the original passive movement. This leads to an overall decrease in correlation values for all conditions, and is not expected to impact the trends observed across rate and amplitude.

Table 5.2: Average replay correlation values for the specified stimulus amplitude and rate.

			Stimulation Rate		
			1x	4x	8x
Stimulus Amplitude µA	5		0.074	0.089	0.086
	7		0.063	0.193	0.180
	10		0.094	0.156	0.132
	15		0.168	0.266	0.256
			Mean Correlation Values		

5.4.2 Importance of Stimulus Timing

During testing there was evidence that the relative timing of individual pulses delivered to multiple channels, on the order of a few milliseconds, affected the observed cortical response. Relative pulse timing has been shown to play a significant role in previous experiments as well. When stimulating on all channels in the DRG at the same time, it is possible to generate large limb movements (Bourbeau 2011). However, by altering the timing (randomly) of the stimulus pulses to reduce the number of channels that stimulate simultaneously, the evoked forces were often eliminated.

Analysis of the cortical responses to replay stimulation would occasionally show an unusual amount of 'banding' in the response (Figure 5.4A). In other words, certain action potentials in the response seemed to vary little in their timing with repeated presentations of the stimulus. This is referred to as a “reliable” response. Upon closer examination (Figure 5.4B) it

was possible to see that the variation in response time was less than 1 ms. In Figure 5.4C stimuli have been aligned to the cortical response by removing a conduction delay of approximately 15 ms. This shift revealed that simultaneous stimulation on channels 3 and 5 was responsible for eliciting the two reliable responses shown in 5.4B. This synchronization between channels 3 and 5 was simply a result of the naturally occurring spike timing used to generate the replay stimulus train. Of the 23 times when the cathodic phase of the stimuli on channels 3 and 5 overlapped, 19 occurrences elicited a reliable response in the cortex. By comparison, this occurred just 3 of the 231 times that channel 3 was stimulated without 5 (although other channels may have been involved), and 3 of the 53 times for stimulus channel 5 (without 3). Importantly, stimulus channels 3 and 5 were located next to each other (400 μm apart).

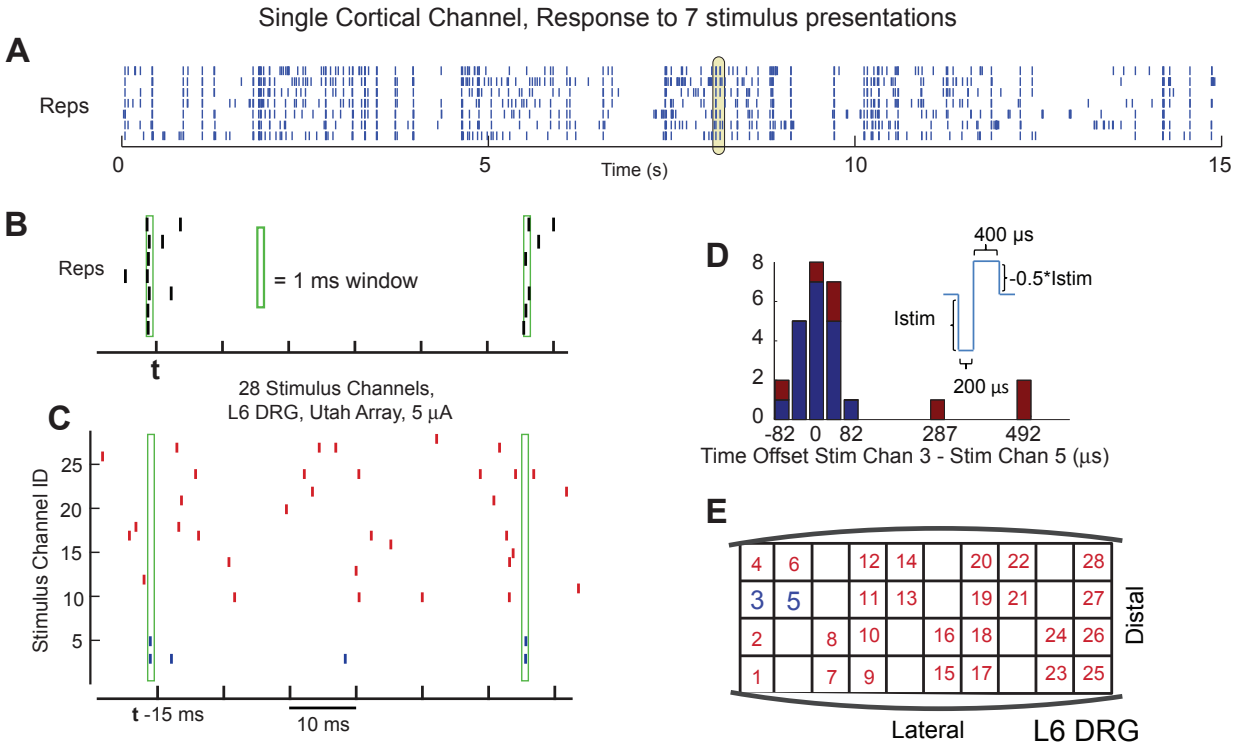

Figure 5.4: Unexpected recruitment from simultaneous stimulation. (A) Example response of a single cortical channel to seven presentations of a replay stimulus. From this response it appears like there are highly synchronized cortical responses. (B) A closer view of a section of this response indicates that these responses are tightly time locked. Any time the cortical channel elicited a response to 5 or more of the 7 stimuli within a 1 ms window, the response was considered "reliable." This occurred 42 times. (C) The stimulus that elicited the response shown in (B). After correcting for conduction delays it appears that this response is due to simultaneous stimulation on stimulus channels 3 and 5. (D) Of 26 stimulus presentations of channels 3 & 5 that occurred within 1 ms of each other, 23 occurred within 200 µs such that the cathodic pulses would be overlapping, and 19 of these elicited a reliable response (blue). Stimulus channel 3 occurred by itself (without stimulus channel 5) 231 times, of which 3 of these stimuli were within 1 ms of the appropriate conduction delay for having elicited a reliable response. Similarly, channel 5 occurred 53 times without channel 3, and again 3 of these times might have elicited reliable responses. (E) Spatially channels 3 and 5 are located close together (400 µm apart) suggesting that simultaneous stimulation might recruit additional neurons.

In a different experimental session, the relative timings of the stimuli were intentionally manipulated during replay stimulation (cat 2). First, cortical recordings were made during a normal presentation of a replay stimulus. Following this trial, a stimulus offset of 0 – 10 ms was

applied to each stimulus channel. The offsets were chosen to minimize simultaneous stimulation on any pair of channels. Since any stimulus channel was at most only 5 ms away from the group mean, the coarse spatio-temporal stimulus pattern was maintained.

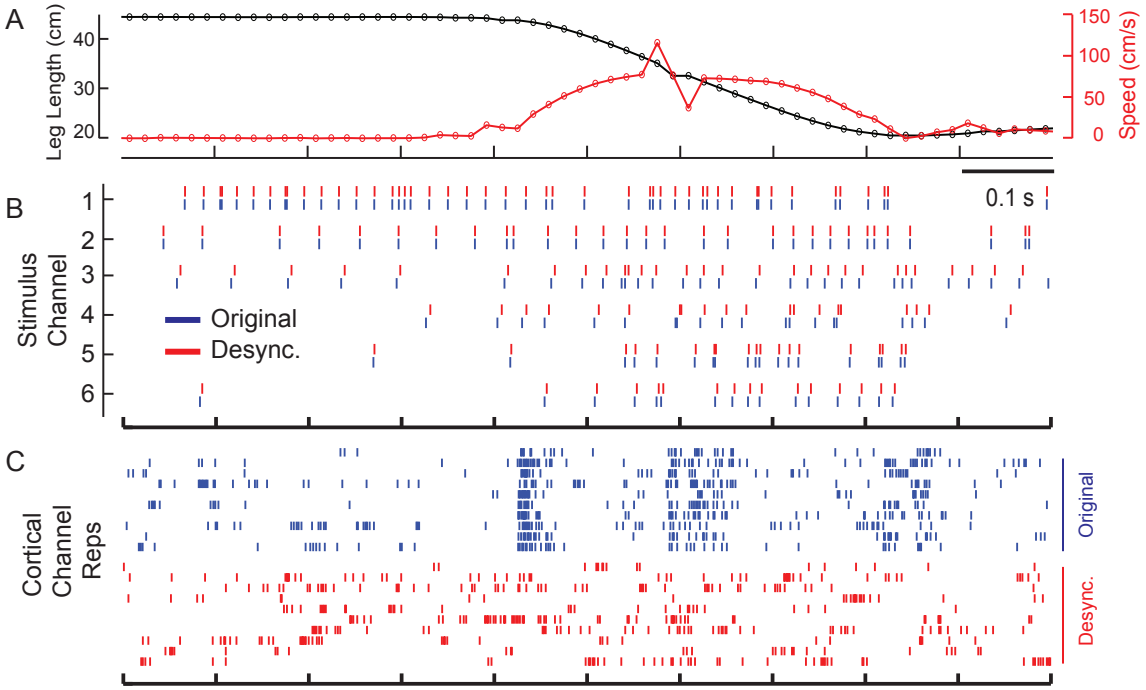

Figure 5.5: Stimulus timing manipulation (cat 2). Only one second of data is shown to highlight the small stimulus timing changes made. (A) The hindlimb was manipulated in a flexion-extension pattern. (B) The response to this passive movement was measured in the L6 DRG (32 channels, only 6 shown) and used as the basis for replay stimulation. In a second trial each stimulus channel was assigned a stimulus offset between -5 and 5 ms. For each stimulus channel, each stimulus pulse on the channel was shifted by the channel offset amount relative to a global stimulus time. Offsets for each stimulus channel were chosen so as to try and minimize simultaneous stimulation between channels. (C) Cortical response on a single channel to the original replay stimulus (10 reps) and the desychronized stimulus (10 reps) at 10 μA. There is a large increase in activity about halfway through the shown data, which is only present when the original simultaneous stimuli are present. The cortical channel responds strongly to movement onset, as well as some small perturbation (mid-flexion), and finally a bit as the movement stops. This type of result was seen on other cortical channels as well and serves as motivation for exploring the changes in neural recruitment that occur during simultaneous stimulation.

Figure 5.5 shows the results of this manipulation for a single cortical channel. There was a strong response to the original replay stimulus that corresponded with a response during movement of the limb. After desynchronization of the stimuli, the response was eliminated.

It is possible that the changes in activity as measured in somatosensory cortex could be due to changes in neural recruitment or changes in recruitment of downstream neurons from synaptic integration (or both). This result suggests that a better understanding of neural recruitment during simultaneous and near-simultaneous stimulation is required and that it is important to examining the integrative properties of synapses in the pathway. This first issue will be examined in Chapter 6.

5.5 DISCUSSION

A stimulation approach in which primary afferent recordings serve as the basis for stimulation was developed. As an initial test of the stimulation paradigm, the instantaneous stimulation rate and the spatial organization of the stimuli were manipulated to determine their impact on the evoked cortical response as compared to passive movement.

5.5.1 Manipulation of the Stimulus Rate

Increasing the instantaneous stimulus rate from 1x to 4x led to an increase in replay correlation values. This effect was not present at the population level at 5 μA, but was expressed at higher stimulus amplitudes. It is possible that at 5 μA insufficient neuronal recruitment occurred, limiting the discernible impact of increased rate across the cortical population. The largest

increase in correlation values occurred at 7 μA. It is tempting to think that 7 μA might show the largest effect given our hypothesized mechanism of action; that it is possible to replace a lack of spatial input (spatial summation) with increased temporal summation. This relationship has been anecdotally observed in amputee patients where lower stimulus amplitudes require a higher range of stimulus rates (Dhillon et al. 2005). Low stimulation amplitudes are meant to make the stimulus more realistic, and as such, higher stimulus rates may be needed to compensate. Although 7 μA showed the highest correlation differences between 1x and 4x, it was not significantly different than 15 μA ($p = 0.4068$, t-test).

Perhaps surprisingly, and contrary to the example shown in Figure 5.3, there was no significant difference in replay correlation values between 1x and 8x. This result corroborates the results seen in Figure 4.2, where there was a decrease in detectable stimulus channels at high stimulus rates, following an initial increase when transitioning from 10 to 100 pps.

Three considerations should be kept in mind in the interpretation of these results. First, the data presented here come from a small sample size further experiments should be conducted before definitive conclusions can be made. Second, the population level statistics do not necessarily represent what occurs on individual channels. At the single channel level, examples can be found that both support and refute the original hypotheses. Because of these observations, a major challenge that remains to be solved is understanding why stimulus rate scaling, or any other manipulation, can be effective on some cortical channels but perform poorly on others. Importantly, with multichannel stimulation this could require learning how to adjust stimulus channels on an independent basis, instead of changing the stimulus rate (or amplitude) for all stimulation channels together. Third, rate scaling could have two different types of effects on the nervous system. One impact, which our manipulation is targeting, is changes in recruitment at

the synaptic level. The other impact is a possible change in the number of primary afferent neurons that are recruited. For an increase in stimulus rate the likelihood of coincident stimulation on channels increases, which could lead to a change the recruited neural tissue. If additional neural tissue is recruited during simultaneous stimulation on multiple channels, and this recruitment is not appropriate, it could explain the observed decrease in performance at the 8x stimulus rate.

5.5.2 Shuffling the spatial location of stimuli

Shuffling the stimuli resulted in changes in the cortical response as would be expected if significantly different stimulus profiles are spatially swapped. However, shuffling the stimuli did not lead to a statistical decline in the replay correlation values. This suggests that the 'replay' nature of the stimulus is minimal and that the precise spatial pattern of the stimulation was less important than the overall temporal pattern. It is possible that with more stimulus channels, smaller stimulus amplitudes on those channels, and more selectivity when choosing neurons to stimulate, that the ‘replay’ nature of the stimulus might become more important. These changes might lead to a higher fidelity replay stimulus, and subsequently a significant drop in performance when shuffling the stimuli.

Shuffling the stimuli did not always lead to lower replay correlation values. As an example, Figure 5.3 shows that the replay correlation values were slightly lower for the shuffled conditions. Similar to rate scaling, some cortical channels had higher replay correlation values without shuffling, whereas others had higher values with shuffling. Figure 5.6 shows an example from the same trial where the replay correlation was higher than the shuffle correlation for one cortical channel, but where the shuffle correlation was higher than the replay correlation on a

different cortical channel. The top row (blue) is the response of these channels to passive movement, the second row (green) is the response to a replay stimulus at 10 μA and 4x rate, and the third row (red) at 10 μA and 4x rate, but with the stimuli shuffled. For the first cortical channel, shuffling the stimulus led to a decrease in the replay correlation value. However, for the second cortical channel, the same shuffling led to an increase in the replay correlation value. This inconsistent change was observed frequently, both across different cortical channels, as well as within a single cortical channel where one phase of the response might improve (become more similar to the original response) while another phase would decline (become less like the original response). This type of inconsistent response across all channels highlights the need to conduct finer scale manipulations, rather than changing stimuli on all stimulus channels at the same time.

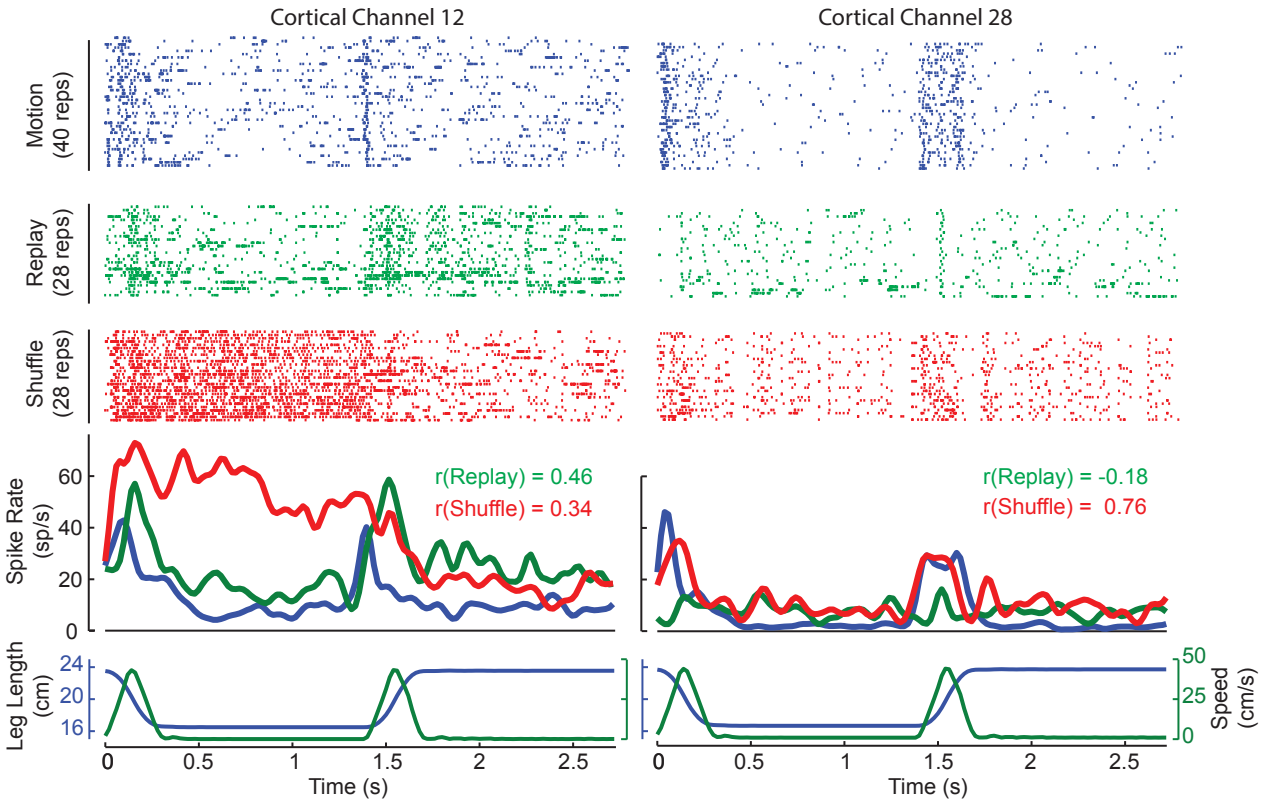

Figure 5.6: Different cortical results from the same stimulus manipulations. Cortical response on two different electrode channels to the same passive movement, replay stimulus, and shuffling of that replay stimulus. Shuffling the replay stimulus led to a decrease in replay correlation for cortical channel 12 (left) while at the same time leading to an increase in replay correlation for another cortical channel (28, right). The top row of responses indicates the cortical response on each channel to passive movement (blue). For channel 12, the response to the replay stimulus (2nd row, green) is more similar to the original response than is the shuffled stimulus (3rd row, red). The opposite is true for cortical channel 28. Smoothed firing rates help to illustrate this effect. The kinematics which led to the passive movement response are shown for reference.

5.5.3 Increasing stimulus amplitude to increase fidelity

From the results in Table 5.2 it is tempting to think that an increase in stimulation amplitude would continue to lead to improved correlation values. Whether this would happen or not remains to be seen. However we expect that the experimental paradigm described here would demonstrate that simply increasing the stimulus amplitude would result in physiologically

inappropriate results. In general it is expected that larger stimulus amplitudes would not be preferable to the subject, since large synchronous coactivation of many primary afferents is unnatural. At high stimulus amplitudes, primary afferent microstimulation has been reported to elicit unnatural, electric sensations (Dhillon et al. 2004).

The stimulation amplitude in our acute studies (cat 1 and others) was limited to 15 μA as we found that higher stimulus amplitudes evoked significant leg movements. The maximum stimulus amplitude was found to be even less in chronic experiments (cat 2 and others) under dexmedetomidine, where the maximum stimulus amplitude was roughly 6 – 8 μA, particularly at higher stimulation rates. To some extent the production of force should be expected and might actually serve as an indicator of appropriate feedback. It is estimated that 35% of the force produced in the cat ankle extensors during stance is produced by reflexes due to muscle length changes (Stein et al. 2000). Thus, lack of movement might be indicative of a failure to adequately convey proprioceptive information.

5.5.4 Experimental Difficulties

With the exception of Figure 5.5, the results presented in this chapter are from a single experiment. This 'replay' stimulation paradigm was attempted in nine different acute experiments, five in which it was the primary goal of the experiment. The following sections describe some of the difficulties encountered in achieving the desired experimental goals.

5.5.4.1 Difficulties: Electrode Mapping

Due to hardware limitations, it was necessary to switch cabling between the recording and stimulation components of the experiments. The hardware numbering of an electrode during recording and stimulation could be different because of this switch. The task of matching system hardware to physical electrode location is known colloquially as the 'electrode mapping problem', and this functionality is typically poorly supported by hardware vendors. This problem was made even more difficult as hardware manufacturers frequently provide incorrect mapping documentation. This occurred either through misinterpretation of connection diagrams from other manufacturers or simple mistakes made within the company. The majority of these mistakes involved confusing pin-out diagrams where it was unclear which part of the connector (male or female) the documentation was referring to, and which perspective the connector was being viewed from (looking at the pins from the top or bottom of the connector). Even when mapping diagrams were correct, incorrect connections as allowed by non-keyed or poorly keyed connectors, meant errors would occur. Ultimately for the replay stimulation paradigm this led to a several experiments in which the replay stimulation paradigm was performed incorrectly. After these failures, significant effort went into designing and implementing documentation and a custom software system that allowed us to easily handle differences in mapping across different devices.

5.5.4.2 Difficulties: Hardware and Software

There was also considerable effort that when into designing and/or using appropriate hardware and software. When these experiments were conceived, there was a general lack of availability of programmable multi-channel microstimulators. Seven years later there have been some improvements, but significant problems remain.

Initially, a switching-headstage that allowed rapid transitions between stimulation and recording, was used during our experiments. However, it was discovered through unexplained 'off' responses in cortical recordings, that during switching from recording to stimulation, or vice-versa, a large electrical transient was delivered to the tissue that led to significant neural activation. This type of transient discharge was later confirmed on the bench and has since been observed in numerous other situations, usually during device hookup, software failure, or connection of monitoring cables to a theoretically electrically isolated stimulus unit. The electrical problems observed with the switching headstage and its physically large size, meant that use of the switching headstage was discontinued, thus leading to the electrode mapping issues described previously.

Monitoring the stimulus output was, and continues to be, an issue with most stimulators. The MS16 stimulator (TDT) had no built in feedback systems, and the stimulus controller battery only lasted 2-3 hours, whereas the experiments described here would frequently take 12-36 hours to complete. Once the battery failed, no stimulation would be delivered. Unless LED indicators on the front of the stimulator were carefully monitored, it became impossible to tell in which trials electrical stimulation had occurred, as a non-response in cortex indicated either an inappropriate stimulation parameter or battery failure. External batteries were eventually purchased to mitigate this problem. Although it has some bidirectional communication, the new TDT stimulator (IZ2) has no programmatically queryable battery status. It also has separate positive and negative voltage batteries. During an experiment one of the batteries failed, leading to a railing of the stimulus output to the other pole. Although the system was aware of the low battery, as indicated by a status LED, the stimulator did not shut down gracefully. This caused significant tissue and electrode damage to occur.

In addition to monitoring the stimulator battery, it is also desirable to be able to monitor the stimulus voltage and delivered current. The MS16 had no such abilities and the IZ2 provided the ability to monitor voltage for 8 of 32 stimulus channels. Custom hardware code was written to maximize observations of stimulus pulses. For random stimulation across all 32 stimulus channels in a single trial, this meant changing the monitoring bank so that just prior to each stimulus pulse the bank was monitoring the appropriate channel. Although not used in these experiments, other stimulators (Blackrock CereStim R96 and Plexon Stimulator 2.0) also lack proper monitoring functionality. Ripple LLC has recently added stimulation support to their Grapevine system, putatively with stimulus feedback on all channels, although our lab has yet to test this system. The ability to monitor stimuli would provide confidence that the experiment was carried out as expected.

Automation of stimulus software was critical to collecting sufficient data for analysis. During initial experiments each trial was started and stopped manually. Stimulus parameters were also adjusted manually. This led to collecting significantly less data, approximately 1/10 the amount that was captured when automated. Additionally, manual entry errors often led to omission of different stimulus conditions.

5.6 CONCLUSION

From the outset there was no expectation and no requirement that stimulation would be able to activate only the neurons that had been recorded and therefore truly replay the pattern of activation (on those neurons) that had occurred during passive movement of the limb. Indeed, given the stimulus amplitudes used, we expect that the replay stimulus activated many more

neurons than just those that had been recorded. If however neurons in the DRG have some somatotopy, then the lack of stimulation specificity might be less problematic.

A primary advantage of the replay stimulation paradigm is that it significantly reduces the complexity of stimulus design. An alternative stimulation paradigm would be to generate the stimulus pattern for each channel based on models of how a population of primary afferents should respond to the passive movement shown. This approach lacks spatial specificity but given the shuffling results in which shuffling the stimuli did not lead to a decrease in replay correlation values, this might not be an issue. This would also mitigate the problem of spike sorting and selection of which action potentials should be included in the stimuli. A hybrid approach might be beneficial, in which model parameters for generating a stimulus are based on the type of recordings observed (e.g. for selection of afferent type).

Ultimately it was clear that the cortical responses to replay stimulation were generally not the same as those recorded during passive movement, however responses were observable. This suggests that cortical recordings under anesthesia, even though not ideal, would be able to indicate relative improvements between stimulus conditions. Initial results on rate scaling would support this claim. Further optimization of the evoked cortical response will likely require changes to individual stimulus channels, as results like Figure 5.6 indicate that a global change may simultaneously improve and worsen the response on different cortical channels. The ability to generalize the results from this type of channel by channel optimization and apply them towards clinical use is unclear, although certainly not impossible.

6.0 THE IMPACT OF COINCIDENT STIMULUS TIMING ON ELECTRODE INDEPENDENCE DURING MULTI-CHANNEL MICROSTIMULATION.

This chapter has been prepared for submission to the Journal of Neural Engineering. The citation will be: *Hokanson JA, Gaunt RA, Weber DJ (2014) The Impact of Coincident Stimulus Timing on Electrode Independence During Multi-Channel Microstimulation. J Neural Eng*.

6.1 INTRODUCTION

Microstimulation using arrays of microelectrodes is being investigated as a technique to modulate neural activity with a range of potential applications including restoration of somatosensation, vision, hearing and motor functions (Weber et al. 2011, Davis et al. 2012, Middlebrooks and Snyder 2007, Normann et al. 2012). For simplicity, many stimulation paradigms using these arrays treat each electrode as an independent source (Normann et al. 2012, Horch and Dhillon 2006). In these paradigms, stimulation through each electrode is thought to activate a discrete set of neural tissue that elicits a functional outcome such as a muscle contraction or sensory percept. Without explicit scheduling of stimuli to avoid simultaneous stimulation, these stimulation paradigms may occasionally (or often) deliver stimulus pulses simultaneously on two or more electrodes. Depending upon the stimulus parameters, tissue

properties, and the configuration of the electrodes, this may lead to significant changes in neural recruitment and the subsequent functional outcomes. For macroelectrodes, these interactions are known to be significant (Fisher et al. 2013, Horsager et al. 2010). If these interactions effects persist at the microelectrode scale, it may become difficult to achieve a desired function, or interpret the results of multichannel microstimulation experiments (Nowak and Bullier 1998, Histed et al. 2009).

In the field of cochlear implants, it has been known for many years that the electric field interactions from neighboring channels must be taken into account when creating stimulation patterns. One of the earliest stimulation paradigms that took this into account is known as continuous-interleaved-stimulation, or CIS (Wilson, 1991). As the name implies, CIS interleaves stimulation on neighboring channels to avoid simultaneous stimulation. This is thought to improve implant performance by providing a more reliable mapping between individual electrodes (and the pitch they are trying to convey), the activated neural tissue, and the perceptions that they elicit. Although these interactions were originally thought to be undesirable, recent stimulation paradigms have begun using these interaction effects to improve feedback (Firszt et al. 2009). Similarly, nerve cuffs for motor stimulation have also tried to take advantage of electric field interactions to target different compartments of the nerve (Grill et al. 1991, Brill and Tyler 2011).

In contrast to cochlear implants and nerve cuffs, penetrating array microelectrodes are typically much closer to excitable tissue than they are to each other. In this case it is unclear whether electric field interactions will play a significant role as they have in other stimulation contexts when using functionally relevant stimulation parameters. For example, in the context of a sensory feedback neuroprosthesis, it may be desirable to only recruit a few neurons to provide

a more realistic percept (Ochoa and Torebjork 1983). However, it is unclear if simultaneous stimulation on two or more electrodes will significantly alter the recruitment patterns at the small amplitudes associated with microstimulation.

Even if a stimulation paradigm explicitly avoids simultaneous stimulation on neighboring channels, it may be impossible to avoid simultaneous stimulation on any set of two or more electrodes in the array. As electrode spacing is reduced (Wark et al. 2013), and more electrodes are able to fit into the same volume, this may become even more of an issue. A decrease in the relative distance between any pair of electrodes will make it more likely that simultaneous stimulation will have a significant impact. Further, if many electrodes are all stimulated at fixed rates, it may become impossible to avoid simultaneous stimulation on electrodes within an array. Therefore it is necessary to understand how different stimulus conditions will impact changes in recruitment between independent and simultaneous stimulation. A better understanding of the changes should allow for improved design of stimulus paradigms that wish to avoid or take advantage of these interactions.

The primary aim of this paper is to determine the extent to which simultaneous stimulation causes changes in neural recruitment compared to the independent stimulation case. We will also briefly consider the results from the perspective of trying to enhance neural recruitment using these interaction effects. In order to address these issues, a computational model has been developed to understand under what conditions, and to what extent, electric field interactions play a role in changing the number of recruited neurons in a peripheral nerve as compared to cases in which all electrodes are temporally independent.

The main finding of this study is that even at low stimulus intensities (2 μA amplitude, 200 μs primary pulse width) simultaneous stimulation on electrodes 400 μm apart can lead to

activation of twice as many neurons as would have been recruited if the electrodes were stimulated independently. These results show that stimulation interactions are a significant factor that cannot be ignored when designing multichannel microstimulation paradigms. These interactions are more significant with larger pulse widths, smaller electrode spacing, and larger fiber diameters.

6.2 METHODS

6.2.1 Initial Steps: Determining the response of a cell to a stimulus

A two-step approach, as pioneered by McNeal (1976), was used to determine neural activation of cells in response to a variety of stimulus conditions. For a single cell and set of stimulus parameters, the first step to determining neural activation involved computing the voltage applied to the cell from the stimulating electrode(s). Second, a simulation of the cell's response to the applied voltage was performed to determine stimulus was sufficient to elicit an action potential for each neuron under those stimulus conditions.

The electrodes were modeled as point sources (McIntyre and Grill 2001) and the tissue was modeled as an infinite, homogenous, anisotropic medium with longitudinal resistivity of 175 Ω-cm (ρ_z) and a transverse resistivity of 1211 Ω-cm (ρ_x and ρ_y) (Ranck and BeMent 1965, Choi et al. 2001). The electric field from a single electrode was computed using Equation 6.1 simplified from a derivation given by Li and Uren (1998). The simplification assumes the resistivity tensor to be a diagonal matrix, or more explicitly, that the principal axes of resistivity are aligned with our coordinate system (also see Equation 1 in Nicholson 1965).

$$V(x,y,z) = \frac{10 * \sqrt{\rho_x \rho_y \rho_z}\, I_{stim}}{4\pi\sqrt{\rho_x(\Delta x)^2 + \rho_y(\Delta y)^2 + \rho_z(\Delta z)^2}}$$

(6.1)

V (mV) indicates the voltage at a point that is a given distance away from the stimulating electrode relative to a distant ground. I_{stim} (μA) represents the stimulation current amplitude for each phase. When the phase changes, the discrete neural solver (NEURON) is updated with a new set of external voltages to apply. The delta values are computed as the difference in location between each electrode and the point where V is being computed (each discrete element of the model, units: μm). The applied electric field from multiple electrodes is computed as the sum of the fields from each individual electrode (McNeal 1976, Peterson, 2011). Neurons run parallel to the z-axis.

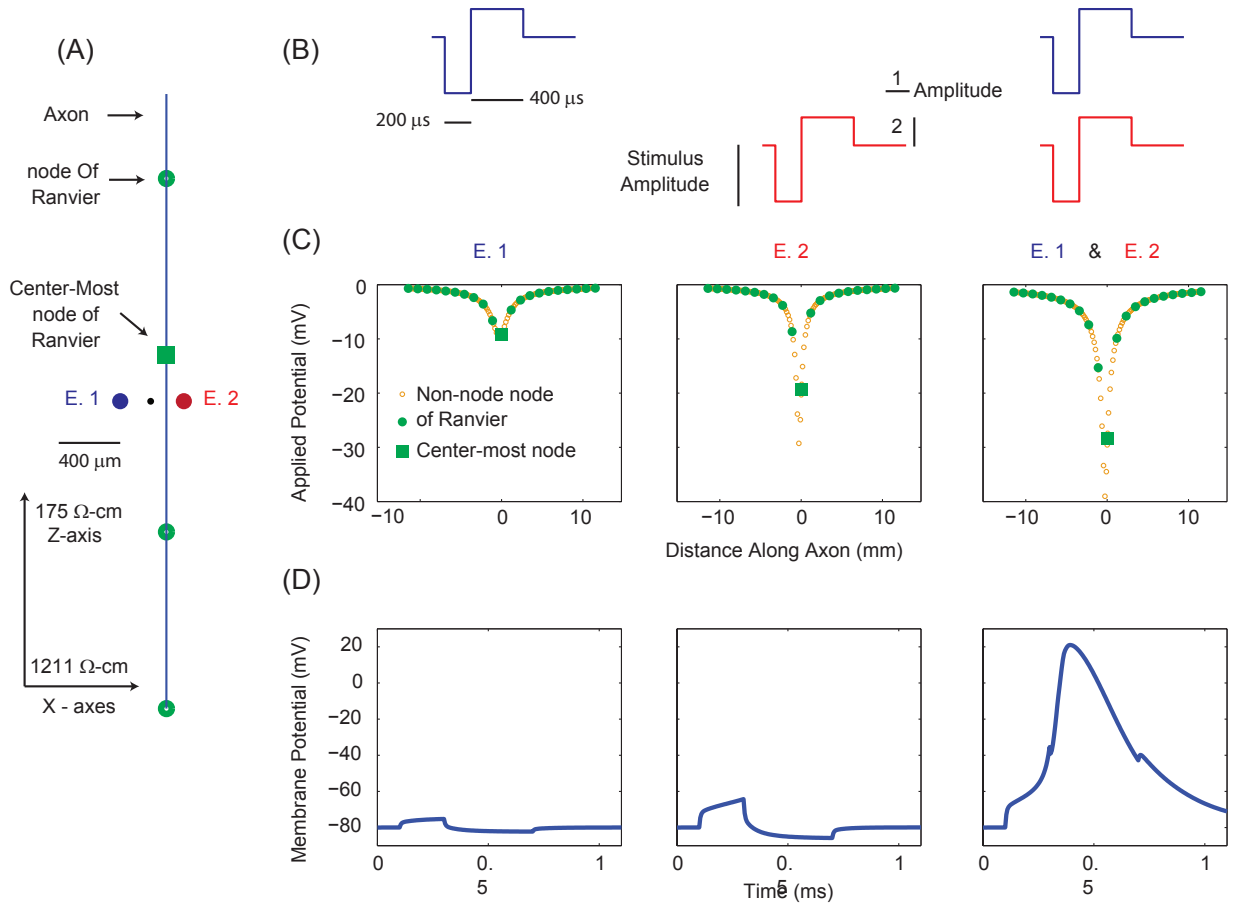

Figure 6.1: Simultaneous versus independent stimulation of a single cell. (A) Spatial layout of the model system. Axons run parallel to the Z-axis. Resistivity along the Z-axis is 175 Ω-cm. Resistivity orthogonal to this is 1211 Ω-cm. A 10 µm diameter fiber is shown with nodes of Ranvier regularly spaced at 1150 µm intervals. In this example, the center node of Ranvier is located at the coordinates [100, 0, 300], and two electrodes are located at [-200, 0, 0] (electrode 1) and [200, 0, 0] (electrode 2). A small black dot indicates the origin. The electrodes are thus separated by 400 µm along the x-axis (transverse pairing). (B) In this example we consider stimulation on electrode 1 and electrode 2, at different times, along with stimulation on both electrodes simultaneously. (C) The potential applied to the model from an 8 µA stimulus. Only the cathodic phase is shown. The anodic phase would have opposite polarity and half the amplitude. The potentials are computed using Equation 6.1. In the case of simultaneous stimulation, the applied potential is the sum of the first two cases. (D) Membrane potential at the centermost node of Ranvier during the simulation. Each electrode individually is unable to cause an action potential. Simultaneous stimulation is sufficient to elicit an action potential at this center node.

Figure 6.1 illustrates the orientation of the coordinate system used for the rest of this paper, as well as some additional setup information. Figure 6.1A shows a portion of an axon oriented parallel to the z-axis. Its centermost node is located at coordinates [100, 0, 300]. The default stimulus waveforms used in this paper are shown in Figure 6.1B. The resulting potentials from applying the first phase of the stimuli from Figure 6.1B (via Equation 6.1) to the entire discrete model of the cell are shown in Figure 6.1C. Although the stimulus waveform is the same for the first and second electrodes, the second electrode is closer to the cell and thus the electric potential along the cell from the second electrode is larger. Stimuli are computed using Equation 6.1. The applied potential for simultaneous stimulation is the sum of the stimuli from both electrodes. Figure 6.1D shows the membrane potential at the center most node of Ranvier of the cell model during the simulation. In this case, when each electrode stimulates independently, the stimulus is insufficient to elicit an action potential. When both electrodes deliver stimulation simultaneously, the cell responds.

Each neuron was modeled using the program NEURON version 7.2 (Hines and Carnevale, 1997). For this analysis, only the axons of cells were modeled (peripheral nerve model). Each axon consisted of 21 nodes of Ranvier and 20 internodal regions. The morphology and channel kinetics came from McIntyre et. al. 2002 as implemented in Model DB #3810 (Hines et al. 2004). Simulations were executed with a fixed time step of 5 μs using the default integration method (backward Euler). The simulation duration was set to 0.4 ms after the final stimulus phase so as to allow an action potential to exceed threshold. This was sufficient time for all tested fiber diameters to propagate an action potential from the site of initiation to the end of the model.

Biphasic stimuli (Figure 6.1B), with a cathodic leading phase followed immediately by an anodic phase (inter-phase delay = 0) of half the amplitude and twice the duration were used unless stated otherwise. Reported stimulus amplitudes correspond to the magnitude of the cathodic phase. The default cathodic pulse width was set to 200 μs. This stimulus waveform was previously used experimentally in our lab (Gaunt et. al. 2009). Stimulus amplitudes were varied from 1 – 30 μA.

6.2.2 Examining the Population Response: Computing a threshold lookup table

It is important to examine recruitment changes at the population level, not just for a single neuron as the results from the population may be difficult to infer from a single neuron (e.g. see McIntyre & Grill 1999). To this end it is common to examine recruitment of a randomly positioned population of neurons (Schiefer et al. 2008, Mahnam et al. 2008). Instead, in this study, thresholds were computed on a uniform grid and details of this approach are described in the following paragraphs. The grid approach allowed for easier computation of the results from multiple channels, each stimulating independently (See Appendix C).

For each tested stimulus condition, the minimum (threshold) stimulus amplitude required to fire an action potential for a neuron of a particular fiber diameter whose center-most node of Ranvier was located at a particular 3D location relative to the stimulating electrode(s) was computed. For the same neuron, this process was repeated in a uniform 3D grid in steps of 20 μm. In preliminary testing this resolution was determined to be an appropriate tradeoff between computation time and accuracy. From selected testing at finer resolutions, interpolation of thresholds on this grid is expected to lead to less than a 0.1 μA threshold error on average. For distances in which a part of the axon was right next to the electrode (numerically 0), Equation

6.1 would yield an infinite stimulus. As a workaround in those cases the cell was moved 1 μm away from the electrode in question. Given the scales the model covered it is expected that moving the cell 1 μm had negligible impact on the results.

Stimulus threshold was determined when a stimulus elicited a propagating action potential. This was detected when the membrane potential at the last node of Ranvier in the model exceeded 10 mV (see Figure 6.1D for referencing the typical action potential shape). A binary search algorithm was used to determine threshold. The threshold value was defined as halfway between maximal subthreshold and minimum suprathreshold amplitudes. The search algorithm stopped when the difference between the two bounding values was less than 0.1 μA. Importantly, subsequent analysis assumed that the cell would respond at all higher stimulus amplitudes (i.e. propagate an action potential). This is not necessarily a valid assumption for monophasic cathodic stimuli (Rattay 1987) but in our experience this assumption holds for biphasic stimuli. Additional tests at 30 μA (i.e. the highest stimulus amplitude used in most figures) confirmed that this assumption held. When two electrodes were stimulated simultaneously, the amplitude of all electrodes was always equal.

6.2.3 Volume of Tissue Activated – proportional to # of neurons recruited

Using this methodology it is also possible to compute the volume of tissue that would be activated by stimulation on one more electrodes at particular stimulus amplitude. The volume of tissue activated (VTA, see Bourbeau et al. 2011, Butson et al. 2007) is a more general term for the more commonly used "sphere of activation" and is preferable in cases in which the recruitment volume is non-spherical. Neurons that have at least one node of Ranvier within this volume will fire an action potential in response to the stimulus. Although the shape of this

volume may be interesting in some cases (e.g. see Butson et al. 2007) our analysis for the most part will not focus on shape, but rather on size of the VTA.

To compute the VTA, the gridded threshold results were numerically integrated. Prior to integration, the threshold values were upsampled via linear interpolation from the original 20 μm resolution to 1 μm in order to more accurately compute the VTA. For each stimulus amplitude in question, all points with thresholds less than the amplitude were counted. To ensure a correctly computed VTA, several additional steps were needed to account for edge cases and are described in Appendix B.

6.2.4 Computing the impact of simultaneous stimulation

The VTA were computed for a set of electrodes with two different timing conditions. In the first timing condition, independent stimulation, the stimulus pulses from each electrode were offset in time so that activation volumes were independent. In the second condition, the stimulus pulses were presented to the tissue simultaneously, at the same amplitude.

To examine the effect of stimulus timing, we computed the ratio of tissue activated from simultaneous stimulation case relative to the independent stimulation case. The ratio of these two values, referred to as the volume ratio, is an indication of how much more neural tissue is recruited due to simultaneous stimulation. The following is an example of the calculation for a pair of electrodes.

$$Volume\ Ratio = \frac{Volume_{simultaneous}}{Volume_{independent}} = \frac{Volume_{(1,2)}}{Volume_{(1)} \cup Volume_{(2)}} \tag{6.2}$$

$Volume_{(1,2)}$ represents the volume of tissue activated by both electrodes stimulating simultaneously whereas $Volume_{(1)}$ and $Volume_{(2)}$ represent the volumes of tissue activated by each electrode, stimulating independently. For details on calculating the union of these two volumes see Appendix C. The VTA was also limited in the z-axis to prevent double counting different nodes of Ranvier from the same neuron (See Appendix B).

For a single cell type uniformly distributed through the tissue, the volume itself is proportional to the number of neurons that we would expect on average to recruit given the stimulus (Bourbeau et al. 2011). For example, if we double the VTA via some change in stimulus, on average we would expect to double the number of neurons that we recruited via that change. Since this scaling factor is constant for the numerator and denominator of the volume ratio, the volume ratio is equivalent to a ratio of the average number of neurons recruited during simultaneous stimulation relative to the number recruited during independent stimulation.

A volume ratio of 1 indicates that simultaneous stimulation recruits no more tissue than independent stimulation, whereas a volume ratio of 2 indicates that simultaneous stimulation recruits twice as much tissue as independent stimulation. This equation is easily generalizable to multiple electrodes, in which case the numerator is the volume of tissue activated from all electrodes stimulating simultaneously, and the denominator is the union of all the volumes from independent stimulation.

This entire process is illustrated in Figure 6.2 for a 10 μm diameter fiber (1175 μm internodal distance). Figure 6.2A shows the thresholds for an axon positioned at different locations relative to two electrodes, stimulating independently. The threshold at each location is the lower of the two stimulus thresholds (see union operator in Equation 6.2 and Appendix C) from the two electrodes. The value at each point shows the minimum stimulus amplitude

required to recruit a neuron with a node of Ranvier at that location. Figure 2B shows the recruitment threshold at each point when the electrodes are stimulated simultaneously. The threshold decreases at all locations due to simultaneous stimulation. Figure 6.2C shows the iso-threshold lines from Figure 6.2A and 6.2B at 5, 10, and 15 μA to illustrate the growth in the volume of recruited tissue due to simultaneous stimulation. This process is repeated in Figure 6.2D-F for a transverse pairing of electrodes. The VTAs for the different stimulus conditions and electrode configurations are shown in Figure 6.2G and 6.2H. The ratio of these recruitment profiles produces the volume ratio profiles shown in Figure 6.2I and 6.2J.

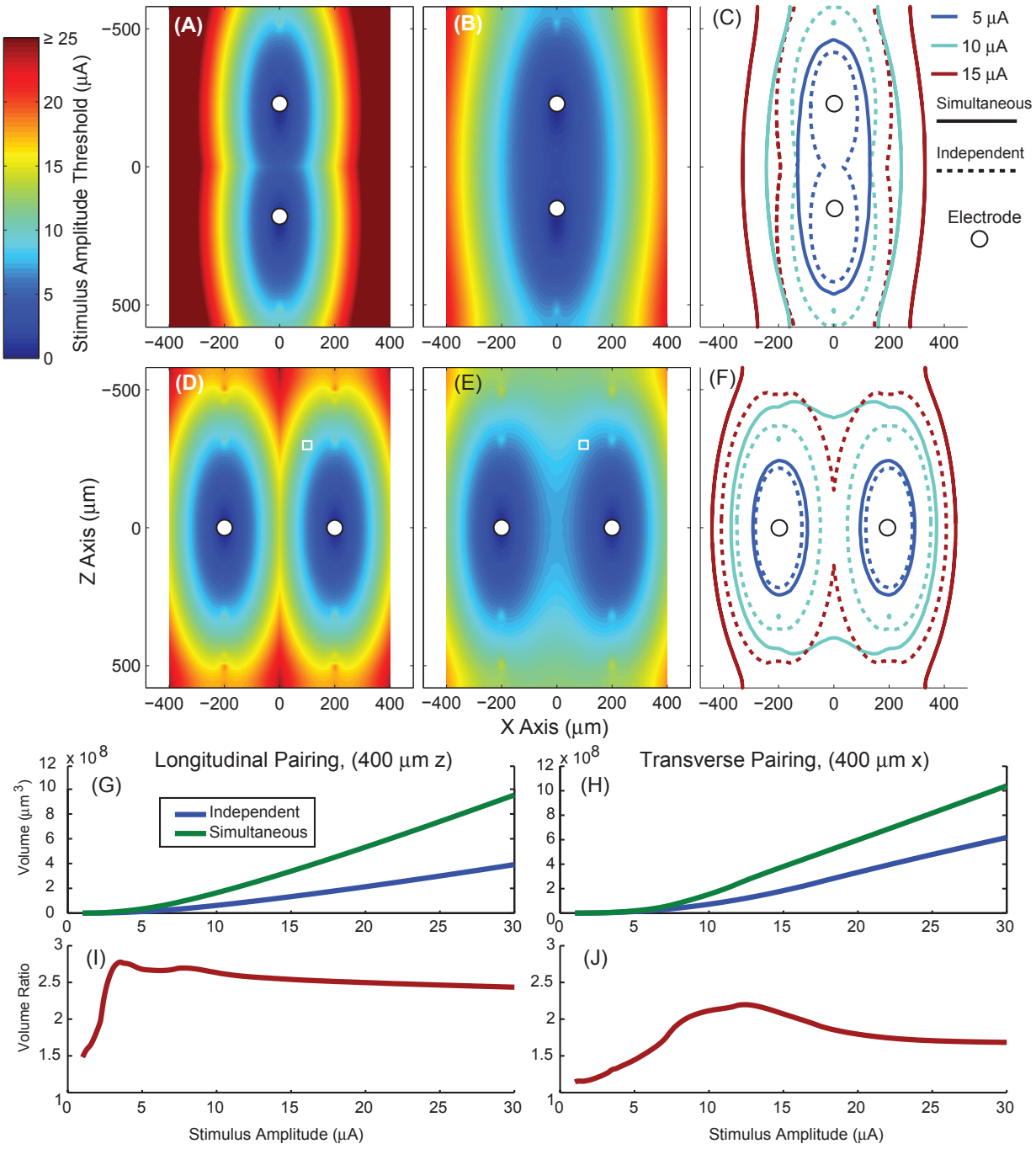

Figure 6.2: Computing the volume ratio. Results for (A),(B),(D) and (E) this figure were computed using a 10 μm diameter fiber. (A) At each location the stimulus threshold of the axon in response to a single electrode stimulus is shown (Independent stimulation case). A single neuron was moved throughout the stimulation space in 20 μm steps to calulate this result. The x-z plane is shown (y = 0) although results were computed in all three dimensions. The final value used during volume integration at each tested cell location was the lowest of any electrodes being considered for simultaneous stimulation (See Appendix C). For panel A the electrodes are separated by 400 μm along the z-axis (longitudinal pairing). The results shown are after upsampling to 1 μm spacing. (B) Similar to (A)

except the threshold at each location is for simultaneous stimulation. (C) Iso-threshold contours at 5, 10, and 15 μA for both the independent and simulataneous stimulation conditions. The solid lines represent the contours for simultaneous stimulation and the dotted lines represent contours for independent stimulation. (D),(E),(F), are the same as (A),(B), and (C) except that they are for a transverse pair of electrodes spaced 400 μm apart. Recruitment volumes are shown in (G) and (H) for the longitudinal and transverse pairing respectively. The ratio of recruitment volumes from simultaneous stimulation over independent stimulation produces the output variable of interest, the volume ratio (I, J). Further details on the shape of the volume ratio as a function of stimulus amplitude can be seen in Appendix D. The small circles in panels A-F represent the location of the electrodes. The small white square in panels (D) and (E) matches the spatial location of the center-most node of Ranvier from an axon relative to the electrodes as shown in Figure 6.1. Stimulus thresholds above 25 μA in (A) are saturated on the color scale shown to provide better visual detail for other other panels.

To determine the impact of the variability of axon locations relative to stimulation electrodes as might be encountered in a peripheral nerve, we generated 10000 different random populations of 14 μm diameter fibers. Center-node locations were generated randomly from a uniform distribution, with the range of the locations limited to a 800x800x1400 μm (x,y,z) cube around the stimulus electrodes. Each population consisted of 2038 axons. Fiber diameter and density were based roughly on Eccles and Sherrington (1930, see also Mahnam et al. 2008). For each population, the number of neurons responding to independent and simultaneous stimuli was determined. Thresholds were determined using linear interpolation between the nearest simulated grid locations. The ratio of the number of neurons recruited during simultaneous stimulation over the number of neurons recruited, or neuron ratio, was calculated. Since the number of neurons recruited is on average proportional to the recruitment volume, the volume ratio and average neuron ratio should be equivalent.

6.3 RESULTS

6.3.1 Volume Ratio and Neuron Ratio Equivalence

To determine the impact that different random populations of axons would have on the volume ratio the neuron ratio from different populations of 14 μm fibers was computed. These results are shown in Figure 6.3. At each stimulus amplitude the distribution of observed neuron ratios was broken down into deciles. Larger variation in the neuron ratio was seen at lower stimulus amplitudes, particularly for the longitudinal pairing. The volume and average neuron ratio were shown to be equivalent below 15 μA. However above 15-20 μA, every neuron in the population is recruited causing the neuron ratio to decrease from what would be expected in an infinitely sized population of neurons. Due to variability in population density and extent, the remaining results will be presented in terms of the volume ratio. However deviations may occur at high stimulus amplitudes, particularly for larger diameter fibers where lower stimulus amplitudes will recruit larger volumes of tissue (McNeal 1976).

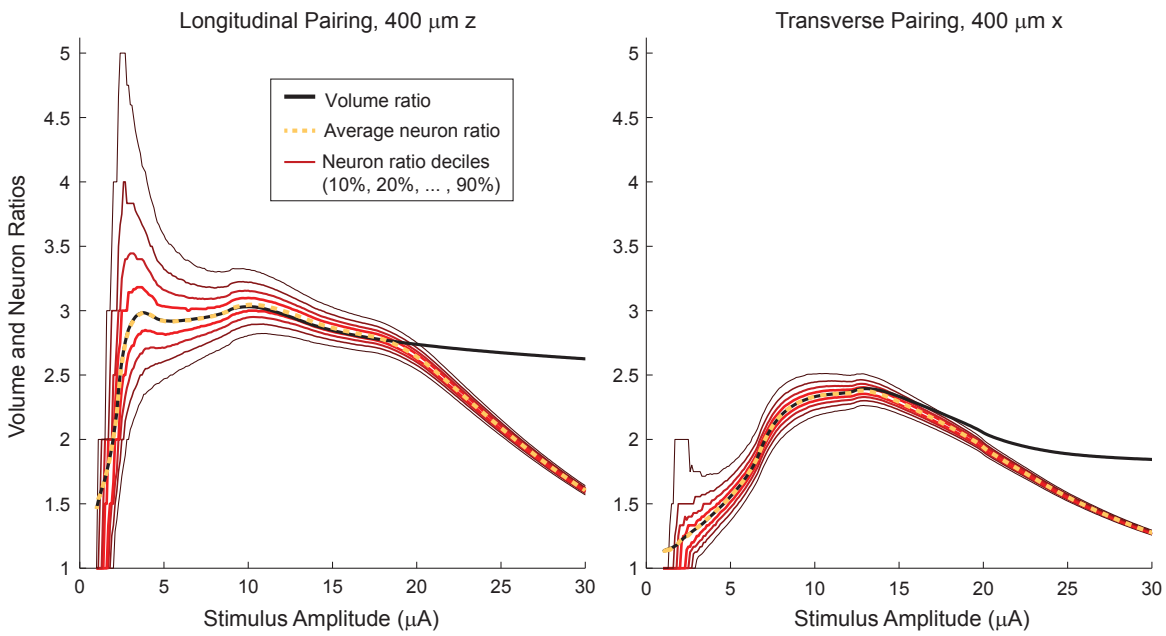

Figure 6.3: Variability in neuron recruitment ratios for a population of 14 μm diameter fibers randomly placed in a 800x800x1400 μm cube. In total, 10000 random populations were generated consisting of 2038 neurons each based on a nodal density of 400 axons for a 400 μm fascicle (Mahnam et al. 2008). Red lines indicate deciles of observed neuron ratios starting at 10% and going to 90%. The average neuron ratio (50%) is shown as a dotted yellow line. The results as predicted from an infinite model (used throughout the rest of the paper, volume ratio) are shown as solid black lines. At smaller stimulus amplitudes, local inhomogeneties in population density lead to more variation in the observed neuron ratios. At higher stimulus amplitudes this effect diminishes and the mean neuron ratios of the random populations approach that expected by the volume ratio. At even higher stimulus amplitudes (> 15-20 μA) the finite nature of the model limits the number of neurons available for recruitment in response to simultaneous stimulation, and the volume ratio decreases from what would be expected with an infinitely large neural population.

6.3.2 Effect of fiber diameter

Peripheral nerves typically contain a wide range of axonal fiber diameters (Boyd and Davey, 1968). Although experimentally we cannot manipulate these fiber diameters, it is important to understand how the results vary depending upon the fiber diameters we encounter in a typical

population. To examine how the volume ratio changes as a function of fiber diameter, we repeated the steps shown in Figure 6.2 for fibers with different diameters. Figure 6.4 shows these results.

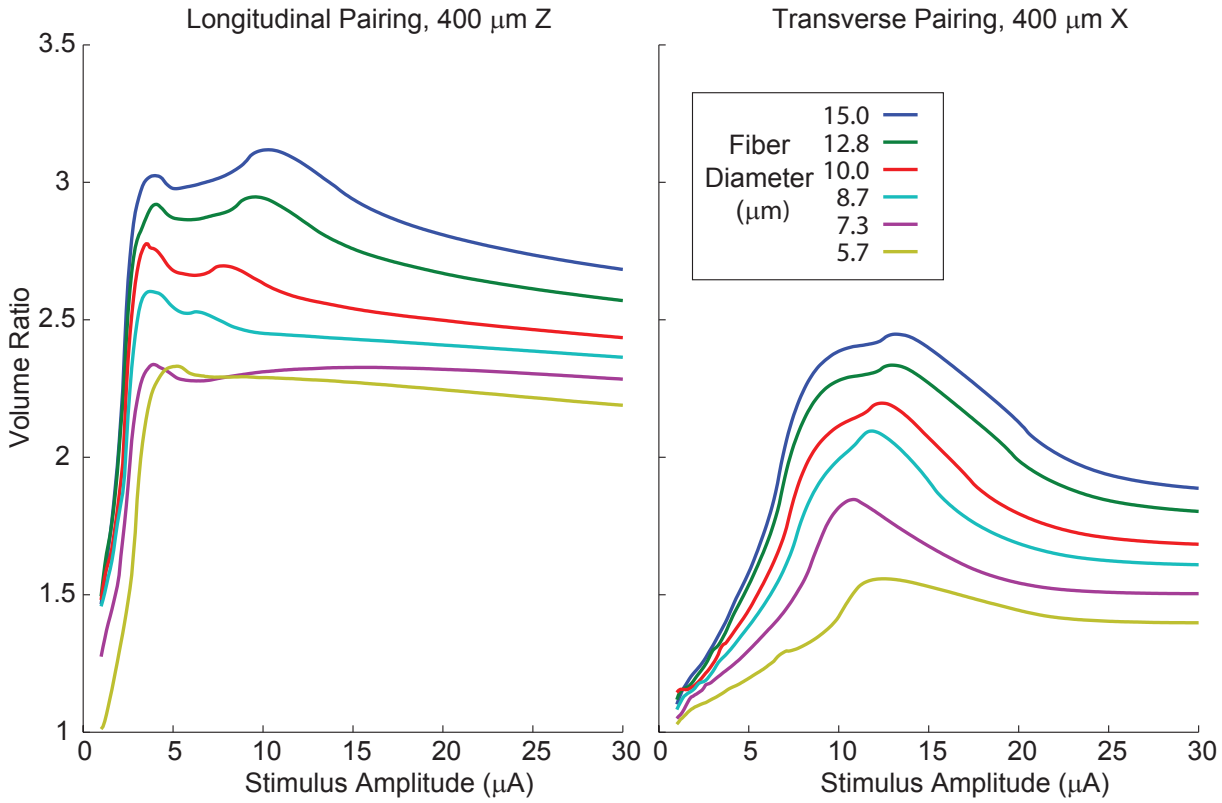

Figure 6.4: Volume ratios as a function of stimulus amplitude and fiber diameter for longitudinal and transverse pairs of electrodes. For the longitudinal pair, the ratios quickly exceed 2 and stay elevated up to the highest stimulus amplitude tested. At all stimulus amplitudes and for all fiber diameters the volume ratios are smaller for the transverse pairing than the longitudinal pairing. The volume ratio also rises at a slower rate in the transverse case. Appendix D explores the factors influencing the shapes of the volume ratio curves as a function of stimulus amplitudes. Figure 6.6 provides further detail on the mechanisms that affect the features of the volume ratio curves.

As was the case for the 10 μm diameter fiber, simultaneous stimulation recruits more neurons than independent stimulation for all tested fiber diameters (volume ratio always greater than 1). However, this effect is stronger for larger diameter fibers than for smaller diameters

fibers across all stimulus amplitudes tested. Longitudinal electrode pairings have larger volume ratios than do transverse electrode pairings. This is because of the lower extracellular resistivity along the main axis of the neuron. Given a pair of electrodes separated by a fixed distance, these electrodes are electrically much closer if separated longitudinally as opposed to transversally. These results demonstrate that the impact of simultaneous stimulation on electrode independence is more important in tissue populations with primarily larger diameter fibers or where activation of large diameter fibers is of primary interest.

6.3.3 Effect of pulse width

In addition to changing stimulus amplitude it is also common to use different stimulus pulse widths. All results presented to this point have used a cathodic pulse width of 200 μs, as described in the methods. Figure 6.5 shows the results of varying stimulus pulse width and amplitude for a 15 μm diameter fiber.

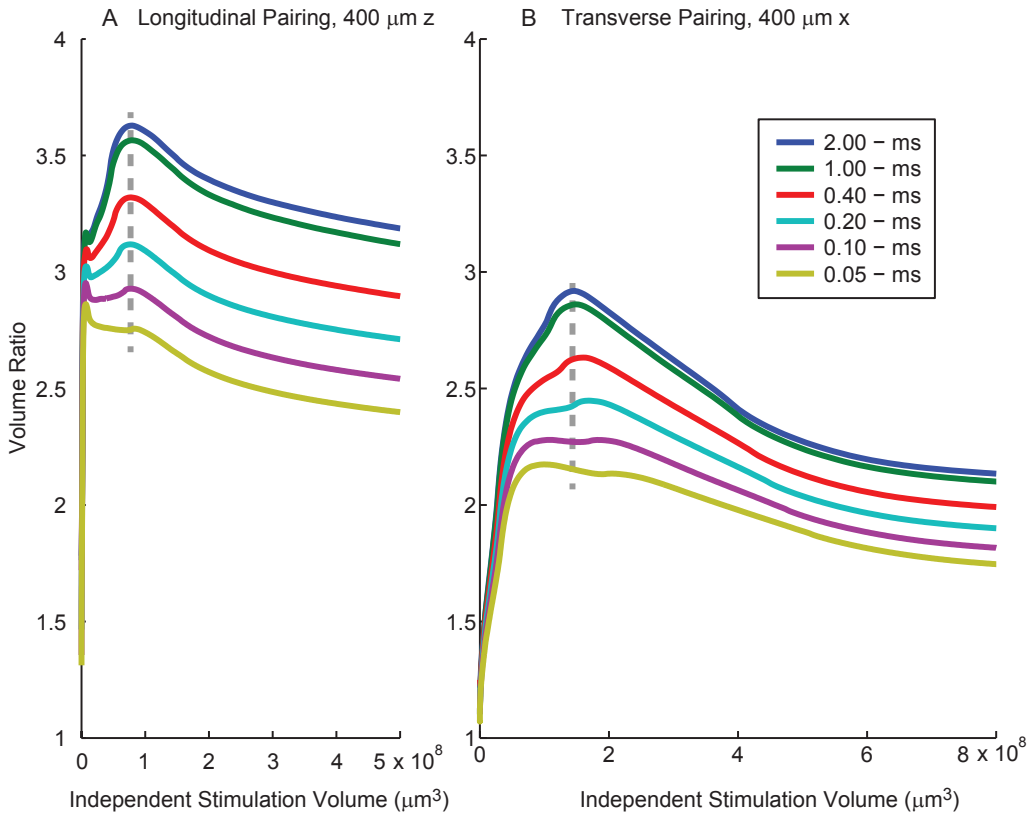

Figure 6.5: Volume ratio for different stimulus pulse durations. Results shown are for a 15 μm diameter separated by 400 μm along the z-axis (longitudinal pairing) or x-axis (transverse pairing). The volume ratio is shown as a function of the volume of tissue recruited from the two electrodes when stimulating independently. For reference, data shown for the 200 μs pulse width spans from 1 – 27.2 μA (longitudinal) and 1 – 28.1 μA (transverse). For narrower pulse widths the stimulus amplitude range is larger. For wider pulse widths, the stimulus amplitude range is narrower. For both pairings the volume ratios for different stimulus widths differ little when recruiting small volumes during independent stimulation. At larger independent stimulation recruitment volumes, longer stimulus durations have larger volume ratios than shorter stimulus durations. The difference in volume ratios between 2 ms and 0.05 ms at the dotted vertical line (chosen based on the volume ratio peak for the 2 ms trace) is 0.87 and 0.77 for the longitudinal and transverse pairings respectively. Similar results are seen at smaller fiber diameters, although the difference in stimulus widths decreases slightly (0.72 and 0.55 for the longitudinal and transverse pairings, 7.3 μm diameter fiber).

For a given stimulus amplitude, wider pulse-widths will recruit more neural tissue than narrower pulse widths (Grill and Mortimer 1996). Instead of examining the volume ratio versus

charge or pulse amplitude, it is possible to examine it as a function of stimulus effectiveness. By our definition, stimuli with the same effectiveness will recruit the same volume of neural tissue. Figure 6.5 shows these results for longitudinal (Figure 6.5A) and transverse (Figure 6.5B) electrode pairings. For reference to other figures the maximum stimulus amplitude shown for the 0.2 ms (200 μs) stimulus width is 27.2 μA and 28.1 μA for Figure 6.5A and 6.5B respectively.

As expected, the longitudinal electrode pairing shows consistently higher volume ratios. For the majority of stimulus efficacies, wider pulses show larger volume ratios than do narrower pulses. Only at the smallest stimulus efficacies is the stimulus is the difference between stimulus widths negligible. Thus if a stimulation paradigm wished to minimize interaction effects, the use of narrower pulse widths would not only lower the likelihood of interaction, but it would also lessen the impact of simultaneous stimulation on electrode independence. This trend holds for smaller diameter fibers (see Figure 6.5 for more details).

6.3.4 Dependence on electrode pairing distance

To reduce the effect of stimulus interactions, it is possible to increase the distance between simultaneously stimulated electrodes. Figure 6.6 shows the effect of stimulus interactions as a function of distance over a range of stimulus amplitudes. As expected, electrodes that are closer together exhibit larger volume ratios. Also, consistent with previous results, electrodes that are paired longitudinally exhibit larger ratios than transverse pairings. However, unlike the data presented in Figures 6.4 and 6.5, the change in the volume ratio as a function of stimulus amplitude for the longitudinal pairing does not show a smooth transition across the parameter being varied. This change, which is particularly noticeable at 1400 μm, is due to the relationship between electrode spacing and the internodal length of the axon. If electrodes are separated

exactly by the internodal length of the axon, then each single electrode will recruit the same tissue during independent stimulation. In general this will lead to an increase in the volume ratio (smaller denominator).

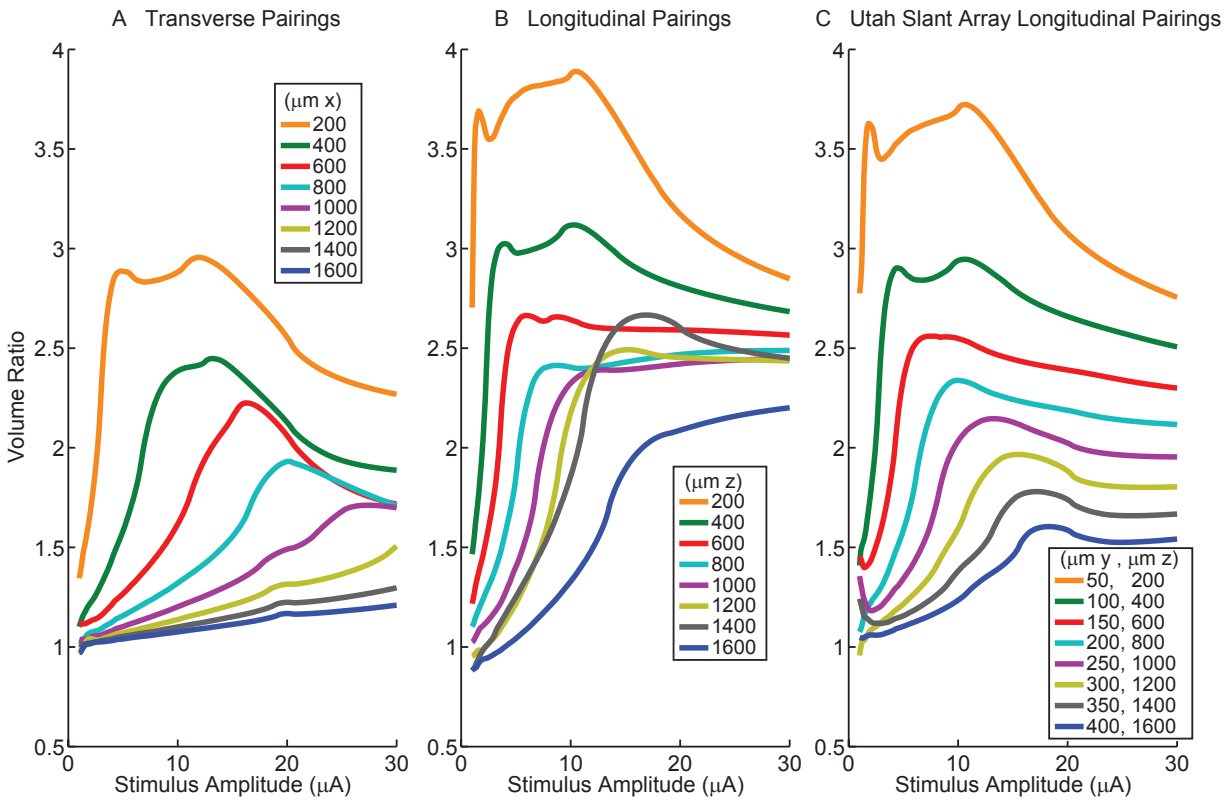

Figure 6.6: Volume ratios as a function of electrode separation for a 15 μm diameter fiber with a 200 μs leading cathodic phase. All results shown are for two electrodes separated by the distances specified in the legends. As with previous results, the volume ratios for transverse pairings are lower than the pairings separated by the same distance along the longitudinal axis. When the longitudinal pairing distance approaches the internodal length of the fiber diameter (1450 μm), the amount of tissue recruited during independent stimulation is reduced, leading to an increase in the volume ratio which is not consistent with the overall trend that larger distances lead to smaller volume ratios. The redundancy of neural activation from purely longitudinal pairings has led to arrays which vary both along the longitudinal and transverse axes, such as the Utah Slant Electrode Array (Branner 2001). Results for this type of electrode are shown in panel C. Unlike panel B, the volume ratios consistently decrease with increasing electrode distances, except for at low stimulus amplitudes which is may be due to interpolation noise.

In the same pairing, the larger electrode spacings also appear to have volume ratios that are less than one, although this effect is minimal. This might be partially explained by the smaller spatial stimulus gradient that is present. The spatial stimulus gradient, in particular the second spatial difference of the applied stimulus is a decent predictor of stimulus threshold (Rattay 1986, Peterson 2011).

Finally, a word of caution should be given at the smallest stimulus amplitudes. Although some of the changes seen may be real, small noise in either simulation condition, simultaneous or independent, can cause the ratio to show a noticeable change. At these smallest amplitudes (1 – 2 μA) the recruitment volume is so minimal that most (if not all) stimulation paradigms will not operate at these ranges.

Although it is difficult if not impossible to prescribe an exact electrode spacing based on these results (see discussion), the electrode spacing we use will likely need to be much larger for longitudinal pairs than transverse pairs.

6.3.5 Resistivity Sensitivity Analysis

To date there are no published values of the resistivity of mammalian peripheral nerve tissue. The majority of studies use values based on measurements of the dorsal columns of the spinal cord (Ranck and BeMent 1965). To examine the impact of the resistivity on our results, the longitudinal resistivity was doubled and halved from the original value, and volume ratios were computed as a function of stimulus amplitudes for a 15 μm diameter fiber. It was found that the change in longitudinal resistivity had little impact on the volume ratios for the longitudinal electrode pairing (Figure 6.7). For the transverse pairing the decrease in resistivity led to an overall decrease in the volume ratios. The opposite effect was seen when the resistivity was

increased. Even in the decreased case the volume ratio still exceeds two over a range of stimulus amplitudes. Similar results were seen for the other fiber diameters. Overall, these data indicate that the results presented are robust to changes in longitudinal resistivity.

Changes in transverse resistivity by ± 200 Ω-cm had minimal impact on the observed results as well. Increasing the transverse resistivity led to a slight decrease in the volume ratio (~0.2) at higher stimulus amplitudes (> 13 μA). Similarly the decrease in transverse resistivity led to a slight increase in the volume ratio at higher stimulus amplitudes.

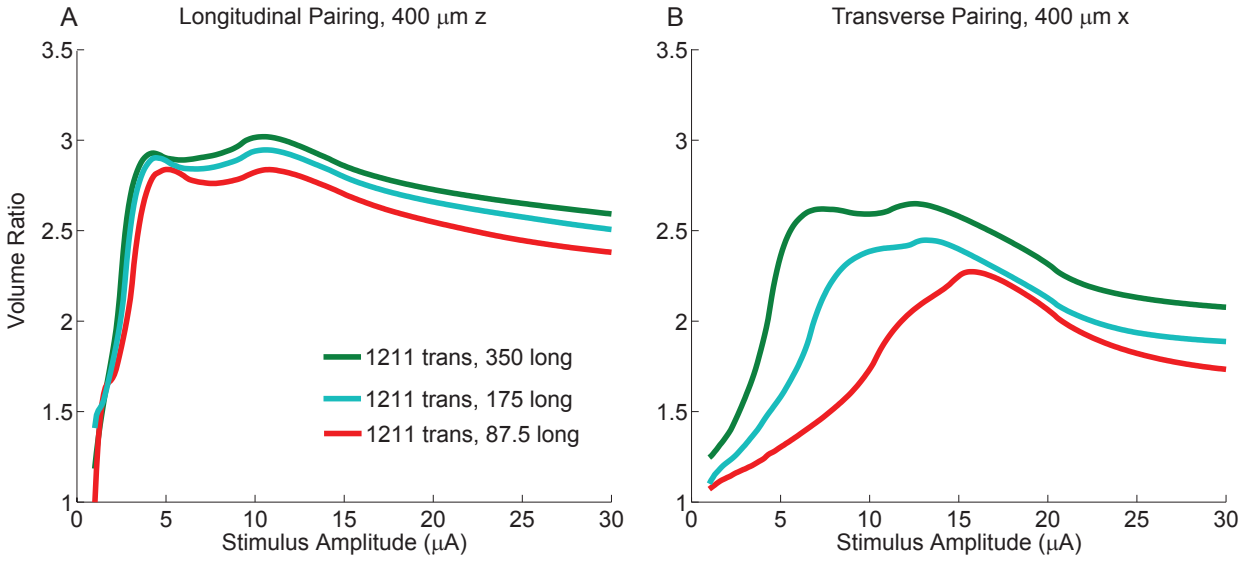

Figure 6.7: Impact of changing longitudinal resistivity on the volume ratio of a 15 μm diameter fiber for electrodes spaced 400 μm apart longitudinally or transversely. The change in the volume ratio for the longitudinal pair is minimal. For the transverse pairing the decrease in longitudinal resistivity led to an overall decrease in the volume ratio, and a shift in the peak to a higher stimulus amplitude. Increasing the longitudinal resistivity led to an increase in the volume ratios and an increase in the range of stimulus amplitudes over which the volume ratios were close to their maximum value.

In general the absolute magnitude of the resistivity is directly proportional to the magnitude of the applied stimulus voltage for a given current. As such, for a given neuron, the stimulus current threshold will change inversely with the change in the modeled resistivity magnitude. For example, in Equation 6.1, doubling the modeled resistivity (multiplying the values of ρ_x, ρ_y, and ρ_z by two), will result in a doubling of the applied stimulus voltage. The threshold stimulus voltage will now occur when the magnitude of the stimulus current is half of its original threshold value. In summary, changing the magnitude of the resistivity only serves to change the interpretation of the stimulus amplitudes and the amount of tissue recruited at a given stimulus amplitude, not the relationships examined in this paper or the values observed for the volume ratios.

6.4 DISCUSSION

6.4.1 General Summary of Results

The key finding of this work is that even at small stimulus amplitudes, simultaneous microstimulation through multiple electrodes can have a large effect on neuronal recruitment. This is especially important in the context of multichannel stimulation, where tens to hundreds of channels may be used and the probability of simultaneous stimulation is high. These modeling results also suggest that the interaction effect between electrodes will be most important for the large diameter axons in a given population (Figure 6.4). However, narrower stimulus pulse widths will lessen the degree of interaction (Figure 6.5). As expected, reducing the interelectrode

spacing was shown to result in stronger interactions during simultaneous stimulation (Figure 6.6). These results were robust to changes in tissue resistivity (Figure 6.7).

6.4.2 Experimental Evidence for Microstimulation Interactions:

Several previous studies of microstimulation using microelectrode arrays lend experimental evidence for the recruitment interaction effects from simultaneous stimulation observed in this modeling study. In these three studies, microstimulation pulses were delivered through neighboring electrode sites both independently and simultaneously, and differences in force recruitment were compared (Rutten et al. 1991 (Figure 3), Yoshida & Horch 1993 (Figure 3), and Branner et. al. 2001 (Figure 9A)). These examples include data that can be used to compute force ratios. These force ratio measurements are similar to the volume ratio computation conducted for this study in that they compute force recruitment from simultaneous stimulation relative to the force data from each of the electrodes stimulating independently. Due to a lack of detail in these reports, direct comparisons to the volume ratio are difficult to make, however the force ratios are similar to, and perhaps even higher than the volume ratios observed in the model (~3 – 30).

6.4.3 Stimulation Scheduling Design:

Given the effect of simultaneous stimulation on neural recruitment, a stimulus paradigm that treats each electrode as an independent channel (e.g. Horch and Dhillon, 2006) should avoid simultaneous stimulation on multiple electrodes. Given high electrode counts in current multielectrode arrays, it may not be possible to stimulate each electrode independently of all

others, especially when high stimulus rates are used. Cochlear implants have partially solved this problem by narrowing the pulse width. In these systems, it is not uncommon to see pulse widths on the order of 40 μs or less (Wilson, 2006). Many cochlear implant stimulation paradigms also place each electrode in a group, where the group constituents are non-neighboring electrodes, in an attempt to minimize interactions. Scheduling stimulation in this way is a useful approach for avoiding simultaneous stimulation by allocating a specific time slot in which each stimulus channel can be active. For arrays in which the electrode variation is primarily limited to a plane such as the Utah Slant Electrode Array (Blackrock Microsystems), the approach used by cochlear implant stimuli can easily be expanded to two dimensions (See Figure 8).

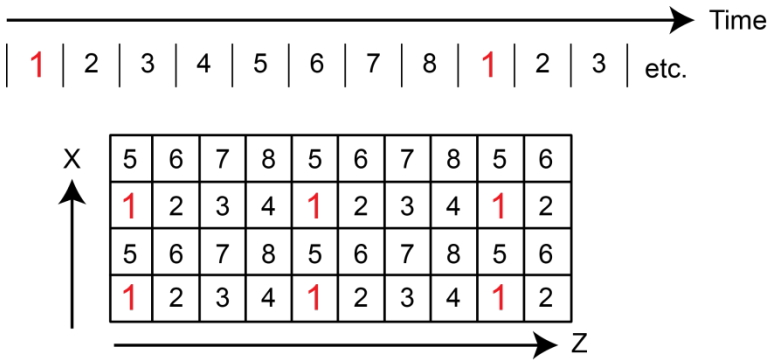

Figure 6.8: Illustration of a two dimensional stimulation schedule. The large rectangle is a 4 x 10 electrode array where each square represents an electrode channel. Each stimulus channel has been assigned to one of eight different time bins in which it can stimulate. Each electrode in a group is spatially separated from the other electrodes in the group. Given the higher volume ratios observed along the z-axis (longitudinal pairings), it will be necessary to have more groups along this axis. This solution highlights the general approach but is not meant to be prescriptive. Eight groups in a 2x4 pattern might not be the best approach. Additionally, it might be better to use a group order which does not progress to a neighboring electrode (e.g. stimulating on three after one, instead of two).

Based on the results presented, it is difficult to prescribe an electrode spacing where interaction effects are not likely to be significant. Two factors make this difficult. The first factor is the interpretation of the significance of the volume ratio magnitude. Although its interpretation is straightforward, the impact that a specific volume ratio may have on a functional outcome is not. For example, if the volume ratio is 1.4, and 10 neurons are recruited by two different electrodes, would the functional outcome be negatively impacted during simultaneous stimulation when 14 neurons are recruited? The second factor is the variability in the ratio as a function the actual neuronal population surrounding the tissue. Although the results from Figure 6.3 show relatively little variability with different random populations, assumptions made about the density and distribution of neurons might be inaccurate, and larger variability is certainly possible.

6.4.4 Channel Interactions and Current Steering/Focusing:

Stimulus interactions due to simultaneous stimulation can be beneficial or detrimental, depending upon the goals of a particular application. Thus far we have considered interactions with the goal of maximizing electrode channel independence. Alternatively one may design stimulation paradigms that take advantage of these stimulus interactions. Known as current steering or focusing, this can lead to tissue activation that is not possible with a single electrode. For example, stimulation paradigms in clinical use for cochlear implants are starting to take advantage of stimulus interactions to improve performance (Firszt et al. 2009).

With penetrating microelectrode arrays, the proximity of the electrodes to tissue has largely led to an avoidance of the topic of field interactions, since selectivity is viewed as being high, and stimulus amplitudes as being relatively low. Additionally, in the field of motor

stimulation, the technique of interleaving stimulation to avoid fatigue has largely led to an avoidance of the issue of stimulus interactions with penetrating arrays (McDonnall et al. 2004).

The increased efficacy of recruitment during simultaneous stimulation that we observed in the model, particularly in recruiting neural tissue between the electrodes, could serve as a current steering mechanism (see Figure 6.2C and 6.2F for examples). Branner reported that individual stimulation through two different electrodes each maximally generated a muscle force of 4N (Branner et al. 2001). When stimulated simultaneously at a level that generated 1N each, a total muscle force of 6N was generated, which was larger than the maximal recruitment of either electrode. However, no explanation for this result was presented. Under the assumption that maximal stimulation through either electrode independently recruited the entire population of motor neurons, this result could be explained by the focused activation of target motor neurons, while avoiding recruitment of antagonist motoneurons. Use of multiple electrodes is now starting to be studied as a method of increasing force recruitment (Hilgart et al. 2012). In contrast to the more common notion of anodal inhibition to provide current steering (Sweeney et al. 1990, Grill et al. 1991), it is simultaneous cathodic stimulation, as was studied in this model, which is being used clinically for current steering in cochlear implants (Firszt et al. 2009). Recent modeling work has also suggested that this type of stimulation would be more advantageous than tripolar stimulation with guarding anodes (Li et al. 2013).

6.4.5 Model Limits, Population Modeling:

One aspect that the model does not attempt to capture is the population response. The recruitment volumes used to calculate the volume ratio do not represent actual counts of recruited neurons and are only valid for a uniform distribution of axons with a single fiber

diameter. If the distribution of fiber diameters is known in the tissue, it is possible to estimate an aggregate response by combining the individual fiber diameter results in proportion to their relative percentage in the aggregate fiber distribution (Bourbeau et al. 2011).

This however assumes a uniform spatial distribution. If the distribution is not uniform, it is easy to come up with spatial arrangements of fibers where simultaneous stimulation has much less or more of an effect than is shown here. For example, if the fibers are predominantly arranged between a set of electrodes, the volume ratio should increase significantly, as simultaneous stimulation tends to primarily activate additional tissue between the two electrodes. If the fibers of interest are predominantly close to the electrodes, and arranged outside the set of electrodes, then simultaneous stimulation should not have as strong an effect, especially at higher amplitudes when all of the tissue of interest has already been recruited.

In general the uncertainty introduced by the arrangement of the population does not invalidate our results. Across a wide range of stimulus amplitudes, the threshold of any particular neuron is significantly reduced during simultaneous stimulation as compared to independent stimulation. Variability should be highest at low stimulus amplitudes (Figure 6.3). As the VTA expands with higher stimulus amplitudes, local inhomogeneities should exert less of an influence on recruitment, and variability should decrease.

6.4.6 Model Limits, Peripheral Nerve Fascicles:

It is well known that fascicles act as a high impedance barrier to charge (see Grinberg et al. 2008). This model does not take into account the fascicle barrier. It is expected that the fascicle barrier would significantly reduce the impact of simultaneous stimulation for electrodes that are inside different fascicles as they are electrically far apart (Schady et al. 1983). However, for

electrodes that are within the same fascicle it is expected that simultaneous stimulation would become a more significant factor, as charge is restricted within the fascicle. This may be one of the reasons why previous experimental data using muscle force to examine the effect of simultaneous stimulation has shown even higher ratios than were seen with this model.

6.5 CONCLUSION

When designing stimulation paradigms using multi-channel microelectrode arrays, it is important to take into account the relative stimulus timing between stimulus channels. Specifically, simultaneous stimulation on neighboring electrode channels can significantly increase the number of recruited neurons in comparison to independent stimulation. This effect is increased for larger diameter fibers, wider stimulus widths, and closer electrodes. In order to maximize electrode independence it is recommended that a stimulation scheduling approach is used where neighboring electrodes are only able to stimulate at non-overlapping times.

7.0 SUMMARY OF RESULTS AND FUTURE WORK

New approaches for stimulus design are needed in order to design advanced somatosensory neuroprostheses. To this end three different approaches have been explored in this thesis: using peripheral nerve recordings to evaluate stimulation recruitment; computational modeling of stimulation recruitment; and cortical recordings to evaluate sensory transmission from the periphery to the brain.

7.1 DORSAL ROOT GANGLIA MICROSTIMULATION RECRUITMENT

Recruitment of primary afferents via DRG microstimulation was examined by recording antidromic propagation of action potentials via a nerve cuff placed around the sciatic nerve.

7.1.1 Summary of Experimental Results

Recruitment of primary afferents occurs at low stimulus amplitudes. 97% of observed neural thresholds were in the range of 1 – 4 μA. At stimulus threshold a wide range of different neuron types were recruited, as judged by conduction velocity.

7.1.2 Future Directions

7.1.2.1 Further Usage

The lack of synapses in the peripheral nervous system makes it an appealing approach for further understanding how stimulation recruitment occurs. In particular the temporal dynamics of stimulation might be well suited to be explored with this approach. Most stimulation paradigms and models tend to treat a stimulus pulse as being equivalent to neural activation. It is well known however that neurons have temporal dynamics that impact their ability to fire action potentials, such as their absolute and relative refractory periods, as well as other fluctuations of the membrane potential following an action potential (McIntyre et al. 2002). Stimulus approaches that take advantage of the underlying channel dynamics could lead to improved stimulation paradigms. It has been shown that manipulation of the stimulus waveform can lead to changes in the current-distance relationship (Grill and Mortimer 1997) and fiber-diameter recruitment order (Fang and Mortimer 1991). Although experimental evidence exists for these phenomena, they are not widely accepted, and further experimental validation and design using the approach used in this thesis would likely be beneficial to increasing acceptance, usage, and performance.

7.1.2.2 Technique Improvement

There also remains considerable work that could be done to improve the experimental model. It is well known that nerve cuff length and spacing have an important impact on the quality of recordings obtained (Stein et al. 1975). Further optimization of the nerve cuff recording hardware is also possible. However, if one truly wants to optimize signal quality more invasive options are also available. By removing the epineurium it is possible to get a significant increase

in SNR (Yoo et al. 2013). Alternatively, penetrating electrodes could be used. Using a beamforming technique such as that used by Wodlinger and Durand (2009), it might be possible to pull out even more spatial information.

In addition to changes in the electrode interface, nerve isolation might also allow for more accurate electrode placement and less of a need for averaging. By isolating the nerve, it becomes physically easier to place electrodes at different locations in the nerve. Nerve isolation also removes spontaneous neural activity which is likely a significant source of noise during recordings. Initial studies on nerve conduction, primarily conducted on the frog sciatic nerve, likely removed the nerve for these reasons (Erlanger et al. 1926). Although surgically removal of the sciatic nerve with the ganglia may be a difficult task, the improvements might be worth the difficulty. Other nerves that do not pass through the pelvis might be more amenable to this approach.

7.2 CORTICAL RECORDINGS DURING DRG MICROSTIMULATION

Recordings were made using penetrating electrodes in somatosensory cortex during DRG microstimulation. Two different stimulation approaches were used. The first stimulation approach involved single channel stimulation and the stimulus rate and amplitude were changed. The second stimulation approach involved multi-channel stimulation and a stimulation spatio-temporal pattern that was based on DRG recordings made during passive movement.

7.2.1 Summary of Results

Recordings in somatosensory cortex were used to detect stimuli in the DRG and to discriminate between these different stimulus channels. At lower stimulus amplitudes (5 and 10 μA), the stimulus rate impacted the ability to detect a stimulus. This effect was not seen at 20 μA. Similarly, for these lower stimulus amplitudes, the cortical responses to two different stimulus electrodes were generally discriminable. However, the cortical responses to two different stimulus electrodes at 20 μA was not as discriminable at smaller distances between the two stimulating electrodes. It was only when considering stimulating electrodes that were greater than 2 mm apart that the average discriminability rose above 80%.

A novel stimulus approach was developed to explore multichannel microstimulation. Initial changes to the stimulus paradigm included manipulating the instantaneous stimulus rate and the spatial relationship of the stimulus pattern. When examining the correlation between the cortical responses to the stimuli and to passive movement, no significant difference was found between shuffled and non-shuffled conditions. Increasing the instantaneous stimulation rate by a factor of four (4x) led to an increase in the correlation values. Increasing the rate further to 8x however did not. Possible explanations for these observations were given in Chapter 5.

7.2.2 Future Directions

For the most part, the cortical results presented are from a single experiment. Future work remains to examine the extent to which these results hold across subjects.

7.2.2.1 Single Channel Stimulation

The parameter space currently explored for single channel stimuli is rather minimal. Significant advances were made in terms of experimental control, which should enable obtaining finer sampling of stimulus amplitude and rate. In particular a fully automated stimulation environment in which a set of stimulus parameters are specified and then data is collected automatically for many hours was created. This led to a significant gain in the amount of data that could be collected. Using nerve cuff and cortical recordings to guide the experiment should also lead to more efficient experiments. If primary afferents don't respond to stimulation on a channel at a high stimulus amplitude, then testing that stimulus channel at a variety of stimulus rates and lower amplitudes doesn't make sense.

The goal of these recordings is to guide stimulus paradigms. Attempts at linking stimulation channels to the type of primary afferent neurons that could be recorded on that channel were lacking. It is likely that the stimulation rate profiles that are appropriate for one type of primary afferent would be different than another primary afferent type (e.g. a Ruffini afferent versus a muscle spindle afferent). Although these would not necessarily be knowable in an amputee, there might be other covariates (e.g. low stimulus threshold, response to a high stimulus rate or not, perception of stimulus) that are, and this extra knowledge would help to reduce testing time or lead stimulus designers down a path that might not otherwise be explored. As such, future experiments should improve upon "unit identification." An initial attempt was made to automate this process but significant work on the project remains.

Expansion of single channel stimulation to two channel stimulation also remains an incompletely explored avenue. One of the challenges in moving to two channel stimulation is the significant growth in testing that is required, due the increase in the number of pairs of stimulus

channels relative to the number of single stimulus channels. As was seen in Chapter 4, this also led to confusing results. It is highly recommended that this type of testing be done with a very specific hypothesis in mind. One possible hypothesis to explore is that low amplitude stimulation on two "muscle spindle" stimulus channels might provide a stronger cortical response than higher stimulation on only one of those stimulus channels. The integration of afferent activity to form a proprioceptive sense of self is not well understood, and current attempts to provide proprioceptive feedback have commented on the difficulty in doing so, hinting that the feedback might require more focus (Horch and Dhillon 2006). Due to the large amount of afferent input that is ultimately believed to give rise to proprioception, multi-channel stimulation is likely to be needed. The current somatosensory feedback stimulation paradigm outlined in Chapter 1 does not extend well to multiple channels which all convey essentially the same type of information. Two channel stimulation might be useful in trying to design a new stimulation paradigm that addresses those shortcomings.

7.2.2.2 Replay Stimulation

Replay stimulation was surprisingly difficult and frustrating to accomplish. Although it probably serves as a decent indicator of the ability (or lack thereof) to provide feedback that is similar to passive movement, significant improvements are needed.

A quantitative understanding of the DRG recordings that are available for stimuli is lacking. This is important if replay stimulation is going to be compared in any meaningful way across experiments. For example, it might be useful to know the coverage of afferents from different muscles. Are muscle spindle recordings present from every muscle? On a more simplistic scale, it would be useful to know if all phases of a movement are represented. If no neurons respond to a flexion or extension phase, it is unlikely that a cortical representation of this

phase will occur. A regression based approach to solving this problem is also inadequate as it does not give an accurate reflection of the robustness of the fit. In order words, a single stimulus channel that represents a flexion or extension phase is likely not equivalent to multiple channels that also represent that phase, in terms of the type of cortical response that they will evoke. Given the difficulties associated with consistent DRG recordings, generated stimuli might be more appropriate. This however also requires quantitative models of the response of different afferents to a stimulus. Fortunately these models exist (Prochazka and Gorassini 1998, Kim et al. 2010), although some work is needed to generate a population of afferents (stimulus inputs).

As the results from Chapter 5 show, individual channel optimization is likely to be needed in order to improve stimulus results. It is possible that the results from single channel stimulation on each individual channel, particularly to stimulus rate manipulation, could be used to guide replay stimulation.

The work of Ted Berger on multiple-input, multiple-output systems is likely relevant here as well (Song et al. 2007, Berger et al. 2010, see also recent work by Millard et al. 2013). Computationally the goal is to create a model that specifies the cortical response in terms of the stimulus inputs. The difficulty in such a model is in learning interaction terms and in having sufficient time to vary the stimulus inputs so as to fully train the model. This type of approach however might prove useful for stimulus optimization.

Stimulus timing needs to be carefully considered and taken into account. The replay nature of the stimulus is completely changed during simultaneous stimulation (Chapter 6). Implementation of a stimulus scheduler might prove useful for stimulus optimization.

Finally, this type of approach is well suited for exploratory analysis. Although 90 channels were implanted in the DRG, only a maximum of 32 channels were available for

stimulation. This was mainly a financial limitation. Additionally, only two ganglia were implanted, even though the neurons that innervate the cat hindlimb go through six different ganglia (Brown and Koerber 1978). It remains to be seen the extent to which this stimulation paradigm can inform which of many electrode configurations is the best at transmitting information to cortex, however it would be interesting and I think informative to try.

7.3 MODELING OF STIMULUS RECRUITMENT

Two different papers were written that used computational modeling of neural recruitment.

7.3.1 Summary of Results

The first computational model was important for highlighting the factors that impact the likelihood of recruiting a neuron: the current-distance relationship, the number of neurons, and the internodal-length. At small stimulus amplitudes these make it roughly twice as likely that a smaller diameter neuron will be recruited before a larger diameter neuron in the L7 ganglia. This model also provides an estimate of the number of fibers being recruited at low stimulus amplitudes. The detectable responses in cortex at 5 μA were likely from about 10 neurons or less. This corroborates data from human microstimulation studies in which stimulation of a single primary afferent is able to elicit responses in cortex that are detectable from FMRI recordings (Trulsson et al. 2001).

The second computational model was designed to investigate the importance of simultaneous stimulation on changing neural recruitment. Simultaneous stimulation leads to a

large change in neural recruitment, even at low stimulus amplitudes. The increase in recruitment is larger for larger diameter fibers, wider stimulus pulses, and more closely spaced electrodes. It is recommended that a stimulation scheduler which explicitly prohibits neighboring electrodes from stimulating at the same time is used if electrode independence is desirable.

7.3.2 Future Directions

Modeling of stimulation recruitment, or even of other aspects of somatosensory feedback, such as synaptic integration, provides an easy way of exploring different stimulation paradigms. Significant opportunities exist to explore modeling of multi-channel stimulation.

Much work also remains in terms of validating these models. Unless an experiment is explicitly performed for model validation, this often involves aggregation of a significant amount of different experimental literature. It would be beneficial to organize this information into a test-suite. Occasionally experiments designed to validate models also yield unexpected results (e.g. consider the stimulus threshold, I_0, observed in Mahnam et al. 2009 which was a factor of 10 larger than the expected threshold). These types of observations should be added to the test-suite that new models should be able to explain.

7.4 FINAL THOUGHTS AND CONCLUSIONS

With rapidly improving technology, the prospects for making improved prosthetics will continue to increase. With technological improvements we will likely need new ways of designing approaches to providing somatosensory feedback. This thesis examined three approaches, two

experimental and one computational. The computational approach has already proven its versatility elsewhere and will likely continue to be a useful tool in understanding neural recruitment. Examining recruitment experimentally in the peripheral nerve is a technique that has been used for decades. Although this approach now is largely clinical for examining nerve damages, the drive to understand artificial recruitment means that this approach might once again become an important scientific tool. Cortical recordings of artificial stimulation offer the promise of understanding one's ability to artificially transmit information into the brain. This approach was found to be quite difficult, however it possible that with methodological improvements that the approach could be useful in guiding stimulus design.

APPENDIX A

CHAPTER 3: DERIVATIONS

This appendix provides additional information on the derivation of equations used to estimate the probability of capturing a node in the VoI. Additionally, we provide an example to illustrate how we estimated the probability of recruiting a given number of fibers from a set of fiber sizes as a function of stimulus amplitude.

To describe the probability of a fiber of given size having a node of Ranvier in the spherical VoI at a certain radial distance from its center, $P(node|I,fD,r_f)$, we divided the length of fiber encapsulated within the VoI (L_f) by the internodal length of the fiber (L_{int}) as in

$$P(node|I, fD, r_f) = \frac{L_f}{inL_{fD}} \qquad \text{(A.1)}$$

We expanded on the definition of L_f

$$L_f = 2\sqrt{r_{VoI}^2 - r_f^2} \qquad \text{(A.2)}$$

using the Pythagorean Theorem with the radial position of the fiber in the transverse plane (r_f) and the radius of the spherical VoI (r_{VoI}) as the hypotenuse (see Figure A.1). We then multiplied the probability of finding a node of Ranvier by the circumference of the circle with radius r_f, then integrated with respect to r_f over the range [0, r_{VoI}]

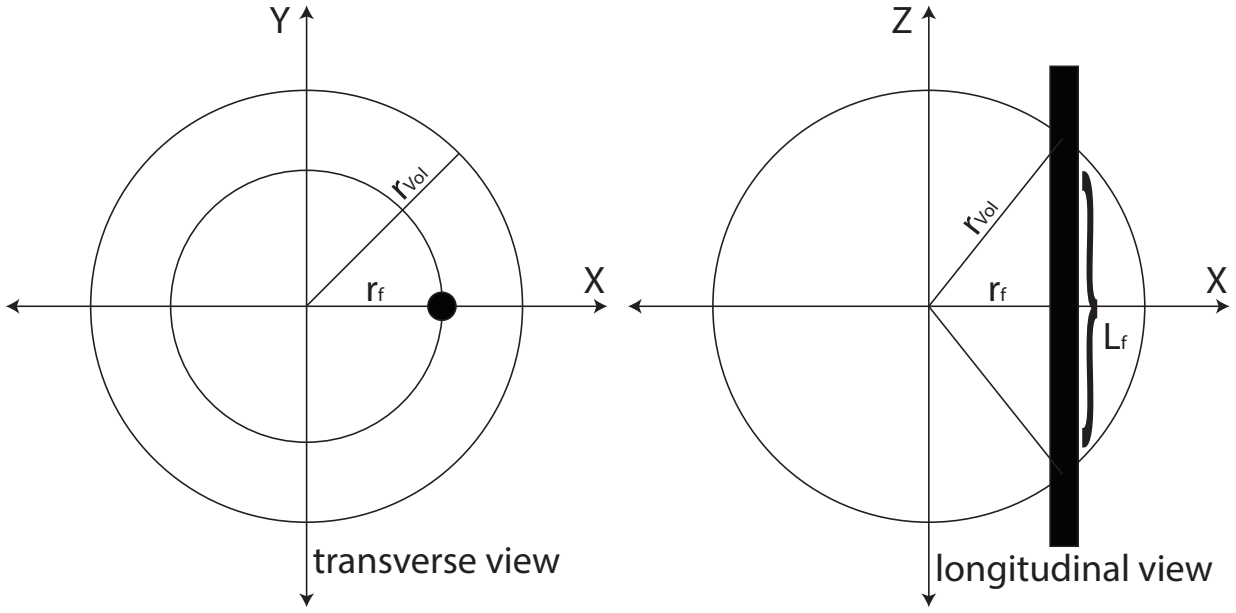

Figure A.1: Schematic depiction of fiber passing through spherical volume of tissue activated (VoI). The outer circle represents the boundary of the VoI, while the filled circle (transverse view) and the thick line (longitudinal view) represent the fiber of passage. The probability of a fiber having a node of Ranvier in the VoI is the ratio of the length of fiber contained within the VoI (L_f) to the internodal length of the fiber (L_{int}). This probability must be calculated for all possible locations of the fiber in the VoI to get a total average probability.

$$P(node|I, fD, inL_{fD} > 2r_{VoI}) = \frac{\int_0^{r_{VoI}} L_f * 2\pi r_f dr_f}{inL_{fD} * \pi r_{VoI}^2} \quad \text{(A.3)}$$

to determine an average value of this probability. The integral was evaluated, using (A.2), to

$$P(node|I, fD, inL_{fD} > 2r_{VoI}) = \frac{-\frac{4\pi}{3}[(r_{VoI} - r_f)(r_{VoI} + r_f)]^{3/2}\Big|_0^{r_{VoI}}}{inL_{fD} * \pi r_{VoI}^2} \quad \text{(A.4)}$$

and then simplified to

$$P(node|I, fD, inL_{fD} > 2r_{VoI}) = \frac{4r_{VoI}}{3inL_{fD}} \quad \text{(A.5)}$$

However, if the diameter of the spherical VoI was larger than the internodal length of the fiber, then the probability of finding a node might exceed 1. We capped this probability at 1 by first setting (A.1) equal to 1 as in

$$P(node|I,fD,r_f) = \frac{2\sqrt{r_{VoI}^2 - r_f^2}}{inL_{fD}} = 1 \qquad \text{(A.6)}$$

and then solving for r_f

$$r_f = \sqrt{r_{VoI}^2 - \left(\frac{inL_{fD}}{2}\right)^2} = r_{inL} \qquad \text{(A.7)}$$

The radial position (r_f) at which the length of fiber encapsulated within the spherical VoI is equal to the internodal length is denoted as r_L. The integral from (A.3) was separated into two integrals to get

$$P(node|I,fD,inL_{fD} \leq 2r_{VoI}) = \frac{\int_0^{r_{inL}} inL*2\pi r_f dr_f + \int_{r_{inL}}^{r_{VoI}} L_f*2\pi r_f dr_f}{inL_{fD}*\pi r_{VoI}^2} \qquad \text{(A.8)}$$

In the first integral, the length of fiber encapsulated within the sphere was set to the internodal length and the integral was taken over the range $[0, r_L]$. The second integral determined the average probability as in (A.3), but over the range $[r_L, r_{VoI}]$. Equation (A.8) was evaluated and then simplified to

$$P\left(node\middle|I,fD,inL_{fD} \leq 2r_{VoI}\right) = \frac{inL_{fD}*r_{inL}^2 + \frac{4}{3}[(r_{VoI} - r_{inL})(r_{VoI} + r_{inL})]^{\frac{3}{2}}}{inL_{fD}*r_{VoI}^2} \qquad \text{(A.9)}$$

In the population model, (A.9) was used to describe the probability of a fiber having a node of Ranvier within the VoI in the case where the diameter of the VoI was larger than the internodal length of the specified fiber. Note that (A.3–5) are only valid for L_{int} greater than $2r_{VoI}$, whereas (A.8) and (A.9) are valid for L_{int} less than or equal to $2r_{VoI}$. In fact, (A.9) simplifies to (A.5) if r_L is set to zero; r_L approaches zero as the interval of r_f values over which the entire internodal length is captured by the VoI approaches zero.

Finally, using probabilities from (A.9), we estimated the probability of recruiting a given number of fibers from a set of fiber sizes as a function of stimulus amplitude (see 9). As an example, let us assume that there are three fiber sizes in a population, termed A, B and C. To

determine the probability of recruiting two fibers among A and B, but no C fibers, we begin by finding that there are three ways to get two fibers: one A and one B; two A's and zero B's; zero A's and two B's. For each combination, the probabilities for each neuron's state are multiplied; these probabilities are then summed across combinations. The equation to get the probability of recruiting two fibers among A or B, without getting any C fibers is expressed as

$$P(2|I,\{A,B\}) = P(1|I,A)P(1|I,B)P(0|I,C) + P(2|I,A)P(0|I,B)P(0|I,C) \ldots + P(0|I,A)P(2|I,B)P(0|I,C). \quad \text{(A.10)}$$

This example illustrates the general means by which we determined the probability of recruiting a given number of fibers from a group of specified fiber sizes, given the probabilities of recruiting various numbers of fibers for all fibers of interest at the specified current level.

APPENDIX B

CHAPTER 6: EDGE CASES WHEN COMPUTING THE VTA

When computed correctly, the volume of tissue activated (VTA) by a stimulus should be proportional to the number of neurons recruited. There are at least two ways in which the calculation of the VTA can be done erroneously. These are described below.

Care was taken to ensure that the simulation bounded all tissue that would be activated by a stimulus. For the x and y axes, orthogonal to the main axis of the neuron, this meant that the lowest stimulus threshold values at the boundaries had to exceed the maximum tested stimulus amplitude. The tested volume was expanded until this was the case. In other words, if the boundary only has maximum stimulus threshold values of 5 μA, it is difficult to make a statement as to the VTA at 30 μA.

In the z-direction it is impossible to set boundaries for the solution in this way, since the threshold rises and falls periodically as different nodes of Ranvier come close to the electrodes and then pass further away, only to have a different node pass closer again. Thus another approach is needed to ensure that the results are accurate, and that the volume is proportional to the number of neurons that we would expect to recruit. In this case the integrated volume of the VTA was limited to the internodal length of the fiber in the z-direction. Since the solution is

periodic (excluding small edge effects), the testing volume was limited in z to ± one half of the internodal length, where electrode pairs were centered at z = 0. A detailed explanation for limiting the volume in the z-direction to the internodal length of the fiber is given in Bourbeau et al. 2011 but is explained here briefly.

For a neuron located at a particular x-y location, its probability of being recruited if it is randomly placed along the z-axis is equal to the length of the VTA (along the z-axis) at that x-y point, divided by the internodal length of the cell. If the VTA extends for 600 μm and the internodal length of the cell is 1000 μm, then when randomly placed along the z-axis on average 60% of the time it will have a node of Ranvier within the VTA. Once the VTA exceeds the 1000 μm, a cell randomly placed at that x-y point will always be recruited. Counting additional points along the z-axis as the VTA expands beyond 1000 μm would invalidate the relationship between volume and number of neurons (i.e. the probability of recruitment at any x-y point cannot exceed 1).

Figure B.1 expounds upon these issues. Both panels show threshold results for a 10 μm diameter fiber at different locations with respect to the electrode(s). Since the nodes or Ranvier of a neuron are periodic along the z-axis, the solution itself becomes periodic along the z-axis. For the results from the single electrode stimulation, the x axis only fully encompasses thresholds for approximately 14.3 μA and less. If one wished to know the solutions for higher stimulus amplitudes, one would need to increase the testing bounds in these dimensions.

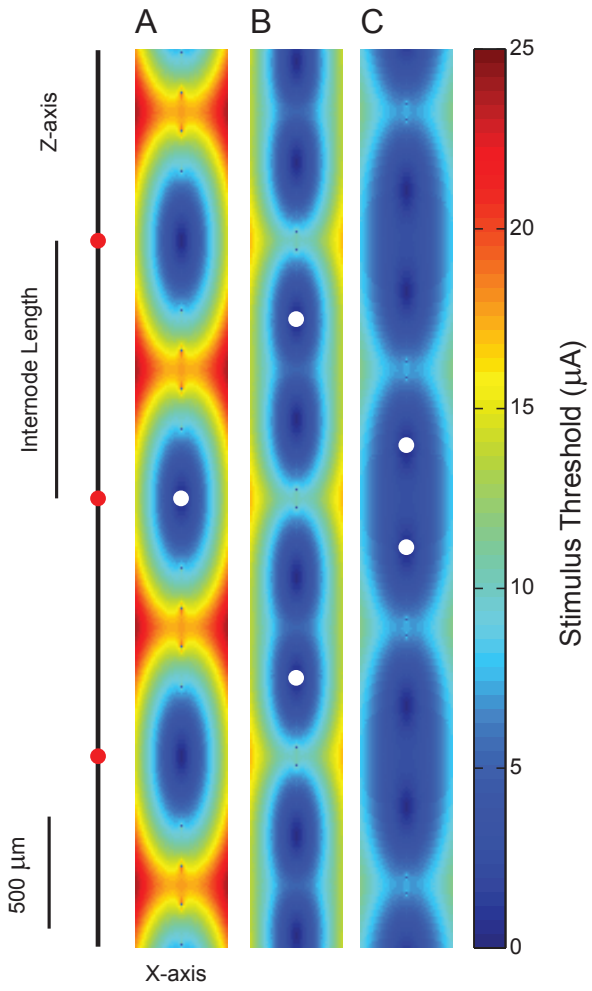

Figure B.1: Stimulus thresholds for a 10 µm diameter fiber whose center-most node of Ranvier is located at different positions relative to a single electrode. (A) and to two electrodes stimulating simultaneously at a separation distance of 1600 µm (B) and 550 µm (C). In all cases the thresholds are periodic in the z-axis, with a spatial period equal to the internodal length of the fiber. This is true even when the electrode separation is larger than the internodal length (as it is in (C)). Importantly, this means that threshold solutions only need to be found over the spatial extent of the internodal length, and that any choice in z-bounds that satisfies this condition will be appropriate. The threshold solutions shown in this figure were obtained by moving the center-most node of Ranvier beyond the typical range in which it was tested. Based on (A), the spatial extent of the solutions obtained (in the x-axis) would limit the stimulus range to roughly 14.3 µA. If we wished to accurately compute the volume ratio for 20 µA, we would need to get thresholds at x-distances larger than those shown in (A). For reference a neuron with nodes of Ranvier, indicated by circles, has been included, with the appropriate internodal spacing.

APPENDIX C

CHAPTER 6: COMPUTING THE SPATIAL UNION OF TWO STIMULI

Given the model assumptions of an infinite homogenous medium, the threshold results from a single electrode are equally valid anywhere within the medium.

For the independent stimulation case, the union of the volumes was calculated by spatially replicating the results from a single stimulus to all involved electrodes (see Figure C.1A) and using the minimum stimulus threshold at any point. Given the assumptions of an infinite homogenous medium, this spatial replication makes sense. There is no specification of stimulus timing between the two electrodes in the independent case, only an implied time, a time that is sufficient to return all neurons to their resting state.

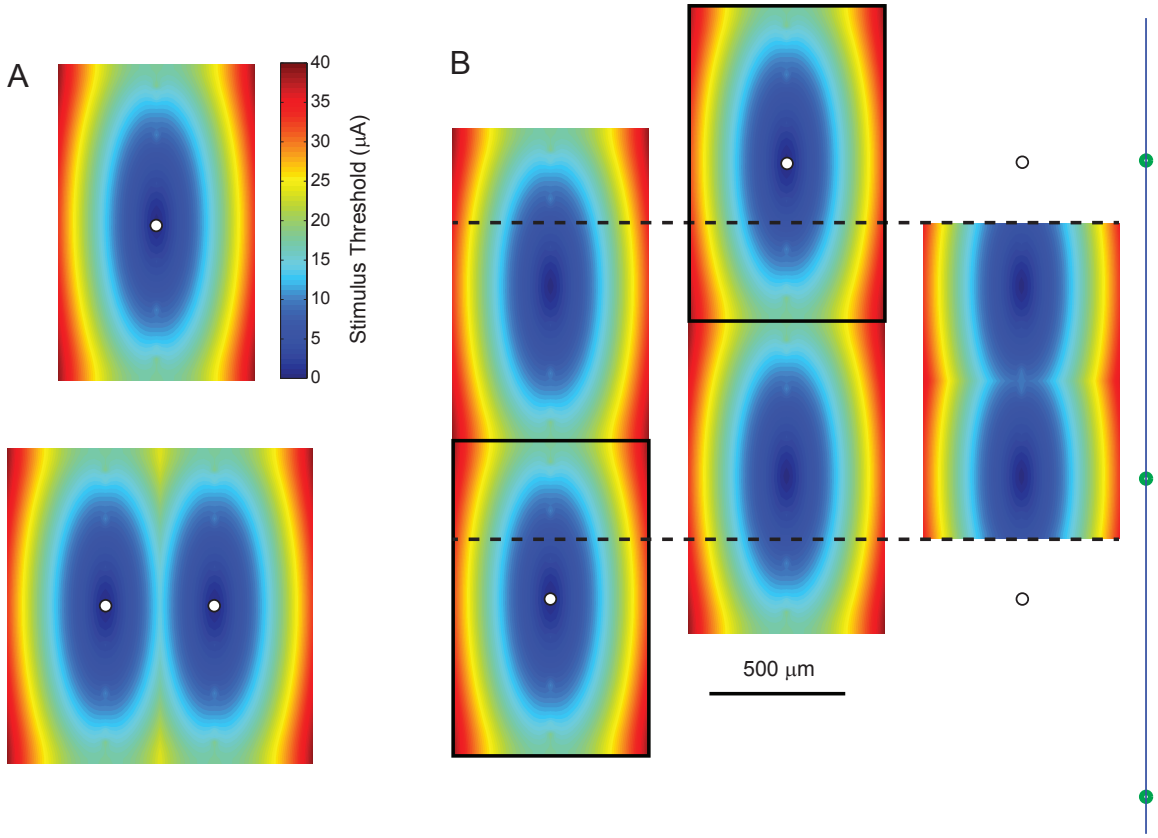

Figure C.1: Spatial replication of stimulus thresholds from a single electrode to derive stimulus thresholds for independent stimulation. (A) Stimulus thresholds for a 10 μm diameter fiber have been calculated at various locations relative to a single electrode. To solve for stimulus thresholds from two electrodes spaced 400 μm apart along the x-axis (transverse pairing), the solution to a single electrode is first spatially replicated. Then at each location, if multiple stimulus thresholds exist, the lowest stimulus threshold at that location is used. This operation corresponds to determining which electrode will activate a given neuron at a lower stimulus threshold. This approach results in the mirror-image solution seen where a neuron on the left side will be activated by the electrode on the left, and neurons on the right will be activated by neurons on the right. (B) Stimulus threshold solution for two electrodes spaced 1600 μm apart along the z-axis. Based on Appendix A, we can repeat the original solutions (pixels surrounded by black boxes) along the z-axis. Once this is done, the same corresponding z-range can be chosen from both electrodes (solutions within the dotted black lines) to form the final solution via the approach shown in (A). The choice of z-range does not matter for the merger, as the solution is periodic (see Appendix B). Notice in this case that the low threshold solution seen in the bottom portion actually corresponds to activation from the top electrode. When a neuron has a node of Ranvier close to the bottom portion of the solution, it has another node of Ranvier close to the top electrode (see axon on far right with circles to illustrate nodes of Ranvier).

An alternative approach used experimentally is to present stimuli on a pair of electrodes, with the stimulus on one shortly following (~1 ms after) stimulus on the other (Fisher et al. 2013). This is done so that neurons activated by the first stimulus will be in a refractory period and not activated by the second stimulus. When done in conjunction with stimuli presented on the pair at a much larger lag, where redundant activation of a subset of the population is possible, this method allows a way to assess stimulus overlap. Since it is expected that the refractory method would yield similar results to the spatial replication method, and since it also significantly increases the computation time, the method was not used for independent stimuli.

Once the single electrode results were spatially replicated, the minimum threshold values at all spatially coincident tests points were used. This corresponds to using the lowest stimulus threshold from any of the electrodes to determine when a neuron at a given location will be activated.

The spatial replication process is slightly more complicated when the replicated electrode locations vary along the z-axis. In this case all electrodes are spatially replicated in x and y as normal, but a different approach is needed for the z-dimension.

To illustrate this point, consider two electrodes that are separated by 1150 μm, which is the internodal length of a 10 μm fiber. Let's also say that at some stimulus amplitude, a volume of tissue is recruited that spans 200 μm (+/- 100 μm from the electrode) along the z – axis. Simple spatial replication would suggest that for two electrodes separated by 1150 μm, there is no overlap. However, due to the periodic nature of the axons, a node of Ranvier that is X μm away from one electrode will also have another node of Ranvier that is X μm away from the other electrode. Thus another approach is needed to perform spatial replication for electrodes that are apart in the z-dimension.

The first step to spatial replication is to replicate as normal in the x and y dimensions. Next, electrodes are moved to their appropriate location in the z-dimension. Because the solution is periodic in z (see Appendix B), each electrode solution is then replicated until all electrodes overlap sufficiently in the z-dimension. Electrodes overlap sufficiently when the overlap region spans one internodal length. Finally, the threshold solutions in the overlap region are merged by taking the minimum threshold at each location. This process is shown in Figure C.1B.

APPENDIX D

CHAPTER 6: VOLUME RATIO PROFILE AS A FUNCTION OF STIMULUS AMPLITUDE

The relationship between the volume ratio and stimulation amplitude is largely influenced by two factors; the merging of recruitment volumes around each electrode, and the saturation in the recruitment volume along the z-axis. These two factors occur in both the numerator and denominator of the volume ratio, depending on the stimulus amplitudes. This appendix further explores these two phenomena.

At small stimulus amplitudes, a small volume of tissue around each electrode is initially recruited. As the stimulus amplitude increases, the recruitment volumes from each individual electrode merge, and the rate of volume recruitment decreases. Intuitively this decrease corresponds to the recruitment volume from one electrode encountering tissue that has already been recruited by the other electrode. When this occurs the instantaneous rate of growth of the recruitment volume must decrease.

Another limit occurs when the recruitment volume begins to exceed the internodal length of the fiber diameter being examined (See Appendix B). This factor also leads to a decrease in the rate of growth of the recruitment volume and occurs at different stimulus amplitudes for the

independent and simultaneous stimulation cases. In terms of the volume ratio, a decrease in the rate of growth of the volumes of the independent or simultaneous stimulation cases will lead to an increase or decrease in the volume ratio respectively.

Figure C.1 shows the underlying changes in recruitment during independent and simultaneous stimulation that lead to the shape of the volume ratio as a function of stimulus amplitude. The volume ratios shown are the same as those shown in Figure 6.2 and have been provided here for reference. The derivatives of the recruitment volumes as a function of stimulus amplitude for independent and simultaneous stimulation are shown in C.1B. These results show that there are stimulus amplitudes where the derivative changes rate. To examine this phenomenon further the second derivative has also been calculated. Stimulus amplitudes at which there were peaks in the second derivative were chosen and their iso-threshold contours plotted in C.1D. These contours show that the peak in the second derivative occurs at nearly the stimulus amplitude where either regions from both electrodes are both to merge, or where this merged region is about to saturate along the z-axis. Some of the second derivative peaks for independent stimulation were not immediately obvious and were chosen post hoc to show this phenomena. There is also some noise in the solution which leads to ripples in the second derivative which cannot be explained. These changes in recruitment rates, combined with the overall curvature of the recruitment rate profiles lead to the observed profiles of the volume ratio.

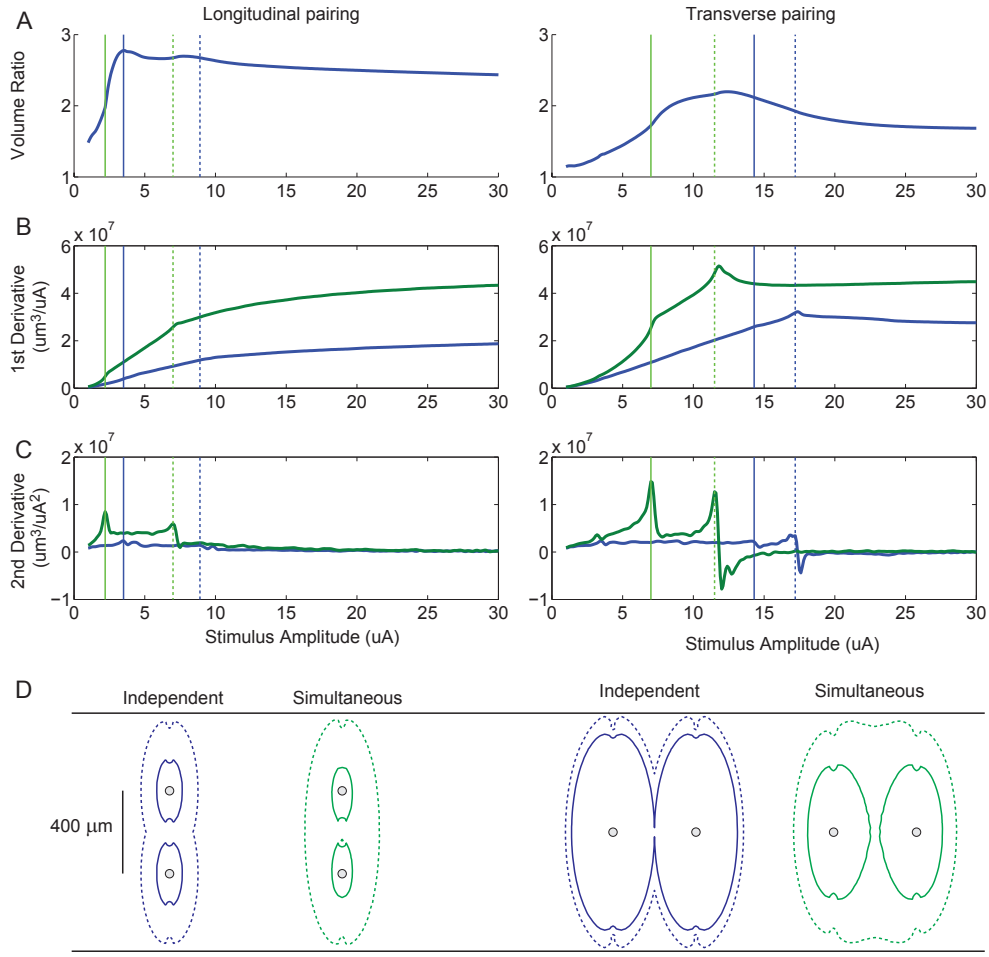

Figure D.1: Exploration of the shape of the volume ratio as a function of stimulus amplitude. Shown are the volume ratios as a function of stimulus amplitude for a 10 µm diameter fiber and a 200 µs stimulus pulse width for electrode spaced 400 µm apart along the x-axis (transverse pairing) and z-axis (longitudinal pairing). The first derivative of the change in recruitment volumes versus stimulus amplitude shows noticeable trend changes at certain stimulus amplitudes. Taking the second derivative shows these changes more clearly. A closer examination of the peaks in the second derivative show that these peaks occur just before the recruitment growth is limited in some way (D). The vertical lines in panel C were chosen to coincide with local peaks in the second derivative. The iso-threshold contours for these stimulus amplitudes are shown in (D) at y = 0. The solid vertical lines indicate a stimulus amplitude where recruitment volumes from the two electrodes are about to overlap. The dashed vertical lines indicate a stimulus amplitude where the volume is about to be limited by the internodal length of the neuron. Horizontal solid lines in (D) are separated by the internodal length of the neuron and indicate recruitment limits. Small circles indicate the location of the electrodes.

BIBLIOGRAPHY

Abbott A (2006) Neuroprosthetics: in search of the sixth sense. Nature 442:125–127.

Adrian ED, Zotterman Y (1926) The impulses produced by sensory nerve-endings. Part 2. The response of a single end-organ. J Physiol 61:151–171.

Alles D (1970) Information Transmission by Phantom Sensations. IEEE Trans Man Mach Syst 11:85–91.

Alter R (1966) Bioelectric Control of Prostheses.

Amir R, Devor M (2003) Electrical excitability of the soma of sensory neurons is required for spike invasion of the soma, but not for through-conduction. Biophys J 84:2181–2191.

Anani AB, Ikeda K, Körner LM (1977) Human ability to discriminate various parameters in afferent electrical nerve stimulation with particular reference to prostheses sensory feedback. Med Biol Eng Comput 15:363–373.

Antfolk C, D'Alonzo M, Controzzi M, Lundborg G, Rosén B, Sebelius F, Cipriani C (2013) Artificial redirection of sensation from prosthetic fingers to the phantom hand map on transradial amputees: vibrotactile versus mechanotactile sensory feedback. IEEE Trans Neural Syst Rehabil Eng 21:112–120.

Antognini JF, Carstens E, Buzin V (1999) Isoflurane depresses motoneuron excitability by a direct spinal action: an F-wave study. Anesth Analg 88:681–685.

Aoyagi Y, Stein RB, Branner A, Pearson KG, Normann R a (2003) Capabilities of a penetrating microelectrode array for recording single units in dorsal root ganglia of the cat. J Neurosci Methods 128:9–20.

Atkins DJ, Heard DCY, Donovan WH (1996) Epidemiologic Overview of Individuals with Upper-Limb Loss and Their Reported Research Priorities. JPO J Prosthetics Orthot 8:2–11.

Bastian HC (1887) The "muscular sense"; its nature and cortical localisation. Brain 10:1–89.

Battye CK, Nightingale A, Whillis J (1955) The use of myo-electric currents in the operation of prostheses. J Bone Joint Surg Br 37-B:506–510.

Beebe X, Rose TL (1988) Charge injection limits of activated iridium oxide electrodes with 0.2 ms pulses in bicarbonate buffered saline. IEEE Trans Biomed Eng 35:494–495.

Beeker TW, During J, Den Hertog A (1967) Artificial touch in a hand-prosthesis. Med Biol Eng 5:47–49.

Belter JT, Segil JL, Dollar AM, Weir RF (2013) Mechanical design and performance specifications of anthropomorphic prosthetic hands: A review. J Rehabil Res Dev 50:599–618.

Berger TW, Song D, Chan RHM, Marmarelis VZ (2010) The Neurobiological Basis of Cognition: Identification by Multi-Input, Multioutput Nonlinear Dynamic Modeling: A method is proposed for measuring and modeling human long-term memory formation by mathematical analysis and computer simulation of nerve-cell . Proc IEEE Inst Electr Electron Eng 98:356–374.

Biddiss E, Beaton D, Chau T (2007) Consumer design priorities for upper limb prosthetics. Disabil Rehabil Assist Technol 2:346–357.

Bourbeau DJ, Hokanson JA, Rubin JE, Weber DJ (2011) A computational model for estimating recruitment of primary afferent fibers by intraneural stimulation in the dorsal root ganglia. J Neural Eng 8:056009.

Boyd IA, Davey MR (1968) Composition of Peripheral Nerves. London: E & S Livingstone Ltd.

Boyd IA, Kalu KU (1979) Scaling Factor Relating Conduction Velocity and Diameter For Myelinated Afferent Nerve Fibres in the Cat Hind Limb. J Physiol 289:277–297.

Branner A, Stein RB, Fernandez E, Aoyagi Y, Normann R a (2004) Long-term stimulation and recording with a penetrating microelectrode array in cat sciatic nerve. IEEE Trans Biomed Eng 51:146–157.

Branner A, Stein RB, Normann RA (2001) Selective stimulation of cat sciatic nerve using an array of varying-length microelectrodes. J Neurophysiol 85:1585–1594.

Brill N, Tyler DJ (2011) Optimizing nerve cuff stimulation of targeted regions through use of genetic algorithms. Conf Proc IEEE Eng Med Biol Soc 2011:5811–5814.

Brown PB, Koerber HR (1978) Cat hindlimb tactile dermatomes determined with single-unit recordings. J Neurophysiol 41:260–267.

Burton H, McFarlane JJ (1973) The organization of the seventh lumbar spinal ganglion of the cat. J Comp Neurol 149:215–232.

Butson CR, Cooper SE, Henderson JM, McIntyre CC (2007) Patient-specific analysis of the volume of tissue activated during deep brain stimulation. Neuroimage 34:661–670.

Butson CR, McIntyre CC (2005) Tissue and electrode capacitance reduce neural activation volumes during deep brain stimulation. Clin Neurophysiol 116:2490–2500.

Butson CR, Miller IO, Normann RA, Clark GA (2011) Selective neural activation in a histologically derived model of peripheral nerve. J Neural Eng 8:036009.

Childress DS (1985) Historical Aspects of Powered Limb Prostheses. Clin Prosthetics Orthot 9:2–13.

Choi AQ, Cavanaugh JK, Durand DM (2001) Selectivity of multiple-contact nerve cuff electrodes: a simulation analysis. IEEE Trans Biomed Eng 48:165–172.

Christiansen R, Contreras-Vidal JL, Gillespie RB, Shewokis PA, O'Malley MK (2013) Vibrotactile feedback of pose error enhances myoelectric control of a prosthetic hand. In: 2013 World Haptics Conference (WHC), pp.531–536. IEEE.

Clark GM, Hallworth RJ, Zdanius K (1975) A cochlear implant electrode. J Laryngol Otol 89:787–792.

Clippinger FW, Avery R, Titus BR (1974) A sensory feedback system for an upper-limb amputation prosthesis. Bull Prosthet Res:247.

Cogan SF, Troyk PR, Ehrlich J, Plante TD (2005) In vitro comparison of the charge-injection limits of activated iridium oxide (AIROF) and platinum-iridium microelectrodes. IEEE Trans Biomed Eng 52:1612–1614.

Cole BYJD, Sedgwick EM (1992) The Perceptions of Force and of Movement in a Man Without Large Myelinated Sensory Afferents Below the Neck. J Physiol 449:503–515.

Creasey G, Elefteriades J, DiMarco a, Talonen P, Bijak M, Girsch W, Kantor C (1996) Electrical stimulation to restore respiration. J Rehabil Res Dev 33:123–132.

Davis TS, Parker R a, House P a, Bagley E, Wendelken S, Normann RA, Greger B (2012) Spatial and temporal characteristics of V1 microstimulation during chronic implantation of a microelectrode array in a behaving macaque. J Neural Eng 9:065003.

Devor M (1999) Unexplained peculiarities of the dorsal root ganglion. Pain Suppl 6:S27–35.

Dhillon GS, Horch KW (2005) Direct neural sensory feedback and control of a prosthetic arm. IEEE Trans Neural Syst Rehabil Eng 13:468–472.

Dhillon GS, Krüger TB, Sandhu JS, Horch KW (2005) Effects of short-term training on sensory and motor function in severed nerves of long-term human amputees. J Neurophysiol 93:2625–2633.

Dhillon GS, Lawrence SM, Hutchinson DT, Horch KW (2004) Residual function in peripheral nerve stumps of amputees: implications for neural control of artificial limbs. J Hand Surg Am 29:605–15;

Dobelle WH, Mladejovsky MG, Girvin JP (1974) Artifical vision for the blind: electrical stimulation of visual cortex offers hope for a functional prosthesis. Science 183:440–444.

Durand DM, Yoo P, Lertmanorat Z (2004) Neural interfacing with the peripheral nervous system. Conf Proc IEEE Eng Med Biol Soc 7:5329–5332.

Eccles JC, Sherrington C (1930) Numbers and Contraction-Values of Individual Motor-Units Examined in some Muscles of the Limb. Proc R Soc London 106:326–357.

Erlanger J, Bishop G, Gasser H (1926) The Action Potential Waves Transmittted Between The Sciatic Nerve and Its Spinal Roots. Am J Physiol 78:574–591.

Erlanger J, Blair EA (1938) Comparative observations on motor and sensory fibers with special reference to repetitiousness. Am J Physiol 121:431–453.

Fang ZP, Mortimer JT (1991) A method to effect physiological recruitment order in electrically activated muscle. IEEE Trans Biomed Eng 38:175–179.

Fetz EE (1969) Operant conditioning of cortical unit activity. Science 163:955–958.

Firszt JB, Holden LK, Reeder RM, Skinner MW (2009) Speech recognition in cochlear implant recipients: comparison of standard HiRes and HiRes 120 sound processing. Otol Neurotol 30:146–152.

Fisher LE, Ayers C a, Ciollaro M, Ventura V, Weber DJ, Gaunt R a (2013a) Chronic recruitment of primary afferent neurons by microstimulation of the feline dorsal root ganglia. Jounral Neural Eng In Review.

Fisher LE, Tyler DJ, Triolo RJ (2013b) Optimization of selective stimulation parameters for multi-contact electrodes. J Neuroeng Rehabil 10:25.

Fitzsimmons NA, Drake W, Hanson TL, Lebedev MA, Nicolelis M a L (2007) Primate reaching cued by multichannel spatiotemporal cortical microstimulation. J Neurosci 27:5593–5602.

Gasser HS (1928) The relation of the shape of the action potential of nerve to conduction velocity. Am J Physiol 84:699–711.

Gaunt RA, Hokanson JA, Weber DJ (2009) Microstimulation of primary afferent neurons in the L7 dorsal root ganglia using multielectrode arrays in anesthetized cats: thresholds and recruitment properties. J Neural Eng 6:55009.

Grill WM, Mortimer JT (1996) The effect of stimulus pulse duration on selectivity of neural stimulation. IEEE Trans Biomed Eng 43:161–166.

Grill WM, Mortimer JT (1997) Inversion of the current-distance relationship by transient depolarization. IEEE Trans Biomed Eng 44:1–9.

Grill WM, Veraart C, Mortimer JT (1991) Selective Activation Of Peripheral Nerve Fascicles: Use Of Field Steering Currents. In: Proceedings of the Annual International Conference of the IEEE Engineering in Medicine and Biology Society Volume 13: 1991, pp.904–905. IEEE.

Grinberg Y, Schiefer MA, Tyler DJ, Gustafson KJ (2008) Fascicular perineurium thickness, size, and position affect model predictions of neural excitation. IEEE Trans Neural Syst Rehabil Eng 16:572–581.

Gustafsson B, Jankowska E (1976) Direct and indirect activation of nerve cells by electrical pulses applied extracellularly. J Physiol 258:33–61.

Hagbarth KE, Vallbo AB (1967) Mechanoreceptor activity recorded percutaneously with semi-microelectrodes in human peripheral nerves. Acta Physiol Scand 69:121–122.

Hilgart DR, Dowden BR, Frankel MA, Warren DJ, Clark GA (2012) Bipolar and multi-electrode intrafascicular nerve stimulation improves both selectivity and strength of motor responses. In: Society for Neuroscience, 2012. New Orleans, LA.

Hines ML, Carnevale NT (1997) The NEURON Simulation Environment. Neural Comput 9:1179–1209.

Hines ML, Carnevale NT (2001) NEURON: a tool for neuroscientists. Neuroscientist 7:123–135.

Hines ML, Morse T, Migliore M, Carnevale NT, Shepherd GM (2004) ModelDB: A Database to Support Computational Neuroscience. J Comput Neurosci 17:7–11.

Histed MH, Bonin V, Reid RC (2009) Direct activation of sparse, distributed populations of cortical neurons by electrical microstimulation. Neuron 63:508–522.

Hochberg LR, Serruya MD, Friehs GM, Mukand JA, Saleh M, Caplan AH, Branner A, Chen D, Penn RD, Donoghue JP (2006) Neuronal ensemble control of prosthetic devices by a human with tetraplegia. Nature 442:164–171.

Hoffer JA, Loeb GE, Pratt CA (1981) Single unit conduction velocities from averaged nerve cuff electrode records in freely moving cats. J Neurosci Methods 4:211–225.

Hokanson JA, Wagenaar JBM, Weber DJ (2008) Recruitment of DRG neurons by electrical microstimulation. In: Society for Neuroscience Annual Meeting. Washington, DC.

Horch KW, Dhillon GS (2006) Towards a Neuroprosthetic Arm. In: The First IEEE/RAS-EMBS International Conference on Biomedical Robotics and Biomechatronics., pp.1125–1128. IEEE.

Horch KW, Meek S, Taylor TG, Hutchinson DT (2011) Object discrimination with an artificial hand using electrical stimulation of peripheral tactile and proprioceptive pathways with intrafascicular electrodes. IEEE Trans Neural Syst Rehabil Eng 19:483–489.

Horsager A, Greenberg RJ, Fine I (2010) Spatiotemporal interactions in retinal prosthesis subjects. Invest Ophthalmol Vis Sci 51:1223–1233.

House WF, Urban J (1973) Long-Term Results of Electrode lmplantation and Electronic Stimulation of the Cochlea in Man. In: Neural organization and its relevance to prosthetics; selected papers and discussions (Fields WS, ed), pp.273–280.

Hubel DH (1957) Tungsten Microelectrode for Recording from Single Units. Science 125:549–550.

Jankowska E, Roberts WJ (1972) An electrophysiological demonstration of the axonal projections of single spinal interneurones in the cat. J Physiol 222:597–622.

Jones EG, Porter R (1980) What is area 3a? Brain Res 203:1–43.

Kaas JH (1983) What, if anything, is SI? Organization of first somatosensory area of cortex. Physiol Rev 63:206–231.

Kandel E, Schwartz J, Jessell T (2000) Principles of Neural Science, 4th ed.

Kim SS, Sripati AP, Bensmaia SJ (2010) Predicting the timing of spikes evoked by tactile stimulation of the hand. J Neurophysiol 104:1484–1496.

Koivuniemi AS, Otto KJ (2011) Asymmetric versus symmetric pulses for cortical microstimulation. IEEE Trans Neural Syst Rehabil Eng 19:468–476.

Kuiken T a., Marasco PD, Lock BA, Harden RN, Dewald JP (2007) Redirection of cutaneous sensation from the hand to the chest skin of human amputees with targeted reinnervation. Proc Natl Acad Sci U S A 104:20061–20066.

Landgren S, Silfvenius H, Landgren BYS (1969) Projection to Cerebral Cortex of Group I Muscle Afferents From the Cat's Hind Limb. J Physiol 200:353–372.

Lebedev M a, Nicolelis M a L (2006) Brain-machine interfaces: past, present and future. Trends Neurosci 29:536–546.

Li CL, Bak A (1976) Excitability characteristics of the A- and C-fibers in a peripheral nerve. Exp Neurol 50:67–79.

Li M, Yan Y, Wang Q, Zhao H, Chai X, Sui X, Ren Q, Li L (2013) A simulation of current focusing and steering with penetrating optic nerve electrodes. J Neural Eng 10:066007.

Li P, Uren NF (1998) Analytical solution for the electric potential due to a point source in an arbitrarily anisotropic half-space. J Eng Math 33:129–140.

LLOYD DPC, CHANG HT (1948) Afferent fibers in muscle nerves. J Neurophysiol 11:199–207.

Loeb GE, Bak MJ, Duysens J (1977) Long-term unit recording from somatosensory neurons in the spinal ganglia of the freely walking cat. Science (80-) 197:1192–1194.

London BM, Jordan LR, Jackson CR, Miller LE (2008) Electrical stimulation of the proprioceptive cortex (area 3a) used to instruct a behaving monkey. IEEE Trans Neural Syst Rehabil Eng 16:32–36.

Lu H, Chestek CA, Shaw KM, Chiel HJ (2008) Selective extracellular stimulation of individual neurons in ganglia. J Neural Eng 5:287–309.

Macefield VG, Gandevia SC, Burke D (1990) Perceptual responses to microstimulation of single afferents innervating joints, muscles and skin of the human hand. J Physiol 429:113–129.

Mahnam A, Hashemi SMR, Grill WM (2008) Computational evaluation of methods for measuring the spatial extent of neural activation. J Neurosci Methods 173:153–164.

Mahnam A, Hashemi SMR, Grill WM (2009) Measurement of the current-distance relationship using a novel refractory interaction technique. J Neural Eng 6:036005.

Malešević NM, Popović Maneski LZ, Ilić V, Jorgovanović N, Bijelić G, Keller T, Popović DB (2012) A multi-pad electrode based functional electrical stimulation system for restoration of grasp. J Neuroeng Rehabil 9:66.

Mann R, Reimers S (1970) Kinesthetic Sensing for the EMG Controlled "Boston Arm." IEEE Trans Man Mach Syst 11:110–115.

Mann RW (1968) Efferent and afferent control of an electromyographic, proportional-rate, force sensing artificial elbow with cutaneous display of joint angle. Arch Proc Inst Mech Eng Conf Proc 1964-1970 (vols 178-184), Var titles Label Vol A to S 183:86–92.

Marasco PD, Kim K, Colgate JE, Peshkin M a, Kuiken T a. (2011) Robotic touch shifts perception of embodiment to a prosthesis in targeted reinnervation amputees. Brain 134:747–758.

Maurer MS, Burcham J, Cheng H (2005) Diabetes mellitus is associated with an increased risk of falls in elderly residents of a long-term care facility. J Gerontol A Biol Sci Med Sci 60:1157–1162.

McCreery DB, Agnew WF, Yuen TG, Bullara LA (1992) Damage in peripheral nerve from continuous electrical stimulation: comparison of two stimulus waveforms. Med Biol Eng Comput 30:109–114.

McDonnall D, Clark GA, Normann RA (2004a) Interleaved, multisite electrical stimulation of cat sciatic nerve produces fatigue-resistant, ripple-free motor responses. IEEE Trans Neural Syst Rehabil Eng 12:208–215.

McDonnall D, Clark GA, Normann RA (2004b) Selective motor unit recruitment via intrafascicular multielectrode stimulation. Can J Physiol Pharmacol 82:599–609.

McGlone F, Reilly D (2010) The cutaneous sensory system. Neurosci Biobehav Rev 34:148–159.

McIntyre CC, Grill WM (1999) Model-based design of stimulus waveforms for selective microstimulation in the central nervous system. In: Proceedings of the First Joint BMES/EMBS Conference, pp.384.

McIntyre CC, Grill WM (2000) Selective microstimulation of central nervous system neurons. Ann Biomed Eng 28:219–233.

McIntyre CC, Grill WM (2001) Finite element analysis of the current-density and electric field generated by metal microelectrodes. Ann Biomed Eng 29:227–235.

McIntyre CC, Grill WM, Sherman DL, Thakor N V (2004) Cellular effects of deep brain stimulation: model-based analysis of activation and inhibition. J Neurophysiol 91:1457–1469.

McIntyre CC, Richardson AG, Grill WM (2002) Modeling the excitability of mammalian nerve fibers: influence of afterpotentials on the recovery cycle. J Neurophysiol 87:995–1006.

McKenzie DS (1965) The Russian Myo-electric Arm. J Bone Joint Surg Br 47:418–420.

Mckenzie DS (1965) The Clinical Application of Externally Powered Artificial Arms. J Bone Joint Surg Br 47:399–410.

McNeal DR (1976) Analysis of a model for excitation of myelinated nerve. IEEE Trans Biomed Eng 23:329–337.

Meier JH, Rutten WLC, Zoutman AE, Boom H, Bergveld P (1992) Simulation of multipolar fiber selective neural stimulation using intrafascicular electrodes. IEEE Trans Biomed Eng 39:122–134.

Mendell LM, Henneman E (1971) Terminals of single Ia fibers: location, density, and distribution within a pool of 300 homonymous motoneurons. J Neurophysiol 34:171–187.

Micera S, Navarro X (2009) Bidirectional interfaces with the peripheral nervous system., 1st ed. Elsevier Inc.

Middlebrooks JC, Snyder RL (2007) Auditory prosthesis with a penetrating nerve array. J Assoc Res Otolaryngol 8:258–279.

Middlebrooks JC, Snyder RL (2010) Selective Electrical Stimulation of the Auditory Nerve Activates a Pathway Specialized for High Temporal Acuity. J Neurosci 30:1937–1946.

Millard DC, Wang Q, Gollnick C a, Stanley GB (2013) System identification of the nonlinear dynamics in the thalamocortical circuit in response to patterned thalamic microstimulation in vivo. J Neural Eng 10:066011.

Milner TE, Stein RB, Gillespie J, Hanley B (1981) Improved estimates of conduction velocity distributions using single unit action potentials. J Neurol Neurosurg Psychiatry 44:476–484.

Mooney V (1976) Sensory feedback in upper-extremity amputees. Clin Orthop Relat Res:274–275.

Moritz CT, Perlmutter SI, Fetz EE (2008) Direct control of paralysed muscles by cortical neurons. Nature 456:639–642.

Mountcastle VB (1997) The columnar organization of the neocortex. Brain 120 (Pt 4:701–722.

Musallam S, Bak MJ, Troyk PR, Andersen R a (2007) A floating metal microelectrode array for chronic implantation. J Neurosci Methods 160:122–127.

Mushahwar VK, Collins DF, Prochazka A (2000) Spinal cord microstimulation generates functional limb movements in chronically implanted cats. Exp Neurol 163:422–429.

Mushahwar VK, Jacobs PL, Normann R a, Triolo RJ, Kleitman N (2007) New functional electrical stimulation approaches to standing and walking. J Neural Eng 4:S181–97.

Nannini N, Horch KW (1991) Muscle recruitment with intrafascicular electrodes. IEEE Trans Biomed Eng 38:769–776.

Navarro X, Krueger TB, Lago N, Micera S, Stieglitz T, Dario P (2005) A critical review of interfaces with the peripheral nervous system for the control of neuroprostheses and hybrid bionic systems. J Peripher Nerv Syst 10:229–258.

Nicholson PW (1965) Specific impedance of cerebral white matter. Exp Neurol 13:386–401.

NIH (1995) NIH consensus conference. Cochlear implants in adults and children. JAMA 274:1955–1961.

Nilsson I, Berthold CH (1988) Axon classes and internodal growth in the ventral spinal root L7 of adult and developing cats. J Anat 156:71–96.

Normann RA, Dowden BR, Frankel M a, Wilder a M, Hiatt SD, Ledbetter NM, Warren D a, Clark GA (2012) Coordinated, multi-joint, fatigue-resistant feline stance produced with intrafascicular hind limb nerve stimulation. J Neural Eng 9:026019.

Northmore-Ball MD, Heger H, Hunter GA (1980) The below-elbow myo-electric prosthesis. A comparison of the Otto Bock myo-electric prosthesis with the hook and functional hand. J Bone Joint Surg Br 62:363–367.

Nowak LG, Bullier J (1998) Axons, but not cell bodies, are activated by electrical stimulation in cortical gray matter. I. Evidence from chronaxie measurements. Exp Brain Res 118:477–488.

O'Doherty JE, Lebedev M a., Ifft PJ, Zhuang KZ, Shokur S, Bleuler H, Nicolelis M a L (2011) Active tactile exploration using a brain–machine–brain interface. Nature:1–5.

O'Doherty JE, Lebedev MA, Li Z, Nicolelis MAL (2012) Virtual active touch using randomly patterned intracortical microstimulation. IEEE Trans Neural Syst Rehabil Eng 20:85–93.

Ochoa JL, Torebjörk HE (1983) Sensations evoked by intraneural microstimulation of single mechanoreceptor units innervating the human hand. J Physiol 342:633–654.

Ohara S, Weiss N, Lenz F a (2004) Microstimulation in the region of the human thalamic principal somatic sensory nucleus evokes sensations like those of mechanical stimulation and movement. J Neurophysiol 91:736–745.

Owings MF, Kozak LJ (1998) Ambulatory and inpatient procedures in the United States, 1996. Vital Health Stat 13:1–119.

Panizza M, Nilsson J, Roth BJ, Grill SE, Demirci M, Hallett M (1998) Differences between the time constant of sensory and motor peripheral nerve fibers: further studies and considerations. Muscle Nerve 21:48–54.

Panizza M, Nilsson J, Roth BJ, Rothwell J, Hallett M (1994) The time constants of motor and sensory peripheral nerve fibers measured with the method of latent addition. Electroencephalogr Clin Neurophysiol 93:147–154.

Peckham PH, Mortimer JT, Marsolais EB (1980) Controlled prehension and release in the C5 quadriplegic elicited by functional electrical stimulation of the paralyzed forearm musculature. Ann Biomed Eng 8:369–388.

Peterson EJ, Izad O, Tyler DJ (2011) Predicting myelinated axon activation using spatial characteristics of the extracellular field. J Neural Eng 8:046030.

Pfeiffer E a (1968) Electrical stimulation of sensory nerves with skin electrodes for research, diagnosis, communication and behavioral conditioning: a survey. Med Biol Eng 6:637–651.

Pfeiffer E a, Rhode CM, Fabric SI (1969) An experimental device to provide substitute tactile sensation from the anaesthetic hand. Med Biol Eng 7:191–199.

Prats-Galino a, Puigdellívol-Sánchez a, Ruano-Gil D, Molander C (1999) Representations of hindlimb digits in rat dorsal root ganglia. J Comp Neurol 408:137–145.

Priplata A, Niemi J, Salen M, Harry J, Lipsitz L, Collins J (2002) Noise-Enhanced Human Balance Control. Phys Rev Lett 89:238101.

Prochazka A, Gorassini M (1998) Models of ensemble firing of muscle spindle afferents recorded during normal locomotion in cats. J Physiol 507 (Pt 1:277–291.

Prochazka A, Westerman R a, Ziccone SP (1976) Discharges of single hindlimb afferents in the freely moving cat. J Neurophysiol 39:1090–1104.

Proske U, Gandevia SC (2012) The proprioceptive senses: their roles in signaling body shape, body position and movement, and muscle force. Physiol Rev 92:1651–1697.

Rampil IJ, King BS (1996) Volatile anesthetics depress spinal motor neurons. Anesthesiology 85:129–134.

Ranck JB (1975) Which elements are excited in electrical stimulation of mammalian central nervous system: a review. Brain Res 98:417–440.

Ranck JB, BeMent SL (1965) The Specific Impedance of the Dorsal Columns of Cat: An Anisotropic Medium. Exp Neurol 11:451–463.

Rattay F (1986) Analysis of models for external stimulation of axons. IEEE Trans Biomed Eng 33:974–977.

Rattay F (1987) Ways to approximate current-distance relations for electrically stimulated fibers. J Theor Biol 125:339–349.

Reswick JB, Mooney V, Schwartz A, McNeal DR, Su N, Bekey G, Bowman B, Snelson R, Irons G, Schmid P, Sperry C (1975) Sensory Feedback Prosthesis Using Intra-Neural Electrodes. In: Proc. of 5th Int. Symp. On External Control of Human Extremities, pp.9–25.

Risling M, Aldskogius H, Hildebrand C, Remahl S (1983) Effects of sciatic nerve resection on L7 spinal roots and dorsal root ganglia in adult cats. Exp Neurol 82:568–580.

Riso RR (1999) Strategies for providing upper extremity amputees with tactile and hand position feedback--moving closer to the bionic arm. Technol Health Care 7:401–409.

Robles L, Ruggero M a (2001) Mechanics of the mammalian cochlea. Physiol Rev 81:1305–1352.

Romo R, Hernández A, Zainos A, Salinas E (1998) Somatosensory discrimination based on cortical microstimulation. Nature 392:387–390.

Rutten WLC, van Wier HJ, Put JH (1991) Sensitivity and selectivity of intraneural stimulation using a silicon electrode array. IEEE Trans Biomed Eng 38:192–198.

Sainburg RL, Poizner H, Ghez C (1993) Loss of proprioception produces deficits in interjoint coordination. J Neurophysiol 70:2136–2147.

Sanes JN, Mauritz KH, Evarts E V, Dalakas MC, Chu A (1984) Motor deficits in patients with large-fiber sensory neuropathy. Proc Natl Acad Sci U S A 81:979–982.

Saunders E, Cohen L, Aschendorff A, Shapiro W, Knight M, Stecker M, Richter B, Waltzman S, Tykocinski M, Roland T, Laszig R, Cowan R (2002) Threshold, comfortable level and impedance changes as a function of electrode-modiolar distance. Ear Hear 23:28S–40S.

Schady WJL, Ochoa JL, Torebjörk HE, Chen LS (1983) Peripheral projections of fascicles in the human median nerve. Brain 106 (Pt 3):745–760.

Schiefer M a, Triolo RJ, Tyler DJ (2008) A model of selective activation of the femoral nerve with a flat interface nerve electrode for a lower extremity neuroprosthesis. IEEE Trans Neural Syst Rehabil Eng 16:195–204.

Schwartz AB, Cui XT, Weber DJ, Moran DW (2006) Brain-controlled interfaces: movement restoration with neural prosthetics. Neuron 52:205–220.

Scott RN (1990) Feedback in Myoelectric Prostheses. Clin Orthop Relat Res 256:58–63.

Shannon GF (1979) A myoelectrically-controlled prosthesis with sensory feedback. Med Biol Eng Comput 17:73–80.

Song D, Chan RHM, Marmarelis VZ, Hampson RE, Deadwyler SA, Berger TW (2007) Nonlinear dynamic modeling of spike train transformations for hippocampal-cortical prostheses. IEEE Trans Biomed Eng 54:1053–1066.

Spoendlin H, Schrott a (1989) Analysis of the human auditory nerve. Hear Res 43:25–38.

Stein RB, Charles D, Davis L, Jhamandas J, Mannard a, Nichols TR (1975) Principles underlying new methods for chronic neural recording. Can J Neurol Sci 2:235–244.

Stein RB, Misiaszek JE, Pearson KG (2000) Functional role of muscle reflexes for force generation in the decerebrate walking cat. J Physiol 525 Pt 3:781–791.

Stewart JD (2003) Peripheral nerve fascicles: anatomy and clinical relevance. Muscle Nerve 28:525–541.

Suh YS, Chung K, Coggeshall RE (1984) A study of axonal diameters and areas in lumbosacral roots and nerves in the rat. J Comp Neurol 222:473–481.

Suminski AJ, Tkach DC, Fagg AH, Hatsopoulos NG (2010) Incorporating feedback from multiple sensory modalities enhances brain-machine interface control. J Neurosci 30:16777–16787.

Suner S, Fellows MR, Vargas-Irwin C, Nakata GK, Donoghue JP (2005) Reliability of signals from a chronically implanted, silicon-based electrode array in non-human primate primary motor cortex. IEEE Trans Neural Syst Rehabil Eng 13:524–541.

Sweeney JD, Ksienski DA, Mortimer JT (1990) A nerve cuff technique for selective excitation of peripheral nerve trunk regions. IEEE Trans Biomed Eng 37:706–715.

Thach WT (1998) A role for the cerebellum in learning movement coordination. Neurobiol Learn Mem 70:177–188.

Tims EF, Nethken RT, Guidry MR (1967) Substitute Tactile Senses for Denervated Limbs. In: 1967 SWIEEECO (Dougal AA, ed), pp.11–13–1.

Torebjörk HE, Ochoa JL (1980) Specific sensations evoked by activity in single identified sensory units in man. Acta Physiol Scand 110:445–447.

Trulsson M, Francis ST, Kelly EF, Westling G, Bowtell R, McGlone F (2001) Cortical responses to single mechanoreceptive afferent microstimulation revealed with fMRI. Neuroimage 13:613–622.

Tyler DJ, Durand DM (2002) Functionally selective peripheral nerve stimulation with a flat interface nerve electrode. IEEE Trans Neural Syst Rehabil Eng 10:294–303.

Vallbo AB (1981) Sensations evoked from the glabrous skin of the human hand by electrical stimulation of unitary mechanosensitive afferents. Brain Res 215:359–363.

Veale J, Mark R, Rees S (1973) Differential sensitivity of motor and sensory fibres in human ulnar nerve. J Neurol Neurosurg Psychiatry 36:75–86.

Velliste M, Perel S, Spalding MC, Whitford AS, Schwartz AB (2008) Cortical control of a prosthetic arm for self-feeding. Nature 453:1098–1101.

Veltink PH, van Alsté J a, Boom H (1988) Simulation of intrafascicular and extraneural nerve stimulation. IEEE Trans Biomed Eng 35:69–75.

Veltink PH, van Alsté JA, Boom HB (1989a) Multielectrode intrafascicular and extraneural stimulation. Med Biol Eng Comput 27:19–24.

Veltink PH, van Veen BK, Struijk JJ, Holsheimer J, Boom H (1989b) A modeling study of nerve fascicle stimulation. IEEE Trans Biomed Eng 36:683–692.

Venkatraman S, Carmena JM (2011) Active sensing of target location encoded by cortical microstimulation. IEEE Trans Neural Syst Rehabil Eng 19:317–324.

Veraart C, Grill WM, Mortimer JT (1993) Selective control of muscle activation with a multipolar nerve cuff electrode. IEEE Trans Biomed Eng 40:640–653.

Volkmann J, Herzog J, Kopper F, Deuschl G (2002) Introduction to the programming of deep brain stimulators. Mov Disord 17 Suppl 3:S181–7.

Wall PD (1960) Cord cells responding to touch, damage, and temperature of skin. J Neurophysiol 23:197–210.

Wark H a C, Sharma R, Mathews KS, Fernandez E, Yoo J, Christensen B, Tresco P, Rieth L, Solzbacher F, Normann RA, Tathireddy P (2013) A new high-density (25 electrodes/mm(2)) penetrating microelectrode array for recording and stimulating sub-millimeter neuroanatomical structures. J Neural Eng 10:045003.

Weber DJ, London BM, Hokanson J a, Ayers C a, Gaunt R a, Torres RR, Zaaimi B, Miller LE (2011) Limb-state information encoded by peripheral and central somatosensory neurons: implications for an afferent interface. IEEE Trans Neural Syst Rehabil Eng 19:501–513.

Weber DJ, Stein RB, Everaert DG, Prochazka A (2006) Decoding sensory feedback from firing rates of afferent ensembles recorded in cat dorsal root ganglia in normal locomotion. IEEE Trans Neural Syst Rehabil Eng 14:240–243.

Weber DJ, Stein RB, Everaert DG, Prochazka A (2007) Limb-state feedback from ensembles of simultaneously recorded dorsal root ganglion neurons. J Neural Eng 4:S168–80–S168–80.

Wessels W (1993) A rostrocaudal somatotopic organization in the brachial dorsal root ganglia of neonatal rats. Clin Neurol Neurosurg 95:S3–11.

Wessels WJ, Feirabend HK, Marani E (1990) Evidence for a rostrocaudal organization in dorsal root ganglia during development as demonstrated by intra-uterine WGA-HRP injections into the hindlimb of rat fetuses. Brain Res Dev Brain Res 54:273–281.

Wiener N (1951) Problems of sensory prosthesis. Bull Am Math Soc 57:27–36.

Wilson BS (2006) Speech processing strategies. In: Cochlear Implants - A Practical Guide (Cooper HR, Craddock LC, eds), pp.21–69.

Wilson BS, Dorman MF (2008) Cochlear implants: a remarkable past and a brilliant future. Hear Res 242:3–21.

Wilson BS, Finley CC, Lawson DT, Wolford R, Eddington DK, Rabinowitz WM (1991) Better speech recognition with cochlear implants. Nature 352:236–238.

Wise KD, Anderson DJ, Hetke JF, Kipke DR, Najafi K (2004) Wireless Implantable Microsystems: High-Density Electronic Interfaces to the Nervous System. Proc IEEE 92:76–97.

Wodlinger B, Durand DM (2009) Localization and recovery of peripheral neural sources with beamforming algorithms. IEEE Trans Neural Syst Rehabil Eng 17:461–468.

Yoo PB, Lubock NB, Hincapie JG, Ruble SB, Hamann JJ, Grill WM (2013) High-resolution measurement of electrically-evoked vagus nerve activity in the anesthetized dog. J Neural Eng 10:026003.

Yoshida K, Horch KW (1993a) Selective stimulation of peripheral nerve fibers using dual intrafascicular electrodes. IEEE Trans Biomed Eng 40:492–494.

Yoshida K, Horch KW (1993b) Reduced fatigue in electrically stimulated muscle using dual channel intrafascicular electrodes with interleaved stimulation. Ann Biomed Eng 21:709–714.

Zaaimi B, Ruiz-Torres R, Solla S a, Miller LE (2013) Multi-electrode stimulation in somatosensory cortex increases probability of detection. J Neural Eng 10:056013.

Zehr EP, Duysens J (2004) Regulation of arm and leg movement during human locomotion. Neuroscientist 10:347–361.

Zhou HH, Mehta M, Leis a a (1997) Spinal cord motoneuron excitability during isoflurane and nitrous oxide anesthesia. Anesthesiology 86:302–307.

Ziegler-Graham K, MacKenzie EJ, Ephraim PL, Travison TG, Brookmeyer R (2008) Estimating the prevalence of limb loss in the United States: 2005 to 2050. Arch Phys Med Rehabil 89:422–429.

Zrenner E (2002) Will retinal implants restore vision? Science (80-) 295:1022–1025.